

AD-A103 057

DIKEWOOD INDUSTRIES INC ALBUQUERQUE NM

F/G 20/3

INTEGRAL-EQUATION SOLUTIONS AND MEASUREMENTS FOR CURRENTS AND C--ETC(U)

JUN 80 R W KING

F29601-79-C-0149

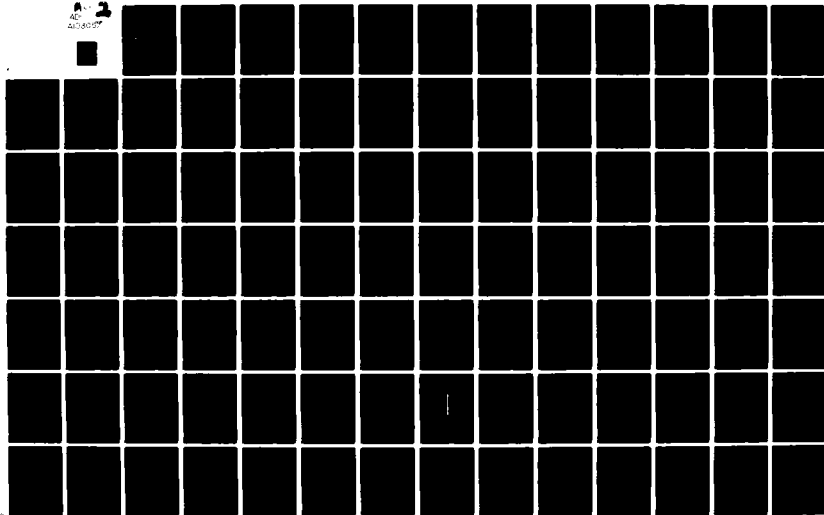
DC-FR-1289-4

AFWL-TR-79-135

NL

UNCLASSIFIED

AD-A103 057



① LEVEL II

AD A103057



INTEGRAL-EQUATION SOLUTIONS AND  
MEASUREMENTS FOR CURRENTS AND CHARGES  
ON TABULAR CYLINDERS AND INTERSECTING  
CYLINDERS--JUNCTION AND BOUNDARY  
CONDITIONS

Ronold W. P. King

Dikewood Industries, Inc  
1009 Bradbury Drive, SE  
Albuquerque, NM 87106

June 1980

Final Report

DTIC  
SELECTED  
JUN 1981  
B

Approved for public release; distribution unlimited.

AIR FORCE WEAPONS LABORATORY  
Air Force Systems Command  
Kirtland Air Force Base, NM 87117

81 8 18 086

This final report was prepared by the Dikewood Industries, Inc, Albuquerque, New Mexico, under Contract F29601-76-C-0149, Job Order 12090606 with the Air Force Weapons Laboratory, Kirtland Air Force Base, New Mexico. Dr. Michael G. Harrison (NTYE) was the Laboratory Project Officer-in-Charge.

When US Government drawings, specifications, or other data are used for any purpose other than a definitely related Government procurement operation, the Government thereby incurs no responsibility nor any obligation whatsoever, and the fact that the Government may have formulated, furnished, or in any way supplied the said drawings, specifications, or other data, is not to be regarded by implication or otherwise, as in any manner licensing the holder or any other person or corporation, or conveying any rights or permission to manufacture, use, or sell any patented invention that may in any way be related thereto.

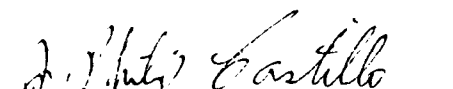
This report has been authored by a contractor of the United States Government. The United States Government retains a nonexclusive, royalty-free license to publish or reproduce the material contained herein, or allow others to do so, for the United States Government purposes.

This report has been reviewed by the Public Affairs Office and is releasable to the National Technical Information Service (NTIS). At NTIS, it will be available to the general public, including foreign nations.

This technical report has been reviewed and is approved for publication.



MICHAEL G. HARRISON, PhD  
Project Officer



J. PHILIP CASTILLO, PhD  
Chief, Electromagnetics Branch

FOR THE DIRECTOR



THOMAS W. CIAMBRONE  
Colonel, USAF  
Chief, Applied Physics Division

UNCLASSIFIED

SECURITY CLASSIFICATION OF THIS PAGE (When Data Entered)

REPORT DOCUMENTATION PAGE		READ INSTRUCTIONS BEFORE COMPLETING FORM
1. REPORT NUMBER AFWL-TR-79-135	2. GOVT ACCESSION NO. AD A03057	3. RECIPIENT'S CATALOG NUMBER 7
4. TITLE (and Subtitle) INTEGRAL-EQUATION SOLUTIONS AND MEASUREMENTS FOR CURRENTS AND CHARGES ON TUBULAR CYLINDERS AND INTERSECTING CYLINDERS--JUNCTION AND BOUNDARY CONDITIONS		5. TYPE OF REPORT & PERIOD COVERED Final Report
7. AUTHOR(s) Ronold W. P. King		6. PERFORMING ORG. REPORT NUMBER DC-FR-1289-4
9. PERFORMING ORGANIZATION NAME AND ADDRESS Dikewood Industries, Inc. 1009 Bradbury Drive, SE Albuquerque, NM 87106		8. CONTRACT OR GRANT NUMBER(s) F29601-76-C-0149
11. CONTROLLING OFFICE NAME AND ADDRESS Air Force Weapons Laboratory (NTYE) Kirtland Air Force Base, NM 87117		10. PROGRAM ELEMENT, PROJECT, TASK AREA & WORK UNIT NUMBERS 64711F/37630115
14. MONITORING AGENCY NAME & ADDRESS (if different from Controlling Office)		12. REPORT DATE June 1980
		13. NUMBER OF PAGES 98
		15. SECURITY CLASS. (of this report) Unclassified
		15a. DECLASSIFICATION/DOWNGRADING SCHEDULE
16. DISTRIBUTION STATEMENT (of this Report) Approved for public release; distribution unlimited.		
17. DISTRIBUTION STATEMENT (of the abstract entered in Block 20, if different from Report)		
18. SUPPLEMENTARY NOTES		
19. KEY WORDS (Continue on reverse side if necessary and identify by block number) Electromagnetic Cylinder Interaction Measurements		
20. ABSTRACT (Continue on reverse side if necessary and identify by block number) Extensive interaction formulas and data are given for the infinitely long cylinder and the cylinder of finite length for both E- and H-polarization, together with a comparison between theoretical calculations and Laboratory measurements. The formulation of the problem of two intersecting electrically thin cylinders and that of two non-orthogonally intersecting thin cylinders are described in detail with some representative results. The essential interaction features of two intersecting thick cylinders in free space and over a ground plane are briefly discussed.		

DD FORM 1 JAN 73 1473

UNCLASSIFIED

SECURITY CLASSIFICATION OF THIS PAGE (When Data Entered)

# CONTENTS

<u>Section</u>	<u>Page</u>
I INTRODUCTION	7
II THE INFINITELY LONG CYLINDER; $kh = \infty$	11
III THE CYLINDER OF FINITE LENGTH; $kh \geq 1$	16
1. E-POLARIZATION	17
2. H-POLARIZATION	28
IV THE ELECTRICALLY SHORT AND THIN CYLINDER: $ka < kh \leq 1$ (BASED ON REF. [5])	29
1. E-POLARIZATION	29
2. H-POLARIZATION	38
V COMPARISON WITH MEASUREMENTS	48
VI INTERSECTING ELECTRICALLY THIN CYLINDERS; $ka \leq 0.1$	50
VII INTERSECTING ELECTRICALLY THICK CYLINDERS; $ka > 0.1$	65
VIII INTERSECTING ELECTRICALLY THICK CYLINDER ( $ka = 1$ ) AND FLAT PLATE (BASED ON REF. [22])	73
IX NON-ORTHOGONALLY INTERSECTING CYLINDERS	81
X PENETRATION OF FIELDS INTO THE INTERIOR THROUGH AN OPEN END	93
XI SUMMARY AND CONCLUSION	94
REFERENCES	95

Approved for	<input checked="" type="checkbox"/>
by	
on	
for	
Code	
or	
by	
A	

# ILLUSTRATIONS

<u>Figure</u>		<u>Page</u>
1	Junction of Crossed Thin-Walled Tubes Illuminated by a Plane Wave that is (a) Arbitrarily Incident but with Wave Normal $\vec{k}$ Perpendicular to x-Axis, or (b) Normally Incident	9
2	Transverse Distribution of Surface Density of Current on Infinitely Long Tube	14
3	The Complex Fourier Coefficients of the Axial Surface Density of Current $K_z(\theta, z) = A(kz) + B(kz)\cos \theta + C(kz)\cos 2\theta + D(kz)\cos 3\theta$	19
4	Fourier Coefficients in $K_z(\theta, z) = A(kz) + B(kz)\cos \theta$ for Tubular Cylinder in an E-Polarized Field. $A(kz) = A_R(kz) + i A_I(kz)$ , $B(kz) = B_R(kz) + i B_I(kz)$ .	21
5	Axial Distributions of $ K_z(\theta, z) $ and $ cn(\theta, z) $ on Tubular Cylinder; E-Polarization	22
6	Magnitude of Axial Component of Surface Density of Current on Tubular Cylinder in E-Polarized Field	24
7	Magnitude of Axial Component of Surface Density of Current on Tubular Cylinder in E-Polarized Field	25
8	Magnitudes of Surface Densities of Charge and Axial Current on Tubular Cylinder with E-Polarization	26
9	Transverse Distribution of $ K_z(\theta, z) $	27
10	Fourier Coefficients of Surface Density of Axial Current on Tubular Cylinder; E-Polarization	30
11a	Fourier Coefficients of Surface Density of Axial Current on Tubular Cylinder; E-Polarization	31
11b	Fourier Coefficients of Surface Density of Axial Current on Tubular Cylinder; E-Polarization	32
12a	Surface Density of Axial Current on Tubular Cylinder; E-Polarization	34

# ILLUSTRATIONS (Continued)

<u>Figure</u>		<u>Page</u>
12b	Surface Density of Axial Current on Tubular Cylinder; E-Polarization	35
13a	Transverse Distribution of Surface Density of Axial Current on Tubular Cylinder; E-Polarization	36
13b	Transverse Distribution of Surface Density of Axial Current on Tubular Cylinder; E-Polarization	37
14a	Fourier Coefficient $B'_I(kz)$ of Surface Density of Transverse Current on Tubular Cylinder; E-Polarization	39
14b	Fourier Coefficient $B'_I(kz)$ of Surface Density of Transverse Current on Tubular Cylinder; E-Polarization	40
15a	Magnitude of Normalized Surface Density of Charge on Tubular Cylinder; E-Polarization	41
15b	Magnitude of Surface Density of Charge on Tubular Cylinder; E-Polarization	42
16a	Normalized Magnitude of Surface Density of Charge on Tubular Cylinder; E-Polarization	43
16b	Normalized Magnitude of Surface Density of Charge on Tubular Cylinder; E-Polarization	44
17a	Phase of Surface Density of Charge on Tubular Cylinder; E-Polarization	45
17b	Phase of Surface Density of Charge on Tubular Cylinder; E-Polarization	46
18	Measured Axial and Transverse Current Densities on Tubular Cylinder; E-Polarization. ( $ K $ in Arbitrary Units).	49
19	Currents and Charges Per Unit Length on Crossed Cylinders in Normally Incident Field; $\vec{E}^{(1)} = \vec{1}_z E_z^{(1)}$	61

# ILLUSTRATIONS (Continued)

<u>Figure</u>		<u>Page</u>
20	Currents and Charges Per Unit Length on Crossed Cylinders in Normally Incident Field; $\vec{E}^{(i)} = \hat{1}_z E_z^{(i)}$	62
21	Currents and Charges Per Unit Length on Crossed Cylinders in Normally Incident Field; $\vec{E}^{(i)} = \hat{1}_z E_z^{(i)}$	63
22	Measured Contours of Constant Charge Density $ n(\theta, z) $ on Vertical Members of Crossed Cylinders. ( $ n $ in Arbitrary Units).	67
23	Measured Contours of Magnitude of Surface Density of Charge on Horizontal Member of Crossed Cylinders. ( $ n $ in Arbitrary Units).	68
24	Measured Surface Density of Charge on Crossed Cylinders with $kh = 3.5\pi$ , $ka = 1$ for Two Locations of the Junction and with No Cross. ( $ n $ in Arbitrary Units).	69
25	Measured Contours of Constant Magnitude of Surface Density of Outside Charge on Vertical Member of Crossed Cylinders with Capped Ends; E-Polarization, Normal Incidence, $\lambda = 24$ cm. ( $ n $ in Arbitrary Units).	71
26	Measured Contours of Constant Magnitude of Surface Density of Outside Charge on Horizontal Member of Crossed Cylinders with Capped Ends; H-Polarization, Normal Incidence, $\lambda = 24$ cm. ( $ n $ in Arbitrary Units).	72
27	Diagram of Flat Plate Crossed with an Electrically Thick Cylinder Illuminated by a Normally Incident, Plane-Wave Field	74
28	Contour Diagram of Measured Magnitude of Surface Density of Charge $ n $ on Tubular Cylinder with Crossed Flat Plate Centered at $kh_1 = 2.5\pi$ , $kh = 3.5\pi$ ; $kL$ of Plate = $1.5\pi$ , $kL = 0.5\pi$ , $kT = 0.054\pi$ . ( $ n $ in Arbitrary Units).	75
29	Contour Diagram of Measured Surface Density of Charge on Horizontal Flat Plate. ( $ n $ in Arbitrary Units).	76



# ILLUSTRATIONS (Continued)

<u>Figure</u>		<u>Page</u>
30	Measured Magnitude of Surface Density of Axial Current on Vertical Cylinder with Crossed Flat Plate; $ka = 1$ , $kh = 3.5 \pi$ , $kh_1 = 2.5 \pi$ ; $kl = 1.5 \pi$ , $kL = 0.5 \pi$ , $kT = 0.054 \pi$ , ( $ K_z $ in Arbitrary Units)	77
31	Measured Magnitude of Surface Density of Current $K_z(x, z)$ on Horizontal Plate ( $ K_z $ in Arbitrary Units)	78
32	Measured Magnitude of Surface Density of Current $K_x(x, z)$ on Horizontal Flat Plate ( $ K_x $ in Arbitrary Units)	79
33	Swept-Wing Thin-Wire Cross	82

## TABLES

<u>Table</u>		<u>Page</u>
1	FOURIER COEFFICIENTS IN mA/V FOR INFINITELY LONG CYLINDER; $E_z^{(i)} = 1 \text{ V/m}$	13

## SECTION I

### INTRODUCTION

When an electromagnetic wave impinges on intersecting conductors like the wings and fuselage of an aircraft, currents and charges are induced on all surfaces with distributions that depend on the shape and dimensions of the conductors relative to the wavelength and on the angle of arrival and the polarization of the incident vector field. In general, the surface currents are determined by Maxwell's equations subject to the boundary condition that the tangential component of the electric field vanish on all of the (perfectly) conducting surfaces. A usually convenient formulation of the mathematical boundary-value problem is in terms of integral equations for the components of the vector surface density of current. Except in special cases like the infinitely long cylinder, these equations are coupled.

In order to obtain a qualitative understanding and derive quantitative information about the distributions of current on intersecting conductors, it is expedient to study first conductors with simple shapes, specifically, intersecting tubular cylinders for which fairly complete theoretical and experimental information is available over a wide range of electrical lengths and radii. Furthermore, a cylinder is a good approximation of the fuselage and its open tubular end resembles an open nose covered by a radome. The wings are better approximated by flat plates than by tubular cylinders, but no theory is available for the conducting strip of finite length. However, a theoretical and experimental study of intersecting tubular cylinders can be correlated with an experimental study of a tubular cylinder intersecting with a flat plate when the axial and transverse dimensions are comparable. Since an electromagnetic pulse consists of a spectrum of frequencies, and resonances that yield the greatest amplitudes in the induced currents and charges occur at specific frequencies, it is essential to obtain detailed information about the single-frequency behavior of the currents and charges on single and intersecting conductors.

Let one of the intersecting tubes be oriented along the  $z$ -axis, the other along the  $x$ -axis with their junction, the origin of rectangular coordinates, at the point of intersection of the axes of the cylinders, as shown in

Fig. 1. Instead of allowing the incident plane wave to travel in a completely arbitrary direction, it is advantageous to have its propagation vector or wave normal  $\vec{k}$  be perpendicular to the x-axis but with  $-\vec{k}$  at an arbitrary angle  $\theta$  with respect to the positive z-axis, as indicated by (a) in Fig. 1. Furthermore,  $\vec{E}^{(i)}$  (which is always in the plane of the wave front and perpendicular to  $\vec{k}$ ) may be rotated by an arbitrary angle  $\psi$  with respect to the yz-plane. It follows that

$$E_z^{(i)}(z) = -E_0^{(i)} \cos \psi \sin \theta e^{-ikz \cos \theta} \quad (1a)$$

$$E_x^{(i)} = -E_0^{(i)} \sin \psi \quad (1b)$$

with the time dependence  $e^{-i\omega t} = e^{j\omega t}$  ( $j = -i$ ). (The time dependence  $e^{-i\omega t}$  is usual in the field of scattering and the determination of surface currents on obstacles. Similarly,  $e^{j\omega t}$  is customary in circuit theory and thin-wire antenna theory. Each convention will be used in the appropriate context. With the definition  $j = -i$  one form is readily converted into the other.) In Eqs. (1a) and (1b),  $E_0^{(i)}$  is the magnitude of the incident electric field at the origin of coordinates. The horizontal tube is in the plane of the wave front and experiences a tangential electric field with the same amplitude and phase along its entire length; the vertical tube experiences a tangential electric field that is constant in amplitude but varies linearly and progressively in phase from one end to the other. When  $\psi = 0$ , the electric field has no component along the horizontal tube and currents in it are excited entirely by capacitive coupling to the vertical wire and by charges maintained at the junction. When  $\theta = \pi/2$ , the field is normally incident as indicated by (b) in Fig. 1; with  $\psi = 0$  the electric field is parallel to the vertical tube, with  $\psi = \pi/2$  it is parallel to the horizontal one.

The currents and charges on the conducting surfaces of intersecting tubes of any radius are governed by integral equations derived from the boundary condition  $E_t = 0$ . The continuity of  $E_n$  along the surfaces requires it to vanish at the bottom of each of the grooves that form the junction contours between the horizontal and vertical tubes. As a consequence, the surface density of charge  $\eta$  (which is proportional to  $F_n$ ) must also vanish there and with it the component of current along each groove. This means that the surface density of current  $\vec{K}$  crosses each groove at right angles.

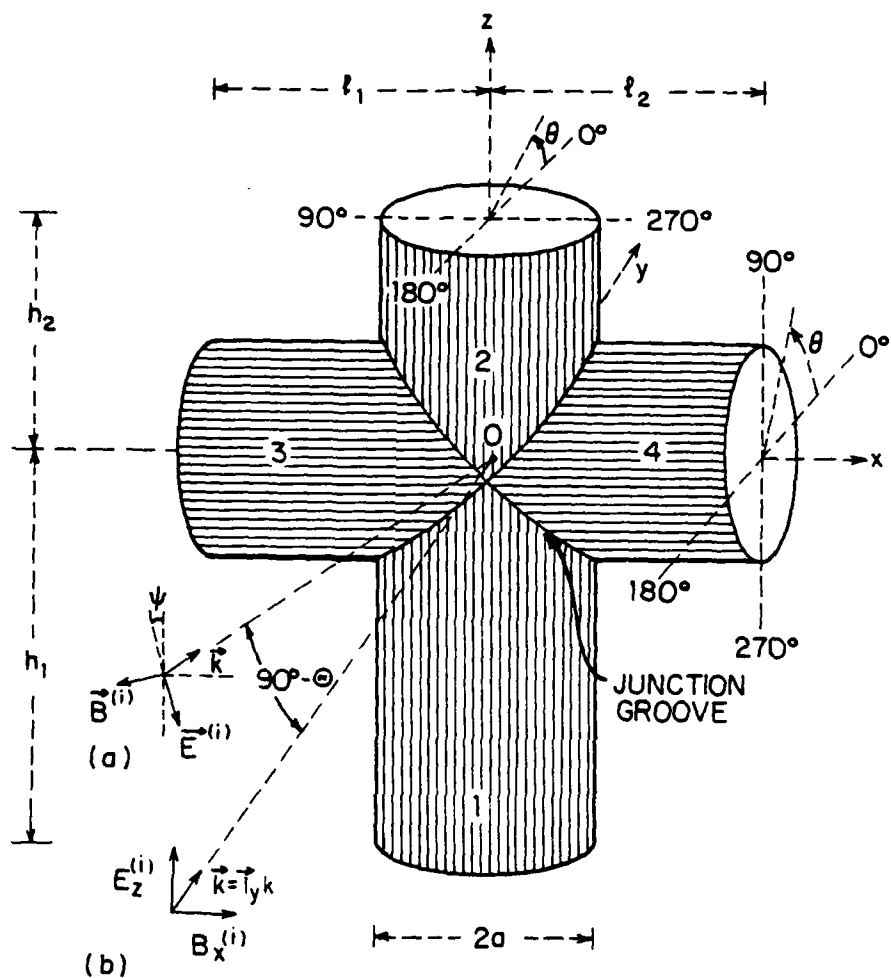


Figure 1. Junction of Crossed Thin-Walled Tubes Illuminated by a Plane Wave that is (a) Arbitrarily Incident but with Wave Normal  $\vec{k}$  Perpendicular to x Axis, or (b) Normally Incident.

In order to understand the currents and charges on intersecting cylinders, it is advantageous to review first the axial and transverse distributions of their surface densities on each tube when isolated, that is,  $\vec{K}(\theta, z)$  and  $\eta(\theta, z)$  on the vertical cylinder extending from  $z = -h$  to  $z = h$  in an E-polarized field,  $\vec{K}(\theta, x)$  and  $\eta(\theta, x)$  on the horizontal tube extending from  $x = -l$  to  $x = l$  in an H-polarized field. (Note that  $\theta$  is the local angular coordinate around either the  $x$  or  $z$  axis with  $\theta = 0^\circ$  at the center of the shadow in each.) It is convenient to examine tubes with electrical half-lengths  $kh$  (or  $kl$ ) in three ranges, viz.,  $kh = \infty$ ,  $1 \leq kh < \infty$ , and  $kh < 1$ . For each range an important special case is the low-frequency or electrically thin range with  $ka \ll 1$ .

The theoretical determination of the currents and charges on tubular cylinders with unrestricted length and radius has been accomplished only with a normally incident plane wave. Since an understanding of the currents and charges on intersecting cylinders depends on the availability of theoretical data for isolated cylinders, the case of normal incidence with E-polarization is considered first. For it the incident electric field is  $\vec{E}^{(i)} = \hat{z} E_z^{(i)}$ ; it is parallel to the vertical cylinder that extends from  $z = -h_1$  to  $z = h_2$ . The associated magnetic vector is  $\vec{B}^{(i)} = \hat{x} B_x^{(i)}$ ; it lies along the horizontal cylinder that extends from  $x = -l_1$  to  $x = l_2$ . The radii of the tubes are initially assumed to be the same and given by  $a$ . With the time dependence  $e^{-i\omega t}$ ,  $E_z^{(i)}(y) = E_{z0}^{(i)} e^{iky} = E_{z0}^{(i)} e^{iko \cos \theta}$ ,  $B_x^{(i)}(y) = E_z^{(i)}(y)/c$  or  $H_x^{(i)}(y) = E_z^{(i)}(y)/Z_0$  where  $c = 3 \times 10^8$  m/sec,  $Z_0 \doteq 120\pi$  ohms, and  $\rho, \theta$  are cylindrical coordinates. The propagation vector is  $\vec{k} = \hat{y} k$ . Note that the center of the illuminated side is at  $\theta = 180^\circ$ , the center of the shadow at  $\theta = 0^\circ$ , and the shadow boundaries at  $\theta = 90^\circ$  and  $270^\circ$ . The dimensions of aircraft and the frequencies in an electromagnetic pulse make electrical radii in the range  $0.01 \leq ka \leq 2$  and arm lengths  $kh$  from several wavelengths to very small fractions of a wavelength of interest. Two important ranges of the electrical radius are  $ka \leq 0.1$  and  $ka > 0.1$ ; the first of these has two subranges defined by  $ka \leq 0.1$ ,  $kh > 1$  and  $ka \leq 0.1$ ,  $kh < 1$ .

SECTION II  
THE INFINITELY LONG CYLINDER;  $kh = \infty$

For infinitely long cylinders the currents induced by E-polarized and H-polarized fields are mutually independent and can be obtained from separate integral equations. This means that an arbitrarily incident field can be resolved into E- and H-polarized components and the currents induced by each determined separately and then combined. When  $kh = \infty$ , the integral equations for the currents are obtained from the boundary condition  $E_t = 0$  at  $\rho = a$ ,  $0 \leq \theta \leq 2\pi$ ,  $-\infty < z < \infty$ . For E-polarization along the z-axis,  $K_\theta(\theta) = 0$  and  $K_z(\theta)$  satisfies the equation:

$$E_{z0}^{(i)} e^{ika \cos \theta} + i\omega\mu_0 a \int_0^{2\pi} K_z(\theta') G(a, \theta; a', \theta') d\theta' = 0 \quad (2a)$$

For H-polarization along the x-axis,  $K_x(\theta) = 0$  and  $K_\theta(\theta)$  satisfies the equation:

$$\frac{\partial}{\partial \rho} [B_{x0}^{(i)} e^{ika \cos \theta}] - \mu_0 a \int_0^{2\pi} K_\theta(\theta') \left[ \frac{\partial^2}{\partial \rho \partial \rho'} G(\rho, \theta; \rho', \theta') \right]_{\rho=\rho'=a} d\theta' = 0 \quad (2b)$$

In Eqs. (2a,b),  $G(\rho, \theta; \rho', \theta') = (i/4) H_0^{(1)}(kR)$  with  $R = [\rho^2 + \rho'^2 - 2\rho\rho' \times \cos(\theta - \theta')]^{1/2}$ . With  $E_z^{(i)} = 1$  V/m and with  $\epsilon_m = 1$ ,  $m = 0$ ;  $\epsilon_m = 2$ ,  $m \neq 0$ , the eigenfunction solutions are:

E-polarization:

$$\begin{aligned} K_z(\theta) &= (2/\pi Z_0 ka) \sum_{m=0}^{\infty} \epsilon_m i^m \cos m\theta / H_m^{(1)}(ka) \\ &= A + B \cos \theta + C \cos 2\theta + D \cos 3\theta + \dots \end{aligned} \quad (3)$$

$$K_\theta(\theta) = 0, \quad \eta(\theta) = 0 \quad (4)$$

H-polarization:

$$\begin{aligned} K_\theta(\theta) &= (2/\pi Z_0 ka) \sum_{m=0}^{\infty} \epsilon_m i^{m-1} \cos m\theta / H_m^{(1)'}(ka) \\ &= A_H + B_H \cos \theta + C_H \cos 2\theta + D_H \cos 3\theta + \dots \end{aligned} \quad (5)$$

$$K_x(\theta) = 0, \quad \zeta\eta(\theta) = (i/ka) \partial K_\theta(\theta) / \partial \theta$$

$$= -(i/ka)[B_H \sin \theta + 2C_H \sin 2\theta + \dots] \quad (6)$$

The complex Fourier coefficients  $A$ ,  $B$ , ..., and  $A_H$ ,  $B_H$ , ..., are functions of  $ka$ . Their numerical values for five values of  $ka$  are in table 1. When  $ka \leq 0.1$ , small argument approximations of the Hankel functions give:  $K_z(\theta) \doteq A + B_R \cos \theta$ ;  $K_\theta(\theta) \doteq A_{HR} + iB_{HI} \cos \theta$  where  $A = A_R + iA_I = (2/\pi Z_0 ka) \{1 - (2i/\pi)[\ln(2/ka) + \gamma]\}$  with  $\gamma = 0.577$ ,  $B_R = -2/Z_0 = -5.30 \times 10^{-3}$  A/V,  $A_{HR} = -1/Z_0 = -2.65 \times 10^{-3}$  A/V, and  $B_{HI} = -2ka/Z_0$ . Note that with E-polarization the rotationally symmetric, zero-order current  $[K_z]_0 = I_z/2\pi a = A$  increases rapidly in amplitude with decreasing  $ka$  while the first-order current  $[K_z(\theta)]_1 \doteq B_R \cos \theta = (-2/Z_0) \cos \theta = -2H_x^{(i)} \cos \theta$  is independent of  $ka$ .  $[K_z(\theta)]_1$  consists of equal and opposite axial currents respectively on the illuminated and shadowed halves of the cylinder. The phase relations are such that  $K_z(\theta)$  is increased on the illuminated side, decreased on the shadowed side as shown in solid lines in Fig. 2. As  $ka$  is increased from 0.1 to 1, the coefficients  $C_I$  and  $D_R$  in Eq. (3) become significant and modify the shape of the curves. With H-polarization, the current with  $ka \leq 0.1$  consists predominantly of a rotationally symmetric circulation around the tube given by  $[K_\theta]_0 = A_{HR} = -1/Z_0 = -H_x^{(i)}$  as shown in broken lines in Fig. 2. As  $ka$  is increased from 0.1 to 1, the coefficients  $B_H = B_{HR} + iB_{HI}$ ,  $C_H = C_{HR} + iC_{HI}$ , and  $D_{HR}$  become significant and the shape of the graphs changes from a horizontal line to a curve with a maximum at  $\theta = 180^\circ$ . Note that when  $ka \leq 0.1$ ,  $K_z(\theta)$  induced by the E-polarized field with  $E_z^{(i)} = 1$  V/m is much greater than  $K_\theta(\theta)$  induced by an equal H-polarized field with  $E_z^{(i)} = H_x^{(i)} Z_0 = 1$  V/m. The two become comparable when  $ka \geq 0.5$ .

With E-polarization, the zero-order part of  $K_z(\theta)$ , viz.,  $[K_z]_0 = A$ , is rotationally symmetric, the first-order part  $[K_z(\theta)]_1 = B \cos \theta$  is equal in magnitude and opposite in direction on the illuminated and shadowed halves as in a balanced, two-conductor transmission line; the second-order part represented by  $C \cos 2\theta$  is equal and codirectional in the illuminated and shadowed quadrants centered respectively at  $\theta = 180^\circ$  and  $0^\circ$ , equal and oppositely directed in the quadrants centered at  $\theta = 90^\circ$  and  $270^\circ$  as in a balanced, four-conductor line. With H-polarization, the zero-order part of  $K_\theta(\theta)$  represented by  $A_H$  is a current that circulates around the cylinder with constant amplitude and phase; the first-order part represented by  $B_H \cos \theta$  is a current that

Table 1

FOURIER COEFFICIENTS IN mA/V FOR INFINITELY LONG CYLINDER;  $E_z^{(i)} = 1$  V/m

## E-POLARIZATION

$$K_z(\theta) = A + B \cos \theta + C \cos 2\theta + D \cos 3\theta + E \cos 4\theta + \dots$$

ka	$A = A_R + iA_I$	$B = B_R + iB_I$	$C = C_R + iC_I$	$D = D_R + iD_I$	$E = E_R + iE_I$
0.01	16.83 + i50.59	-5.30 + i0.00	0.00 - i0.03	0.00 + i0.00	0.00 + i0.00
0.05	6.86 + i13.60	-5.28 + i0.01	0.00 - i0.13	0.00 + i0.00	0.00 + i0.00
0.10	5.03 + i7.74	-5.23 + i0.04	0.00 - i0.26	0.01 + i0.00	0.00 + i0.00
0.50	2.94 + i1.39	-4.47 + i0.74	-0.01 - i1.24	0.16 + i0.00	0.00 + i0.01
1.00	2.18 + i0.25	-3.28 + i1.85	-0.14 - i2.04	0.58 + i0.00	0.00 + i0.10

## H-POLARIZATION

$$K_\theta(\theta) = A_H + B_H \cos \theta + C_H \cos 2\theta + \dots$$

ka	$A_H = A_{HR} + iA_{HI}$	$B_H = B_{HR} + iB_{HI}$	$C_H = C_{HR} + iC_{HI}$	$D_H = D_{HR} + iD_{HI}$	$E_H = E_{HR} + iE_{HI}$
0.01	-2.65 + i0.00	0.00 - i0.05	0.00 + i0.00	0.00 + i0.00	0.00 + i0.00
0.05	-2.64 + i0.01	0.00 - i0.27	0.00 + i0.00	0.00 + i0.00	0.00 + i0.00
0.10	-2.61 + i0.02	0.00 - i0.54	0.01 + i0.00	0.00 + i0.00	0.00 + i0.00
0.50	-2.23 + i0.37	0.48 - i2.62	0.33 + i0.00	0.00 + i0.03	0.00 + i0.00
1.00	-1.64 + i0.92	1.27 - i3.41	1.33 + i0.11	0.00 + i0.21	-0.03 + i0.00



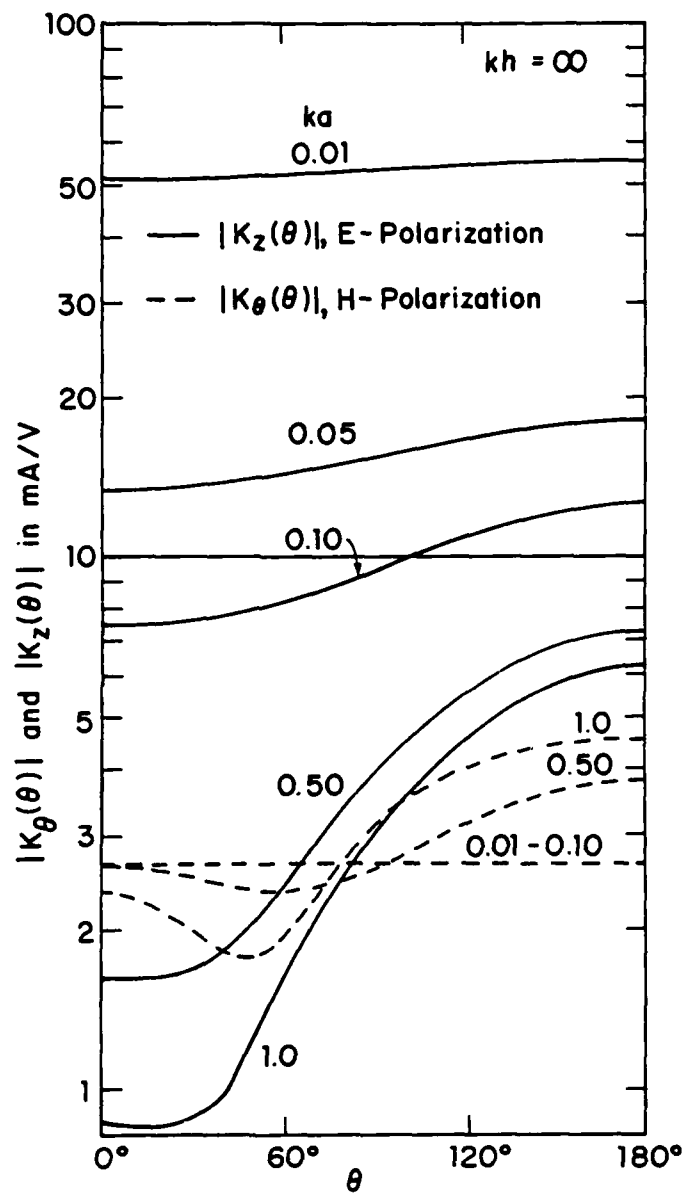


Figure 2. Transverse Distribution of Surface Density of Current on Infinitely Long Tube.

oscillates in a transverse standing-wave pattern on the illuminated and shadowed halves with zero current densities and maximum charge densities of opposite sign at the shadow boundaries.

### SECTION III

#### THE CYLINDER OF FINITE LENGTH; $kh \geq 1$

The currents and charges induced on tubular cylinders of finite length are more complicated in both their axial and transverse distributions than those induced on cylinders that are infinitely long. This is a consequence of multiple reflections at the open ends. The currents are again determined from the boundary condition  $E_t = 0$  on the conductor but this now extends only from  $z = -h$  to  $z = h$  and includes both the inside and outside of the tubular surface. Two coupled integral equations are obtained in Reference 1 for the transverse Fourier components  $K_z(u|n)$  and  $K_\theta(u|n)$ ,  $n = 0, 1, 2, \dots$ , of the total currents  $K_z(\theta, z)$  and  $K_\theta(\theta, z)$ . Both of these components are present with each polarization. Total currents are the sum of the currents on the outside and inside surfaces. When  $ka \leq 1$ , the inside of the tube is well below cut-off for waveguide modes so that the inside current decreases rapidly from the open end inward. Measurements given in Reference 2 have shown that the outside current on a tube with open ends differs little from the current on the same tube with ends closed by flat metal discs. With the notation  $u = kz$ , the equations for E-polarization from Reference 1 are:

$$2 \int_0^{kh} G_\theta(u, u'|n) K_\theta(u'|n) du' = (in/ka) C \sin u + C_\theta(n) \quad (7)$$

$$2 \int_0^{kh} G_z(u, u'|n) K_z(u'|n) du' + (2n/ka) \int_0^{kh} G_{z\theta}(u, u'|n) K_\theta(u'|n) du' = C \cos \theta + C_z(n) \quad (8)$$

The equations for H-polarization in Reference 1 are the same with  $\sin u$  replaced by  $-\cos u$ ,  $\cos u$  by  $\sin u$ . The constant  $C$  is determined from the condition  $K_z(u|n) = 0$  at  $u = kh$ . For E-polarization,  $C_z(n) = -(4\epsilon_n i^n / Z_0 ka) J_n(ka)$ ,  $C_\theta(n) = 0$ ; for H-polarization,  $C_z(n) = 0$ ,  $C_\theta(n) = -(4\epsilon_n i^{n-1} / Z_0 ka) J_n'(ka)$ . The kernels are  $G_\theta(u, u'|n) = (2/Z_0 k^2 a) [M_\theta(u - u'|n) \mp M_\theta(u + u'|n)]$ ,  $G_z(u, u'|n) = (2/Z_0 a) [M_z(u - u'|n) \pm M_z(u + u'|n)]$ ,  $G_{z\theta}(u, u'|n) = (2k/nZ_0) [M_{z\theta}(u - u'|n) \mp M_{z\theta}(u + u'|n)]$ , where the upper sign is for E-, the lower sign for H-polarization and  $\epsilon_n = 1$ ,  $n = 0$ ;  $\epsilon_n = 2$ ,  $n > 0$ . The  $M$ 's are the inverse Fourier transforms of  $\tilde{M}_\theta(\zeta|n) = -(\pi\omega\mu_0 a/2) J_{|n|}(a\xi) H_{|n|}^{(1)'}(a\xi)$ ,  $\tilde{M}_z(\zeta|n) = -(\pi a/2\omega\epsilon_0) J_{|n|}(a\xi) \times H_{|n|}^{(1)}(a\xi)$ ,  $\tilde{M}_{z\theta}(\zeta|n) = (n\pi\zeta/2\omega\xi^2) J_{|n|}(n\xi) H_{|n|}^{(1)}(a\xi)$  with  $\xi^2 = k^2 - \zeta^2$ . The  $n^{\text{th}}$

order Fourier component  $K_\theta(u|n)$  can be determined from Eq. (7) and used in Eq. (8) to obtain  $K_z(u|n)$ . The total currents for E-polarization are, from Reference 1,

$$\begin{aligned} K_z(\theta, z) &= \sum_{n=0}^{\infty} C_z(n) K_z(z|n) \cos n\theta \\ &= A(kz) + B(kz) \cos \theta + C(kz) \cos 2\theta + D(kz) \cos 3\theta + \dots \end{aligned} \quad (9)$$

$$\begin{aligned} K_\theta(\theta, z) &= i \sum_{n=1}^{\infty} C_z(n) K_\theta(z|n) \sin n\theta \\ &= i[B'(kz) \sin \theta + C'(kz) \sin 2\theta + D'(kz) \sin 3\theta + \dots] \end{aligned} \quad (10)$$

For H-polarization, the total currents are given in Reference 1 as:

$$\begin{aligned} K_\theta(\theta, x) &= \sum_{n=0}^{\infty} C_\theta(n) K_\theta(x|n) \cos n\theta \\ &= A_H(kx) + B_H(kx) \cos \theta + C_H(kx) \cos 2\theta + D_H(kx) \cos 3\theta + \dots \end{aligned} \quad (11)$$

$$\begin{aligned} K_x(\theta, x) &= i \sum_{n=1}^{\infty} C_\theta(n) K_x(x|n) \sin n\theta \\ &= i[B'_H(kx) \sin \theta + C'_H(kx) \sin 2\theta + D'_H(kx) \sin 3\theta + \dots] \end{aligned} \quad (12)$$

The associated charge densities are given by

$$\eta(\theta, z) = -(1/c) [\partial K_z(\theta, z) / \partial z + (1/ka) \partial K_\theta(\theta, z) / \partial \theta] \quad (13)$$

for E-polarization and from Eq. (13) with  $x$  written for  $z$  for H-polarization. The number of terms required decreases with  $ka$ . When  $ka = 1$ ,  $K_z(\theta, z)$  and  $K_\theta(\theta, x)$  require four terms; when  $ka \leq 0.1$ , only two are needed.

#### 1. E-POLARIZATION

The complex coefficients  $A(kz)$ ,  $B(kz)$ , ..., (which are functions of  $ka$  and  $kz$ ) generally oscillate about the corresponding coefficients  $A, B, \dots$ , for  $kh = \infty$  with amplitudes that depend on  $ka$ . When  $ka = 1$ , both  $A(kz)$  and  $B(kz)$  have significant resonant amplitudes about the complex constants  $A$  and  $B$ ;  $C(kz)$  and  $D(kz)$  are significant but remain virtually constant at the values  $C$  and  $D$  except very near the open end where they decrease to zero. Higher-order coefficients are negligible. Graphs of these quantities

when  $ka = 1$  are in Fig. 13 and Fig. 14 of Reference 3 for  $kh = 1.5\pi$ , in Figs. 8 and 9 of Reference 4 for a range of values of  $kh$  between  $1.5\pi$  and  $3.5\pi$ . Graphs of the Fourier coefficients when  $ka = 0.5, 0.1, 0.05$ , and  $0.01$  are in Fig. 3 for  $kh = 1.5\pi$ . It is seen that for  $ka = 0.50$  with  $A = A_R + iA_I$ ,  $B = B_R + iB_I$ , ...,

$$K_z(\theta, z) \doteq A(kz) + B(kz)\cos \theta + iC_I(kz)\cos 2\theta + D_R(kz)\cos 3\theta \quad (14)$$

but now only  $A_R(kz)$  has a large resonant amplitude of oscillation about  $A_R$ ,  $A_I(kz)$  and  $B_R(kz)$  have only small oscillatory amplitudes, and  $B_I(kz)$ ,  $C_I(kz)$ , and  $D_R(kz)$  are constant near the values  $B_I$ ,  $C_I$ , and  $D_R$  for  $kh = \infty$  except very near the ends. For  $ka \leq 0.1$ ,

$$K_z(\theta, z) \doteq A(kz) + B_R(kz)\cos \theta \quad (15)$$

$A_R(kz)$  and  $A_I(kz)$  both have large amplitudes of oscillation about  $A_R$  and  $A_I$ ;  $B_R(kz)$  is equal to  $B_R$  except very near the open end. The approximate formula, Eq. (15), is given in Reference 5. It is consistent with the corresponding relation for the axial current density induced on a prolate spheroid as given by Taylor and Harrison in Reference 6.

A convenient approximate representation of the dependence of the Fourier components on the axial variable involves the function  $e(kz)$  which is defined in Reference 4 as follows:

$$e(kz) = 1 \quad , \quad 0 \leq |z| \leq (h - d) \quad ; \quad e(kz) \doteq \sin[\pi(h - |z|)/2d] \quad , \quad h - d \leq |z| \leq h \quad (16)$$

It is usually adequate to set  $d = a$ , where  $a$  is the radius of the tube. With Eq. (16), Eq. (14) is approximated by  $A(kz) \doteq (A + A_I \cos kh)e(kz) + A_I(\cos kz - \cos kh)$ ,  $B(kz) \doteq (B + B_I \cos kh)e(kz) + B_I(\cos kz - \cos kh)$ ,  $C_I(kz) \doteq C_I e(kz)$ ,  $D_R(kz) \doteq D_R e(kz)$  so that

$$ka = 0.50: \quad K_z(\theta, z) \doteq [A + A_I \cos kh + (B + B_I \cos kh)\cos \theta + iC_I \cos 2\theta + D_R \cos 3\theta]e(kz) + (A_I + B_I \cos \theta)(\cos kz - \cos kh) \quad (17)$$

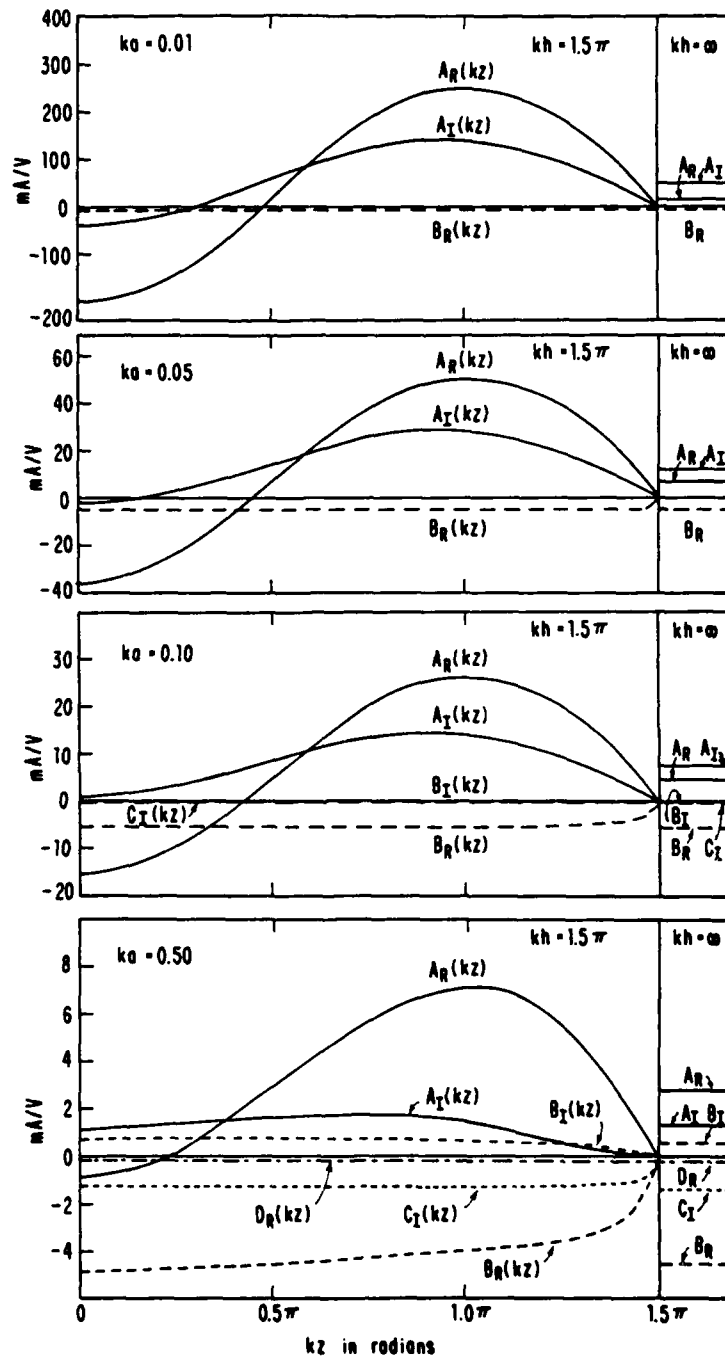


Figure 3. The Complex Fourier Coefficients of the Axial Surface Density of Current  $K_z(\theta, z) = A(kz) + B(kz)\cos \theta + C(kz)\cos 2\theta + D(kz)\cos 3\theta$ .

Similarly, for Eq. (15),

$$ka \leq 0.1: K_z(\theta, z) \doteq [A + A_r \cos kh + B_r \cos \theta]e(kz) + A_r(\cos kz - \cos kh) \quad (18)$$

These formulas are valid when  $kh \geq \pi/2$ . The range  $kh \leq \pi/2$  is discussed in the next section. The amplitudes of the resonant parts of the coefficients are defined as follows:  $A_r = (1/2)[A(0) - A(\pi)]$ ,  $B_r = (1/2)[B(0) - B(\pi)]$ .

In Reference 5 and Fig. 4 are shown Fourier coefficients  $A_r(kz)$ ,  $A_I(kz)$  and  $B_r(kz)$  for long resonant and antiresonant tubes with  $ka = 0.01$  and, respectively, with  $kh = 3.5\pi$  and  $kh = 3\pi$ . Also shown are  $A_r$ ,  $A_I$  and  $B_r$  for  $kh = \infty$ .

Graphs of  $|K_z(\theta, z)|$  and  $|cn(\theta, z)|$  as functions of  $kz$  as computed from Eqs. (9) and (13) for  $\theta = 0^\circ$  (shadow) and  $\theta = 180^\circ$  (illuminated side) are shown in Ref. [5] and in Fig. 5 for  $ka = 0.01$  with  $kh = 3.5\pi$  at the top,  $kh = 3\pi$  at the bottom. When  $kh = 3.5\pi$ ,  $K_z(\theta, z)$  has the axial distribution characteristic of a cylinder in a normally incident, E-polarized field at a resonant length as described in Reference 7. The maxima are alternately larger and smaller for the current and almost constant for the charge. Even with  $ka$  as small as 0.01, the current on the illuminated side is not consistently greater in magnitude than in the shadow as when  $kh = \infty$  (Fig. 2). Actually, the amplitude is higher on the illuminated side than in the shadow only with the larger maxima centered at  $kz = \pi$  and  $3\pi$ , lower with the smaller maxima centered at 0 and  $2\pi$ . The reason for this behavior is obvious from the Fourier components in Fig. 4 where, at the top,  $B_r \cos 180^\circ$  is added to  $A_r(kz)$  along the extremes centered at  $kz = \pi$  and  $3\pi$  and is subtracted from  $A_r(kz)$  along the peaks centered at  $kz = 0$  and  $2\pi$ . Since the current that varies as  $e(kz)$  contributes nothing to the charge except in a short range of length  $d \sim a$  near the open end, the charge density is practically rotationally symmetric everywhere outside this range.

The graphs of  $|K_z(\theta, z)|$  and  $|cn(\theta, z)|$  when  $kh = 3\pi$  are at the bottom of Fig. 5. They show that near axial antiresonance  $|K_z(180^\circ, z)| > |K_z(0^\circ, z)|$  for all values of  $z$ . This follows from the Fourier components in the lower portion of Fig. 4. Since the oscillations in  $A_r(kz)$  and  $A_I(kz)$  are not large enough to become negative, the component  $B_r \cos \theta$  always combines with  $A_r(kz)$  to increase it when  $\theta = 180^\circ$  and decrease it when  $\theta = 0^\circ$ .

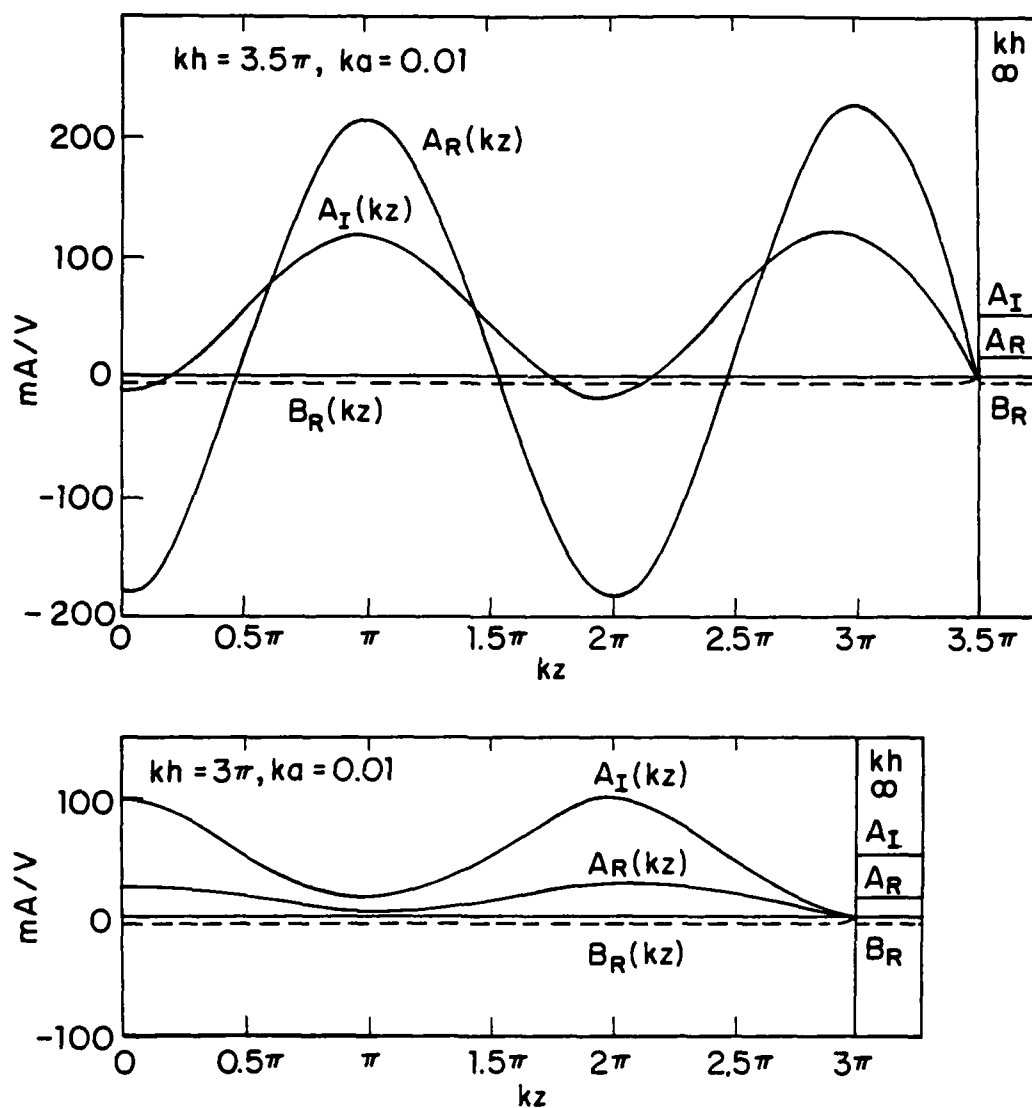


Figure 4. Fourier Coefficients in  $K_z(\theta, z) = A(kz) + B(kz)\cos \theta$  for Tubular Cylinder in an E-Polarized Field.  $A(kz) = A_R(kz) + i A_I(kz)$ ,  $B(kz) = B_R(kz) + i B_I(kz)$ .



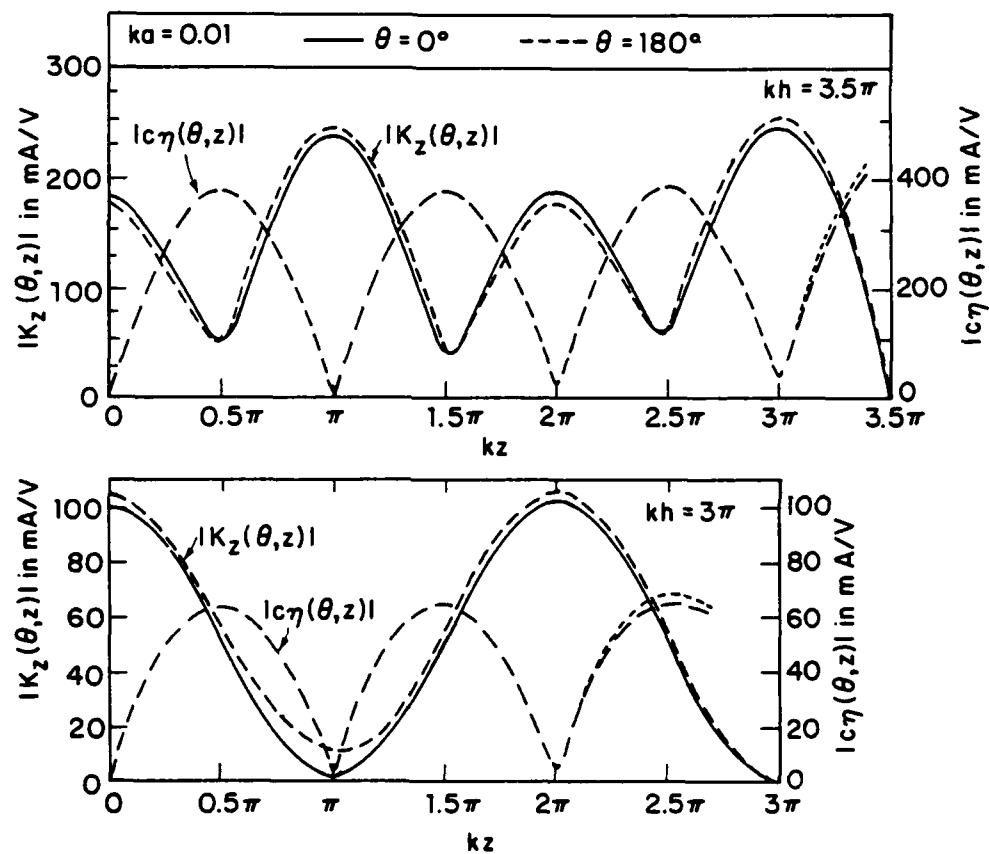


Figure 5. Axial Distributions of  $|K_z(\theta, z)|$  and  $|c\eta(\theta, z)|$  on Tubular Cylinder; E-Polarization.

The transverse distributions of  $|K_z(\theta, z)|$  as a function of  $\theta$  at selected values of  $kz$  are shown in Reference 5 and in Fig. 6 for  $kh = 3.5\pi$  and  $kh = \infty$  with  $ka = 0.01, 0.05, 0.1$ , and  $0.5$  and in Fig. 7 for  $kh = 3\pi$  and  $kh = \infty$  with  $ka = 0.01$ . It is seen in Fig. 6 that for all values of  $ka$  the transverse distributions at  $kz = \pi$  and  $3\pi$  are comparable and increase from  $\theta = 0^\circ$  to  $\theta = 180^\circ$ . For  $kz = 0$  and  $2\pi$  the amplitude decreases as  $\theta$  is increased from zero to reach a minimum at  $\theta = 180^\circ$  for  $ka = 0.01, 0.05$ , and  $0.1$ , at  $\theta = 110^\circ$  for  $ka = 0.5$ . In this last case the relative maximum at  $\theta = 180^\circ$  is smaller than the maximum at  $\theta = 0^\circ$ . At  $kz = \pi/2, 3\pi/2$ , and  $5\pi/2$ , the curves are all similar and show an increasing amplitude from  $\theta = 0^\circ$  to  $\theta = 180^\circ$ . The graph for  $kz = \pi/2, kh = 3.5\pi$ , is almost identical with that for all values of  $kz$  when  $kh = \infty$ . This follows from the fact that the resonant part of the current when  $kh = 3.5\pi$ , viz.,  $\cos kz$ , is zero at  $kz = \pi/2$  and the forced parts are essentially the same on the finite and infinite cylinders except very near the end. In Fig. 7 for  $kh = 3\pi$ , all transverse distributions increase from  $\theta = 0^\circ$  to  $\theta = 180^\circ$ . Those at  $kz = \pi/2, 3\pi/2$ , and  $5\pi/2$  again closely resemble the curve for  $kh = \infty$ .

Axial distributions like those at the top in Fig. 5 for  $kh = 3.5\pi, ka = 0.01$ , and the associated transverse distributions in Fig. 6 are given in Reference 5 and Figs. 8 and 9 for  $kh = 1.5\pi$  - also a resonant length. In addition to graphs for  $ka = 0.01$ , distributions are given for  $ka = 0.05, 0.1$ , and  $0.5$ . These show the growing separation between curves for  $\theta = 0^\circ$  and  $\theta = 180^\circ$  as  $ka$  is increased and serve to emphasize the fact that the transverse distribution of the axial current density  $K_z(\theta, z)$  induced in a conductor of finite length by a normally incident, E-polarized plane wave depends not only on the value of  $ka$  but also on  $kh$  and the location  $kz$  in the standing-wave pattern along the conductor. It differs considerably from the transverse distribution in an infinitely long conductor at all but a few points. The charge distribution is generally rotationally symmetric for  $ka \leq 0.1$  except within short distances of the open end where it is very far from rotationally symmetric even on very thin cylinders. Complete analytical solutions for the axial distributions of the rotationally symmetric current  $I_z(z) = 2\pi a[K_z(z)]_0$  and charge per unit length  $q(z) = 2\pi a[\eta(z)]_0$  for electrically thin and long cylinders have been derived by Chen and Wu in Reference 8 for a normally incident, E-polarized incident field and by Chen in Reference 9 for an arbitrarily

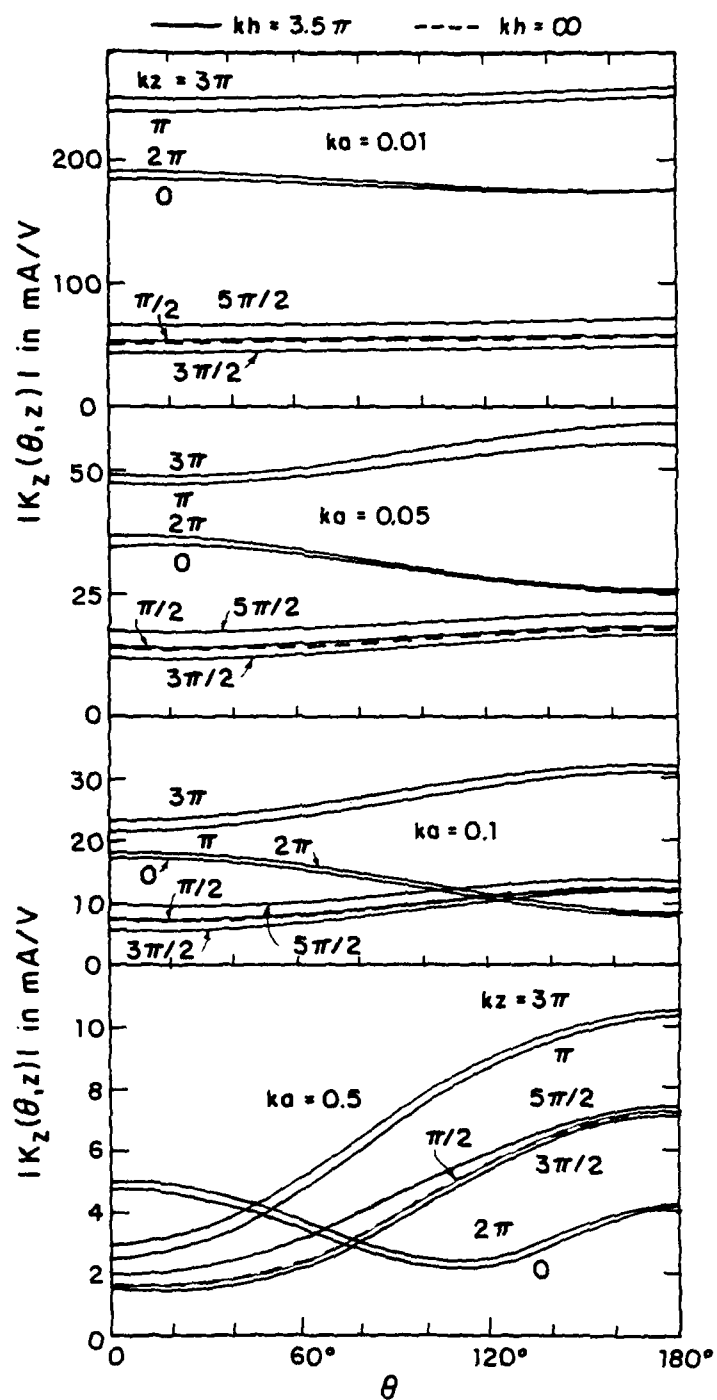


Figure 6. Magnitude of Axial Component of Surface Density of Current on Tubular Cylinder in E-Polarized Field.

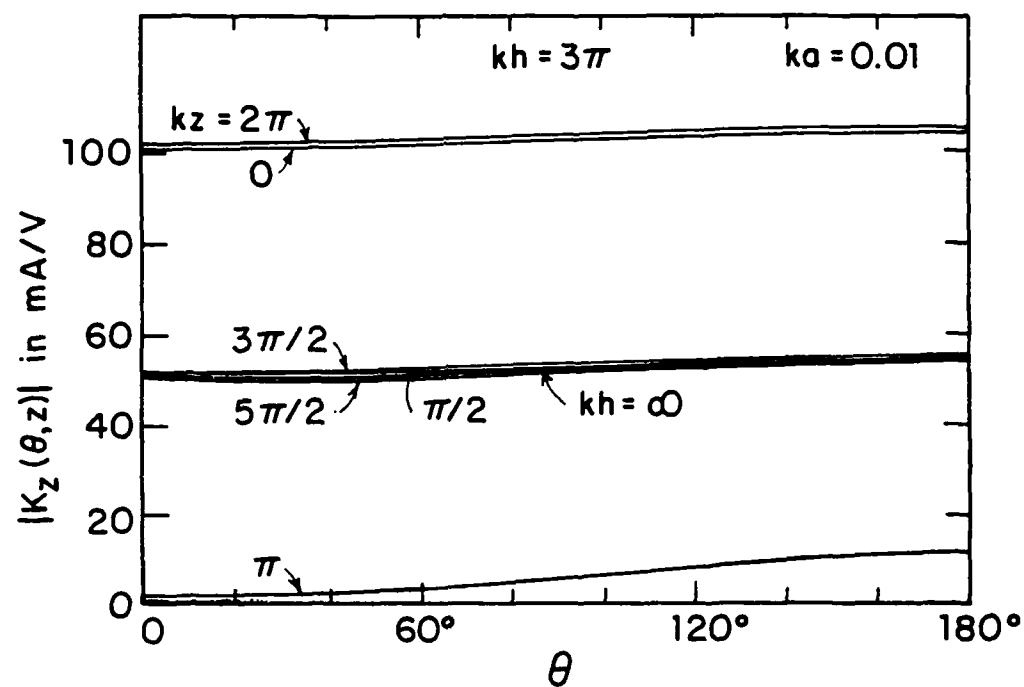


Figure 7. Magnitude of Axial Component of Surface Density of Current on Tubular Cylinder in E-Polarized Field.

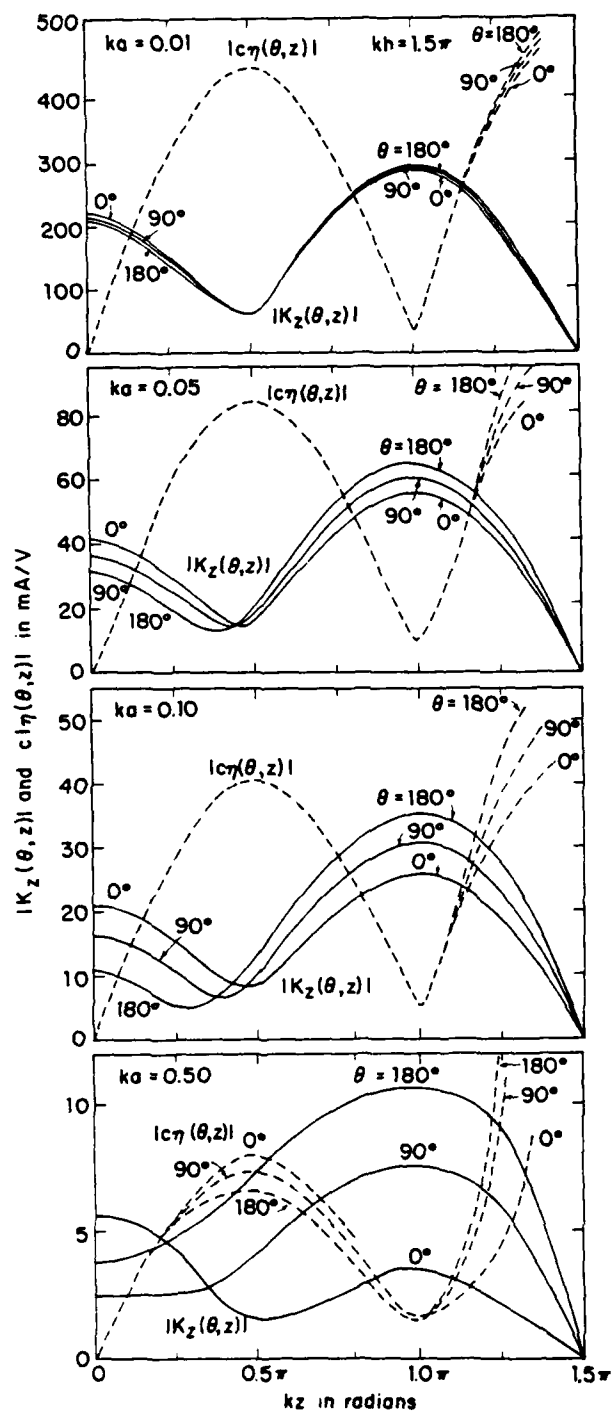


Figure 8. Magnitudes of Surface Densities of Charge and Axial Current on Tubular Cylinder with E-Polarization.

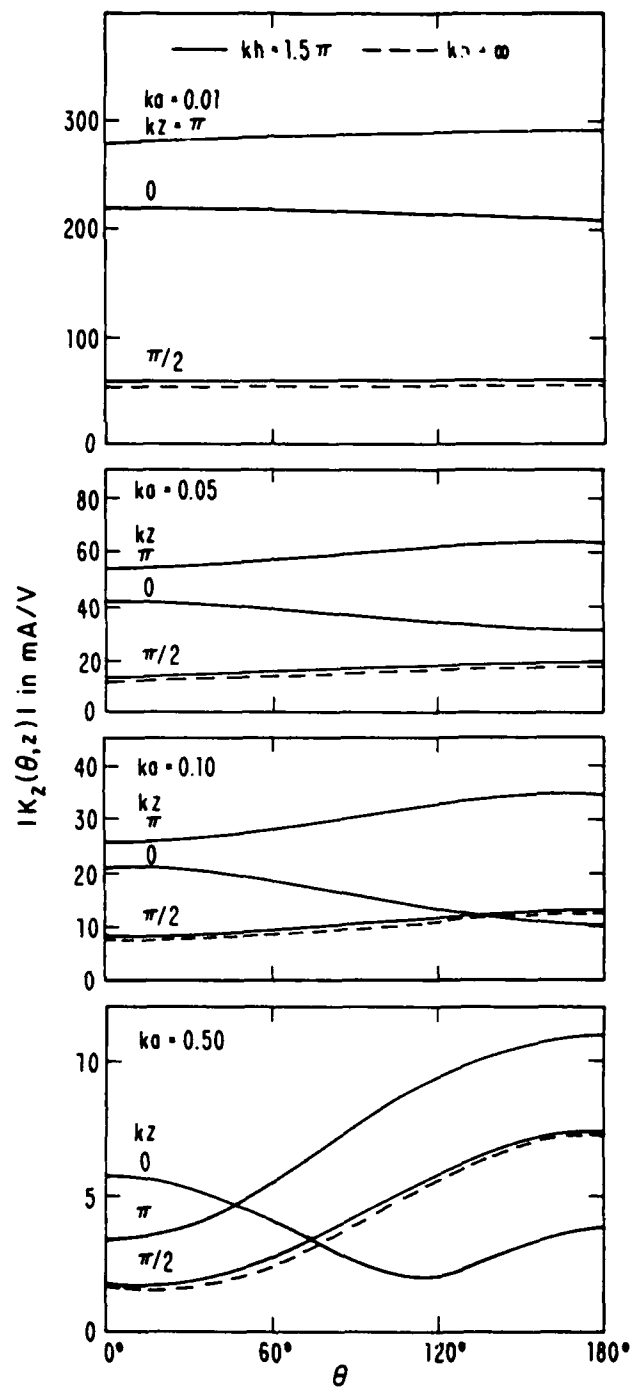


Figure 9. Transverse Distribution of  $|K_z(\theta, z)|$ .

incident field. Graphs of the corresponding numerically calculated currents  $I(z)$  are shown by Harrington in Reference 10. A complete theory for thin cylinders that are not too long in an arbitrarily incident field has been derived by King in References 11 and 12.

The transverse component of current  $K_\theta(\theta, z)$  is very small except within distances  $d \sim a$  of the open end where it rises steeply to large values. Its transverse distribution is proportional to  $\sin \theta$ .

## 2. H-POLARIZATION

The component of surface current  $K_\theta(\theta, x)$  on tubes of finite length differs little from  $K_\theta(\theta)$  for  $kx = \infty$  except within distances  $d \sim a$  of an open end where it rises steeply. For each value of  $ka$ , the Fourier coefficients given in table 1 are good approximations for cylinders of finite length for all values of  $|kx| \leq k(h-d)$  where  $d \sim a$ .

## SECTION IV

### THE ELECTRICALLY SHORT AND THIN CYLINDER: $ka < kh \leq 1$ (BASED ON REFERENCE 5)

#### 1. E-POLARIZATION

The current densities  $K_z(\theta)$  and  $K_z(\theta, z)$  induced in tubular cylinders, respectively, with infinite and finite lengths are well approximated by  $K_z(\theta) \doteq A + B_R \cos \theta$  when  $kh = \infty$  and by  $K_z(\theta, z) \doteq A(kz) + B_R(kz) \cos \theta$  when  $kh$  is finite provided  $ka \leq 0.1$ . The coefficient  $A = A_R + iA_I$  and, so long as  $kh > 1$ , also the coefficient  $A(kz) = A_R(kz) + iA_I(kz)$  increase in magnitude with decreasing  $ka$ . On the other hand,  $B_R$  and  $B_R(kz)$  remain constant and all higher-order coefficients decrease when  $ka$  is reduced. As can be inferred from Figs. 3 and 4,  $A_R(kz)$  and  $A_I(kz)$  oscillate, respectively, about  $A_R$  and  $A_I$  when  $\pi/2 \leq kh < \infty$ . Their amplitudes for each value of  $ka$  are greatest when  $kh$  is at a resonant length, smallest when  $kh$  is at an antiresonant length. When  $kh$  is reduced below the first resonance near  $kh = \pi/2$ , both  $A_R(kz)$  and  $A_I(kz)$  approach zero as  $kh \rightarrow 0$ . This behavior is illustrated in Reference 5 and Fig. 10 at  $kz = 0$  for cylinders with  $ka = 0.01$  and  $0.05$ .  $A_R(0)$ ,  $A_I(0)$ ,  $B_R(0)$  and  $C_I(0)$  are all shown as functions of  $kh$ . It is seen that  $A_I(0)$  dominates when  $kh > 1$ , but decreases rapidly when  $kh$  is reduced so that it becomes equal to  $B_R(0)$  at  $kh = 0.166\pi$  for  $ka = 0.05$  and at  $kh = 0.1\pi$  when  $ka = 0.01$ . When  $kh$  is decreased below these values,  $B_R(0)$  exceeds  $A_I(0)$  and actually dominates when  $kh < 0.06\pi$  with  $ka = 0.05$  or  $kh < 0.04\pi$  when  $ka = 0.01$ . Thus, the current that is very nearly rotationally symmetric when  $ka = 0.01$  and  $kh > 1$  becomes equal and opposite on the illuminated and shadowed sides of the cylinder when  $ka = 0.01$  and  $kh$  is sufficiently small. The three significant Fourier coefficients  $A_R(kz)$ ,  $A_I(kz)$ , and  $B_R(kz)$  are shown in Fig. 11a for  $ka = 0.05$  and in Fig. 11b for  $ka = 0.01$  as functions of  $z/h$  with  $kh$  as the parameter. When  $kh \leq \pi/2$ , the axial distributions have the approximate form

$$A(kz) \doteq A(0) \frac{\cos kz - \cos kh}{1 - \cos kh} \quad ; \quad B_R(kz) \doteq B_R e(kz) \quad (19)$$

where  $A(0) = A + A_I$  and  $A_I$  is the complex amplitude of the oscillatory part of the current. Note the rapid decrease in  $A(kz)$  as  $kh$  is reduced with con-



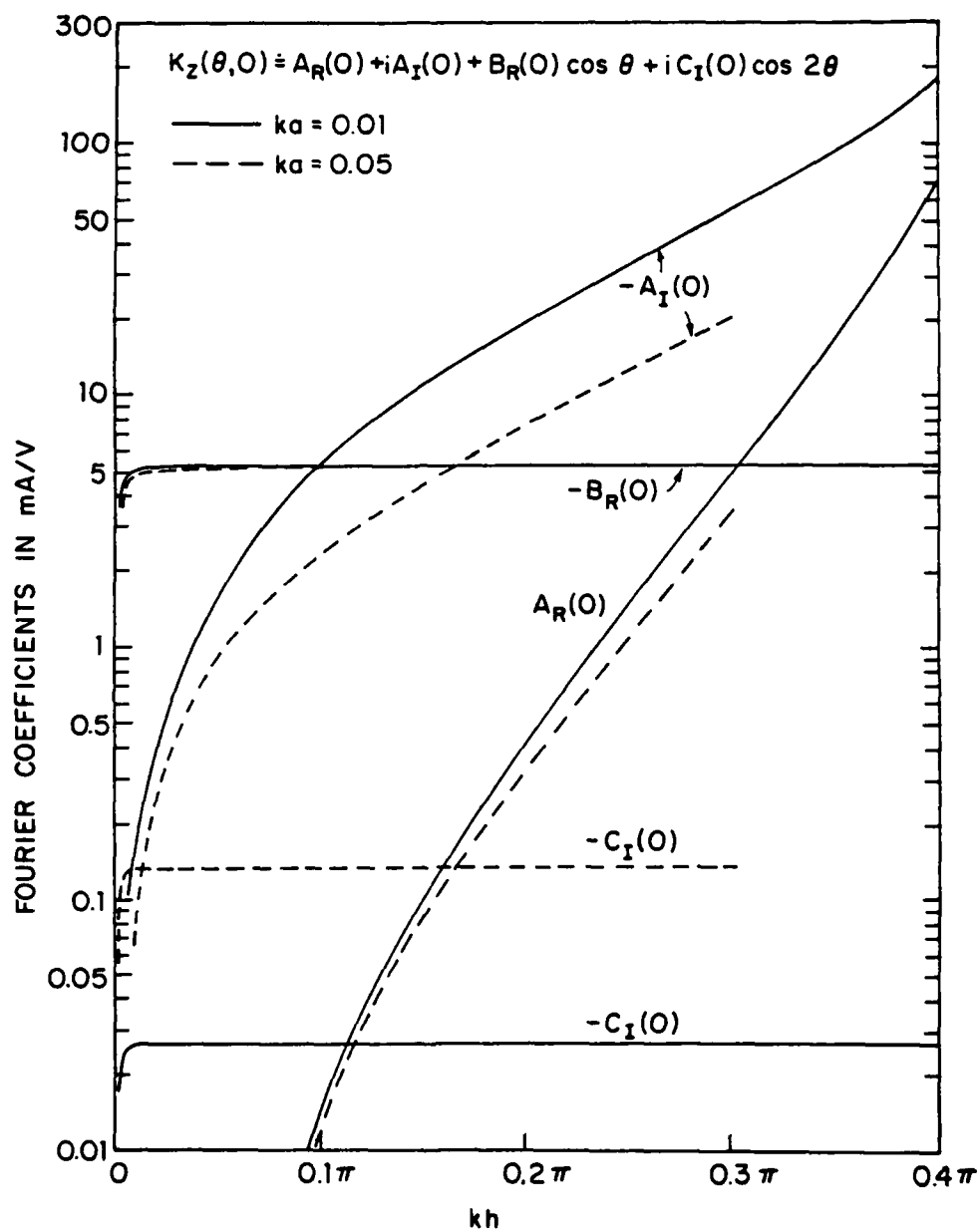


Figure 10. Fourier Coefficients of Surface Density of Axial Current on Tubular Cylinder; E-Polarization.

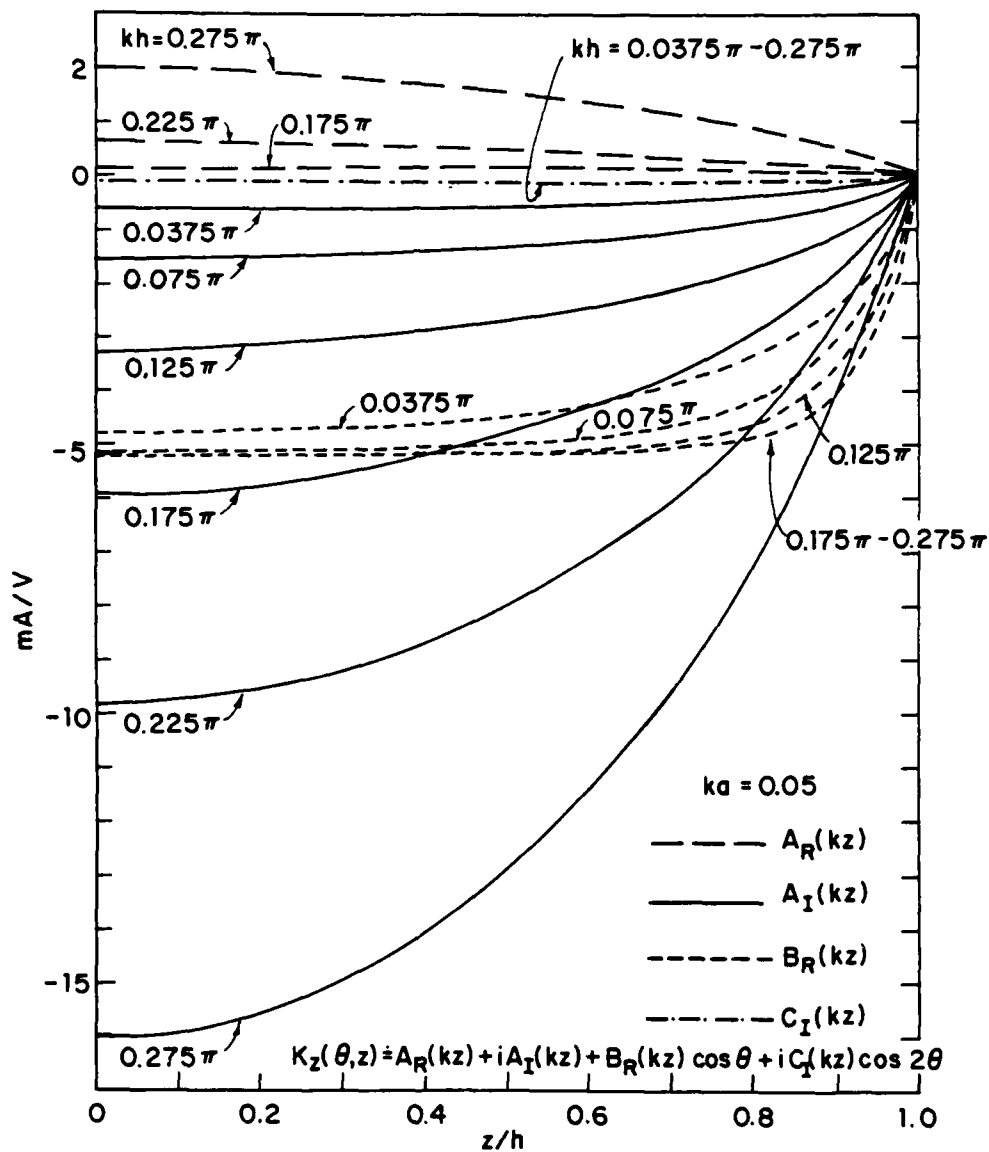


Figure 11a. Fourier Coefficients of Surface Density of Axial Current on Tubular Cylinder; E-Polarization.

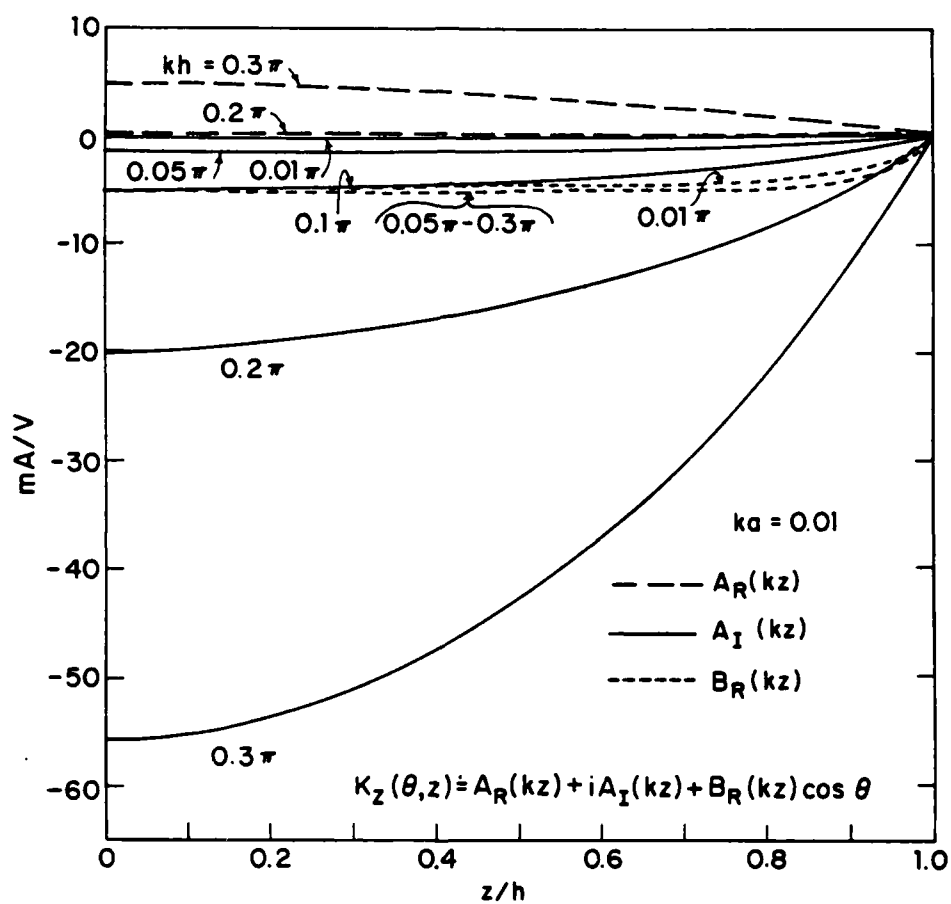


Figure 11b. Fourier Coefficients of Surface Density of Axial Current on Tubular Cylinder; E-Polarization.

stant  $ka$  and the almost complete constancy of the first-order term  $B_R(kz)$  and of the second-order term  $C_I(kz)$ , which is negligibly small.

The axial distribution of the magnitude and phase of the surface density of current on the illuminated side, viz.,  $K_z(180^\circ, z) = A(kz) - B_R(kz)$  is shown as a function of  $kz$  in Reference 5 and in Fig. 12a for  $ka = 0.05$  and Fig. 12b for  $ka = 0.01$ . The total current (sum of outside and inside currents), the outside current and the inside current are shown. Since the latter decreases rapidly inward from the open end, the total and outside currents differ significantly only quite near the open end. The associated transverse distributions at  $z = 0$ , viz.,  $K_z(\theta, 0)$  as a function of  $\theta$  are in Fig. 13a for  $ka = 0.05$  and in Fig. 13b for  $ka = 0.01$ . Note that when  $kh = 0.275\pi$  or  $0.3\pi$ , the amplitude  $|K_z(\theta, z)|$  and the phase angle  $\theta_z$  are both quite constant around the cylinder. As  $kh$  is reduced in steps to  $kh = 0.0375\pi$  with  $ka = 0.05$  or  $kh = 0.01\pi$  with  $ka = 0.01$ ,  $|K_z(\theta, z)|$  develops an increasingly deep minimum at  $\theta = 90^\circ$  and a phase change approaching  $180^\circ$  from the illuminated side ( $\theta = 180^\circ$ ) to the shadowed side ( $\theta = 0^\circ$ ). When  $kh = 0.275\pi$  or  $0.3\pi$ , the zero-order rotationally symmetric component  $A(kz)$  dominates, when  $kh = 0.0375\pi$  or  $0.01\pi$ , the first-order term  $B_R(kz)\cos \theta$  dominates. As  $kz$  approaches  $kh$ , the amplitude of the current decreases but the dip at  $\theta = 90^\circ$  is relatively even deeper.

The multiple reflection of the rotationally symmetric, zero-order current at an open end to generate the standing-wave distribution  $[K_z(z)]_0 = A(kz)$  involves only axially directed currents and charges  $[n(z)]_0$  that are independent of  $\theta$ . The reflection of the higher-order currents is quite different in that it involves not only axial currents like  $[K_z(\theta, z)]_1 = B(kz) \times \cos \theta$  that are not rotationally symmetric, but also transverse currents  $K_\theta(\theta, z)$  that are large particularly within short distances  $d \sim a$  of the end. Actually, what is an open end for the rotationally symmetric zero-order current is effectively a somewhat extended short-circuited end for the two conductor, transmission-line-like first-order current. The transverse current  $K_\theta(\theta, z)$  on an electrically thin cylinder is given by

$$K_\theta(\theta, z) \doteq -B'_1(kz)\sin \theta \quad (20)$$

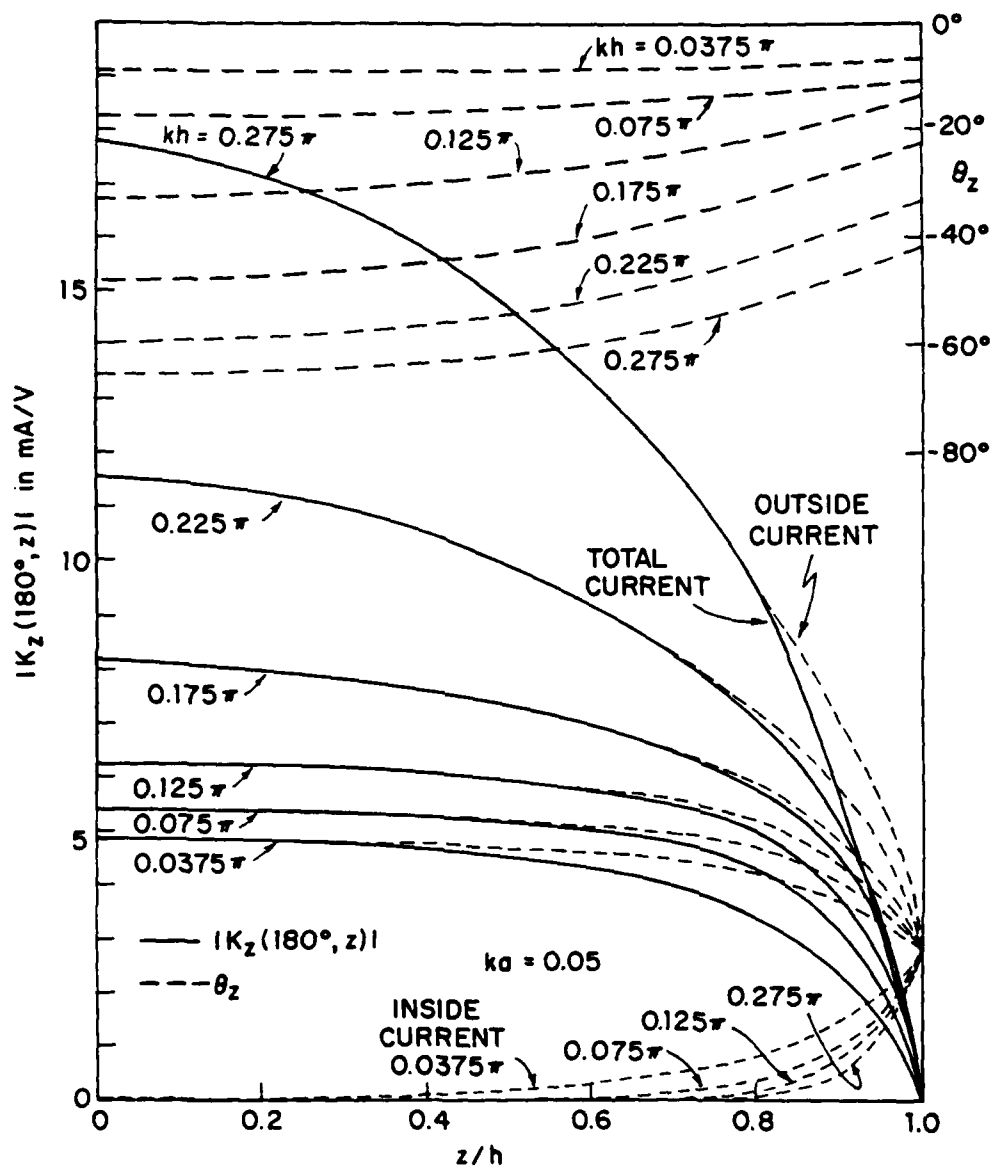


Figure 12a. Surface Density of Axial Current on Tubular Cylinder; E-Polarization.

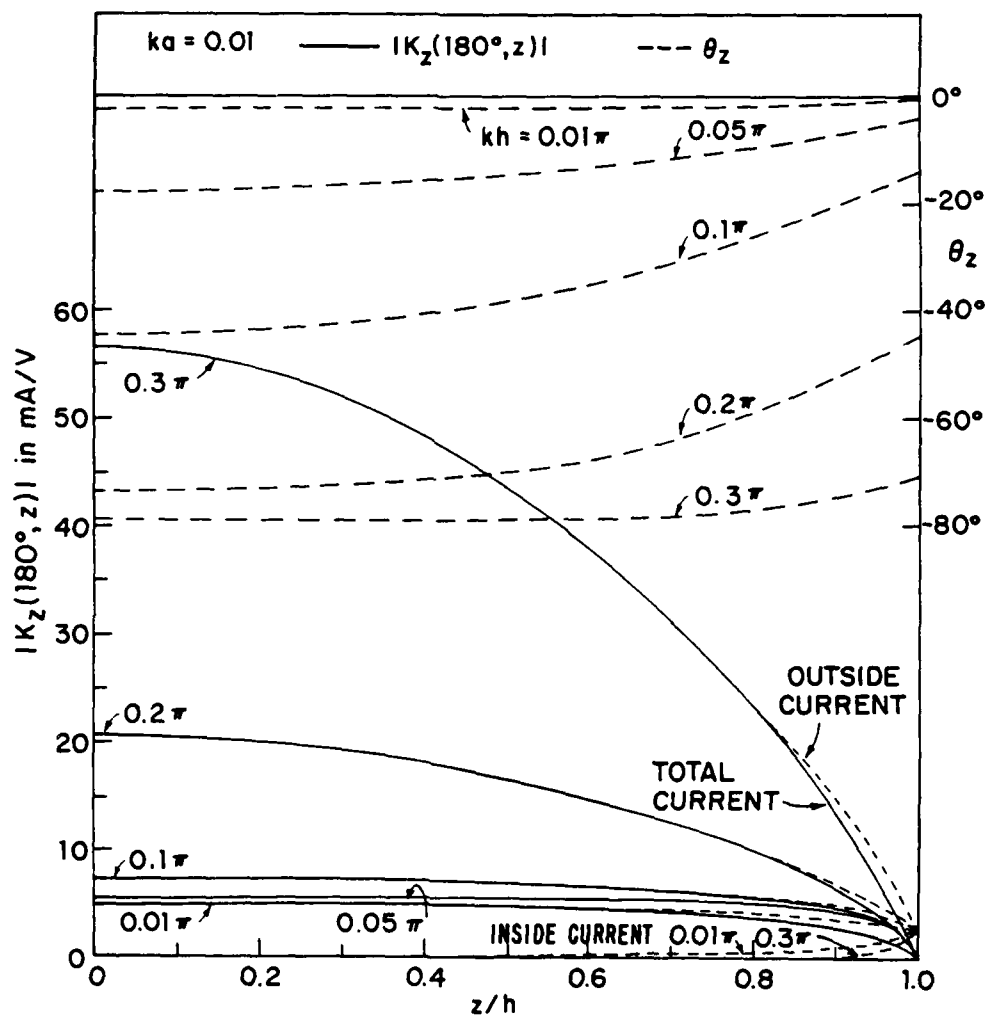


Figure 12b. Surface Density of Axial Current on Tubular Cylinder; E-Polarization.

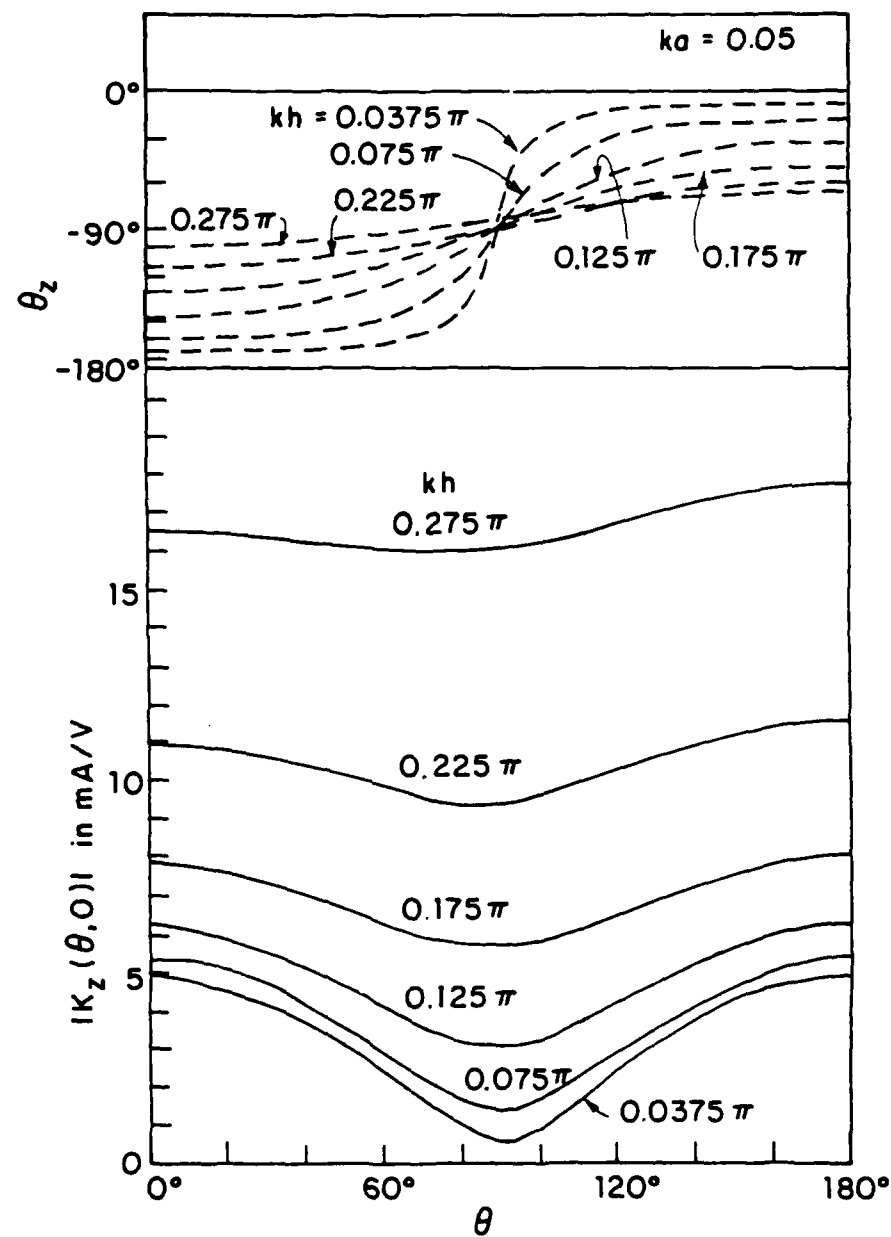


Figure 13a. Transverse Distribution of Surface Density of Axial Current on Tubular Cylinder; E-Polarization.

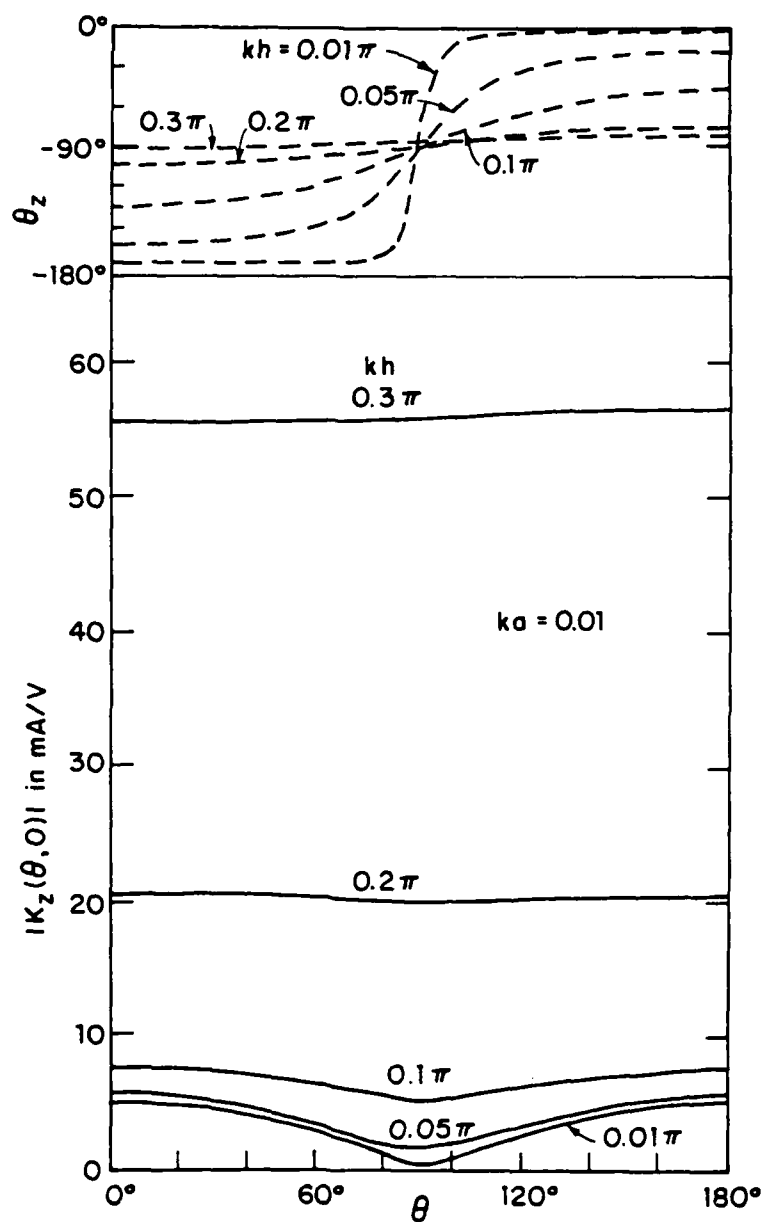


Figure 13b. Transverse Distribution of Surface Density of Axial Current on Tubular Cylinder; E-Polarization.



The real function  $B_I'(kz)$  is shown on a logarithmic scale in Figs. 14a and 14b, respectively, for  $ka = 0.05$  and  $0.01$  as a function of  $z/h$  with  $kh$  as the parameter.  $K_\theta(\theta, z)$  is quite small everywhere except near the open end where it rises steeply to values comparable to those of the associated axial component,  $K_z(\theta, z) \doteq B_R(kz) \cos \theta$ . In effect, the axial current approaches the open end on the illuminated half of the cylinder ( $90^\circ < \theta < 270^\circ$ ), circulates around the cylinder as a transverse current with maxima at  $\theta = 90^\circ, 270^\circ$  near the end, and then continues as an oppositely directed axial current on the shadowed side ( $-90^\circ < \theta < 90^\circ$ ). The transverse current is associated with a rotationally asymmetrical distribution of charge.

Graphs of the magnitude  $|cn(\theta, z)|$  as a function of  $z/h$  are displayed in Reference 5 and in Fig. 15a for  $ka = 0.05$  and Fig. 15b for  $ka = 0.01$ . These show that the charge density rises steeply to a high value at the open end. The transverse distributions of  $|cn(\theta, z)|$ , respectively at  $z/h = 0.2$  and  $0.8$ , as functions of  $\theta$  with  $kh$  as the parameter are in Fig. 16a for  $ka = 0.05$  and in Fig. 16b for  $ka = 0.01$ . The associated phase angles  $\theta_n$  are in Figs. 17a and 17b. It is seen that when  $kh = 0.35\pi$  for  $ka = 0.05$  or  $0.4\pi$  for  $ka = 0.01$ ,  $|cn(\theta, z)|$  is almost rotationally symmetric since the term  $A(kz)$  dominates. On the other hand, when  $kh = 0.0375\pi$  for  $ka = 0.05$  or  $0.01\pi$  for  $ka = 0.01$ ,  $|cn(\theta, z)|$  develops a deep minimum at  $\theta = 90^\circ$  and its phase changes from the illuminated half into the shadowed half by nearly  $180^\circ$ . The entire effect is much more pronounced near the open end at  $z/h = 0.8$  (where the charge density and transverse current are large) than near the center at  $z/h = 0.2$  (where the charge density and the transverse current are very small). Note that when the cylinder is sufficiently short, nearly equal charge densities of opposite sign occur near  $\theta = 0^\circ$  and  $180^\circ$ ; these are associated with the transverse currents  $K_\theta(\theta, z) \sim \sin \theta$  that have maxima at  $\theta = 90^\circ$  and  $270^\circ$ .

## 2. H-POLARIZATION

When  $ka \leq 0.1$ , the surface densities of current induced in tubular cylinders are well approximated by  $K_\theta(\theta) = A_H + B_H \cos \theta$  when  $kh = \infty$  and by  $K_\theta(\theta, x) = A_H(kx) + B_H(kx) \cos \theta$  when  $kh$  is finite. Except within distances  $d \sim a$  of an open end, the coefficients are almost constant along the tube so that  $A_H(kx) \doteq A_H = -1/Z_0 = -2.65 \text{ mA/V}$ , which is independent of  $ka$  and  $kx$ , and  $B_H(kx) \doteq B_H = -i2ka/Z_0 = -15.3ka \text{ mA/V}$ . Specifically when  $ka =$

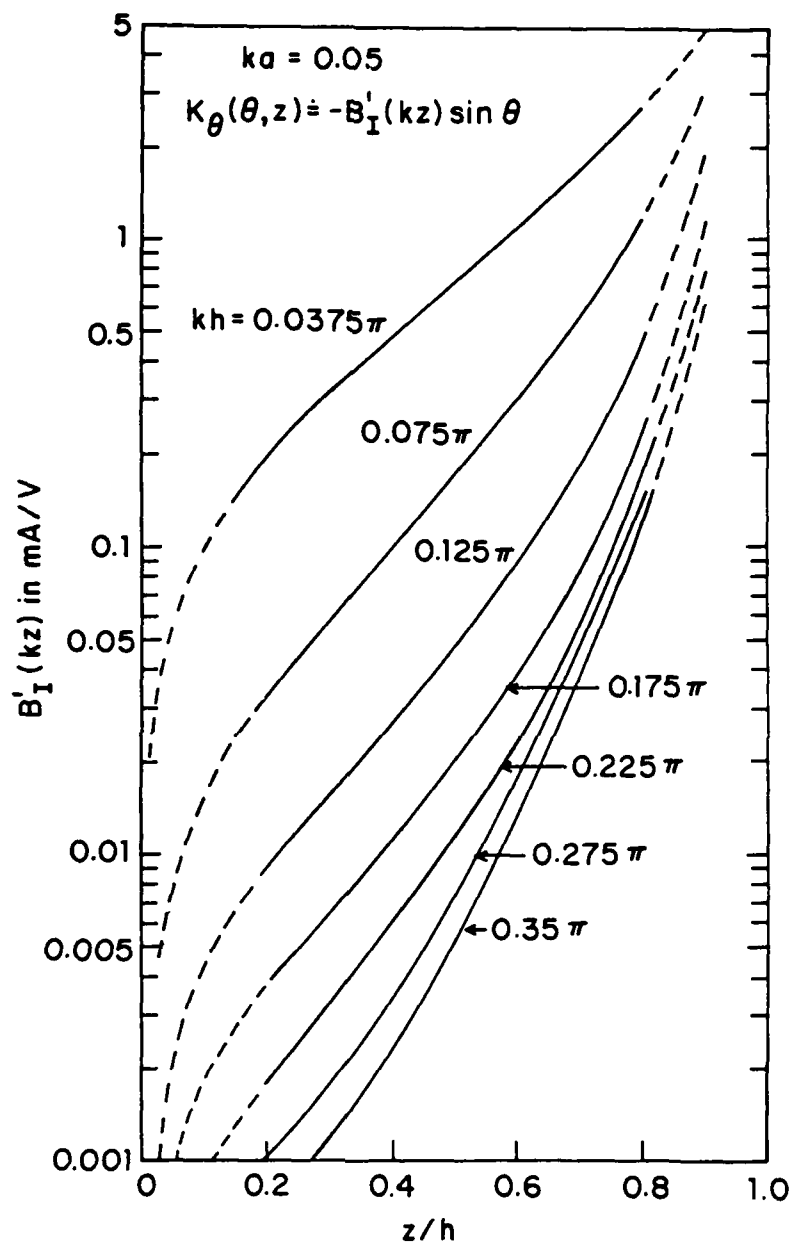


Figure 14a. Fourier Coefficient  $B'_I(kz)$  of Surface Density of Transverse Current on Tubular Cylinder; E-Polarization.

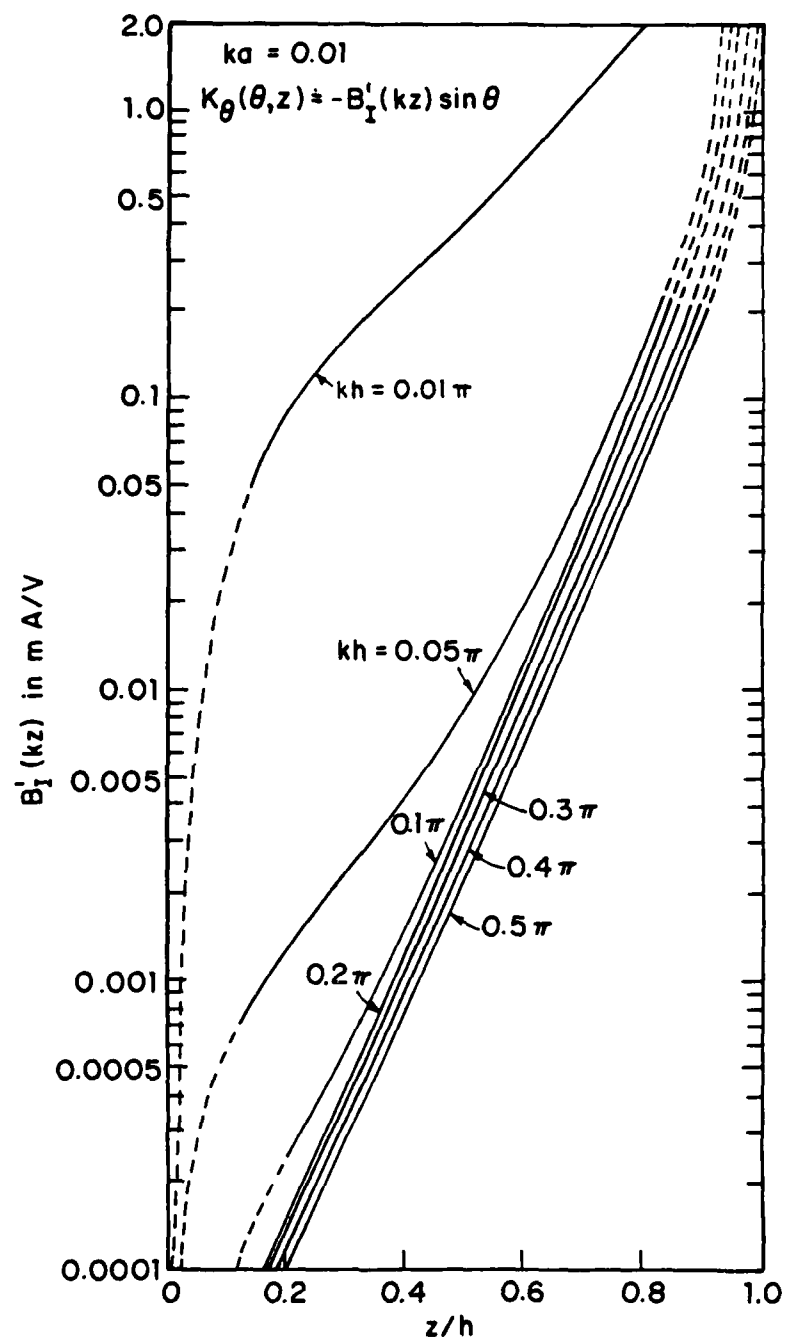


Figure 14b. Fourier Coefficient  $B_I'(kz)$  of Surface Density of Transverse Current on Tubular Cylinder; E-Polarization.

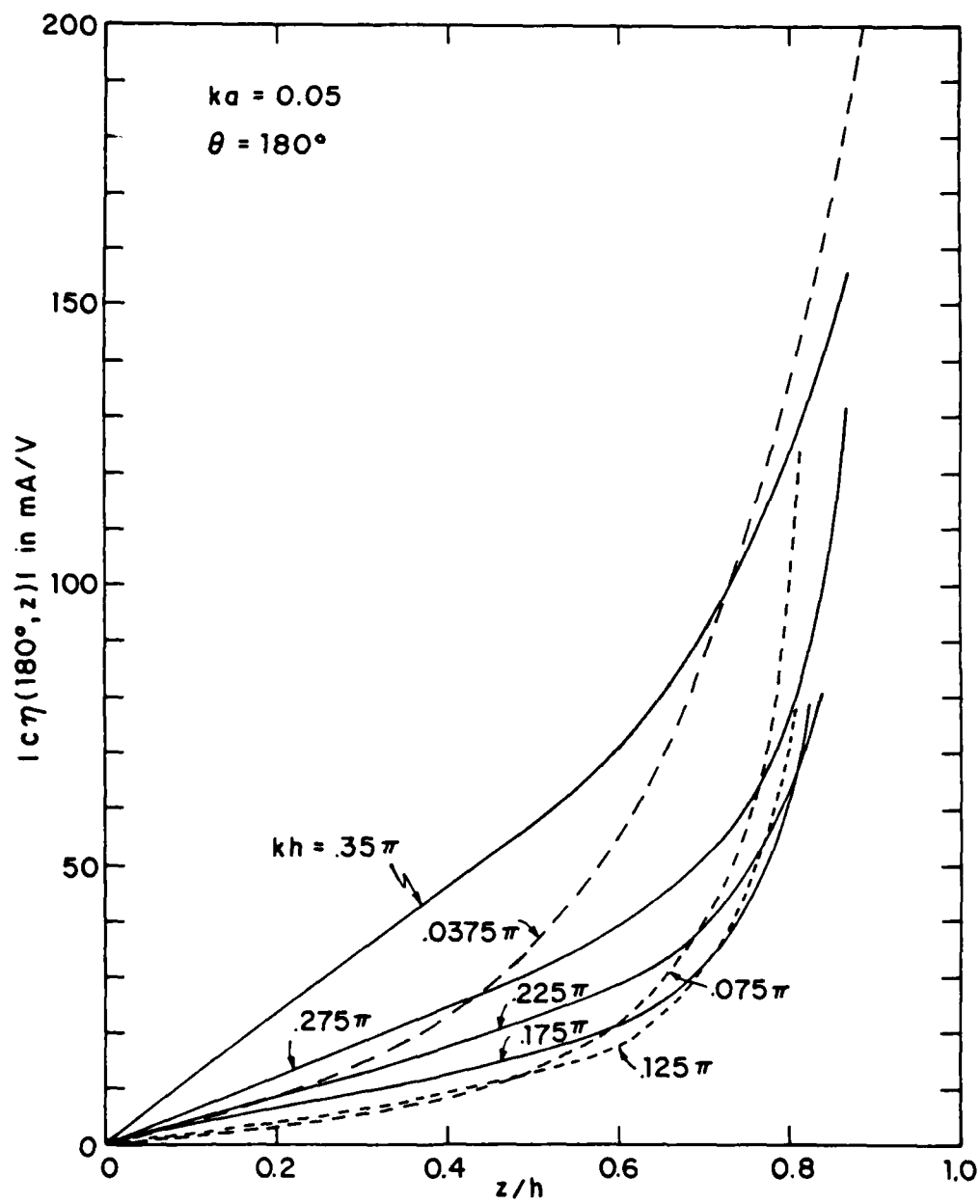


Figure 15a. Magnitude of Normalized Surface Density of Charge on Tubular Cylinder; E-Polarization.

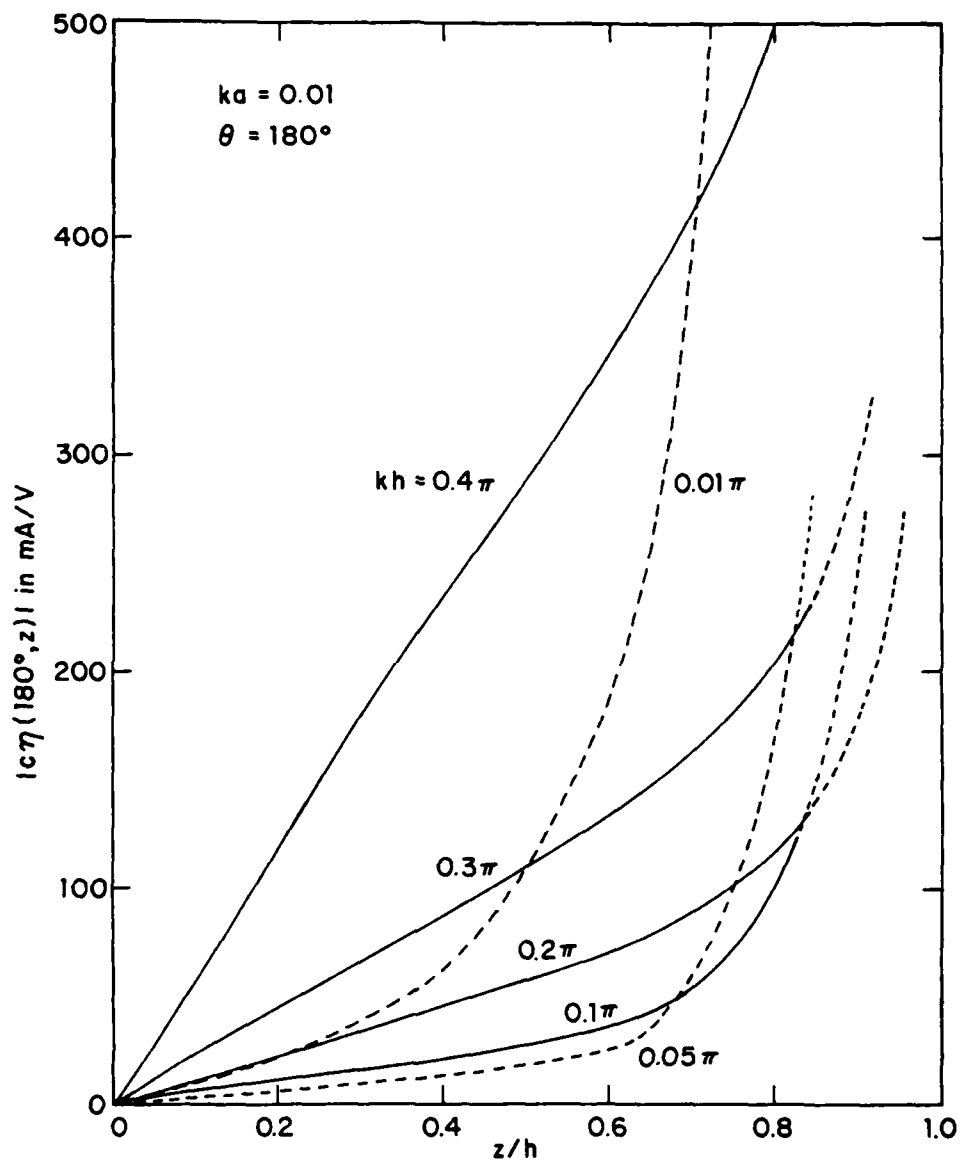


Figure 15b. Magnitude of Surface Density of Charge on Tubular Cylinder; E-Polarization.

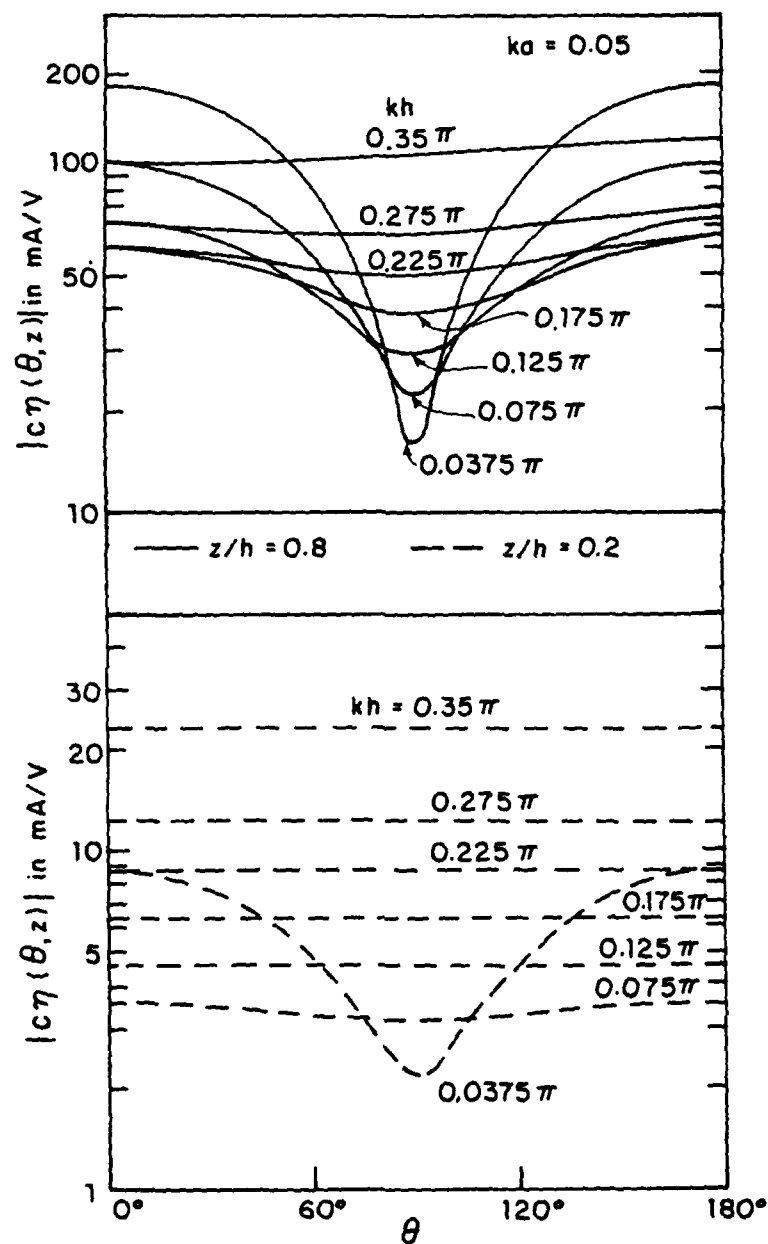


Figure 16a. Normalized Magnitude of Surface Density of Charge on Tubular Cylinder; E-Polarization.

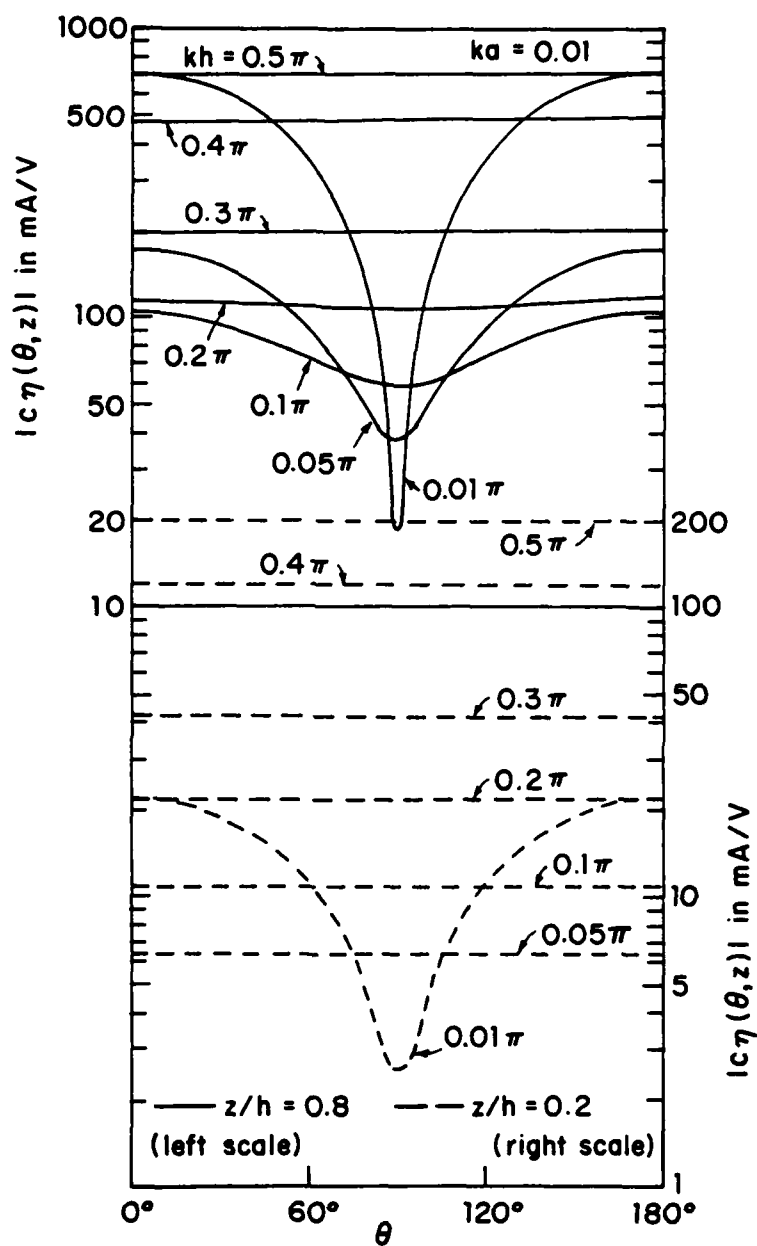


Figure 16b. Normalized Magnitude of Surface Density of Charge on Tubular Cylinder; E-Polarization.

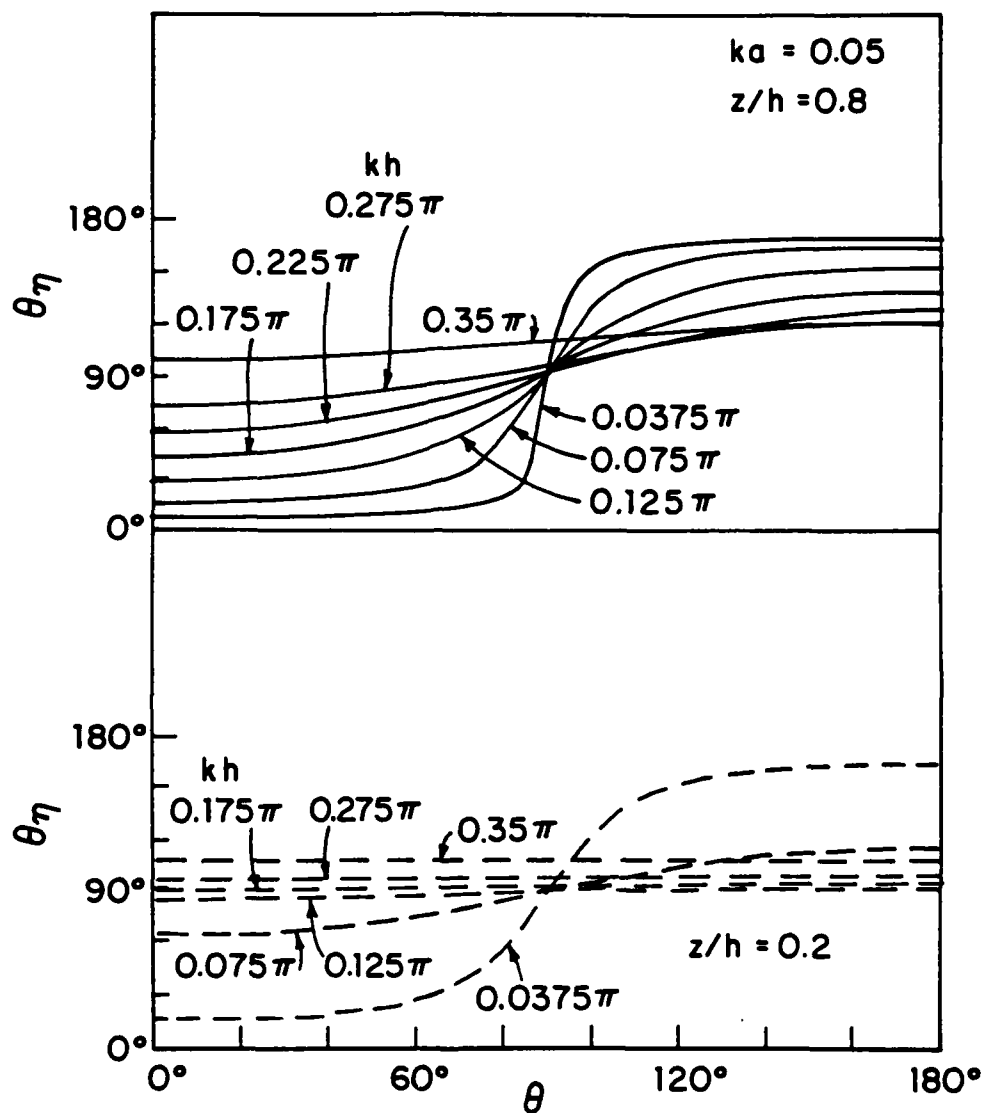


Figure 17a. Phase of Surface Density of Charge on Tubular Cylinder; E-Polarization.



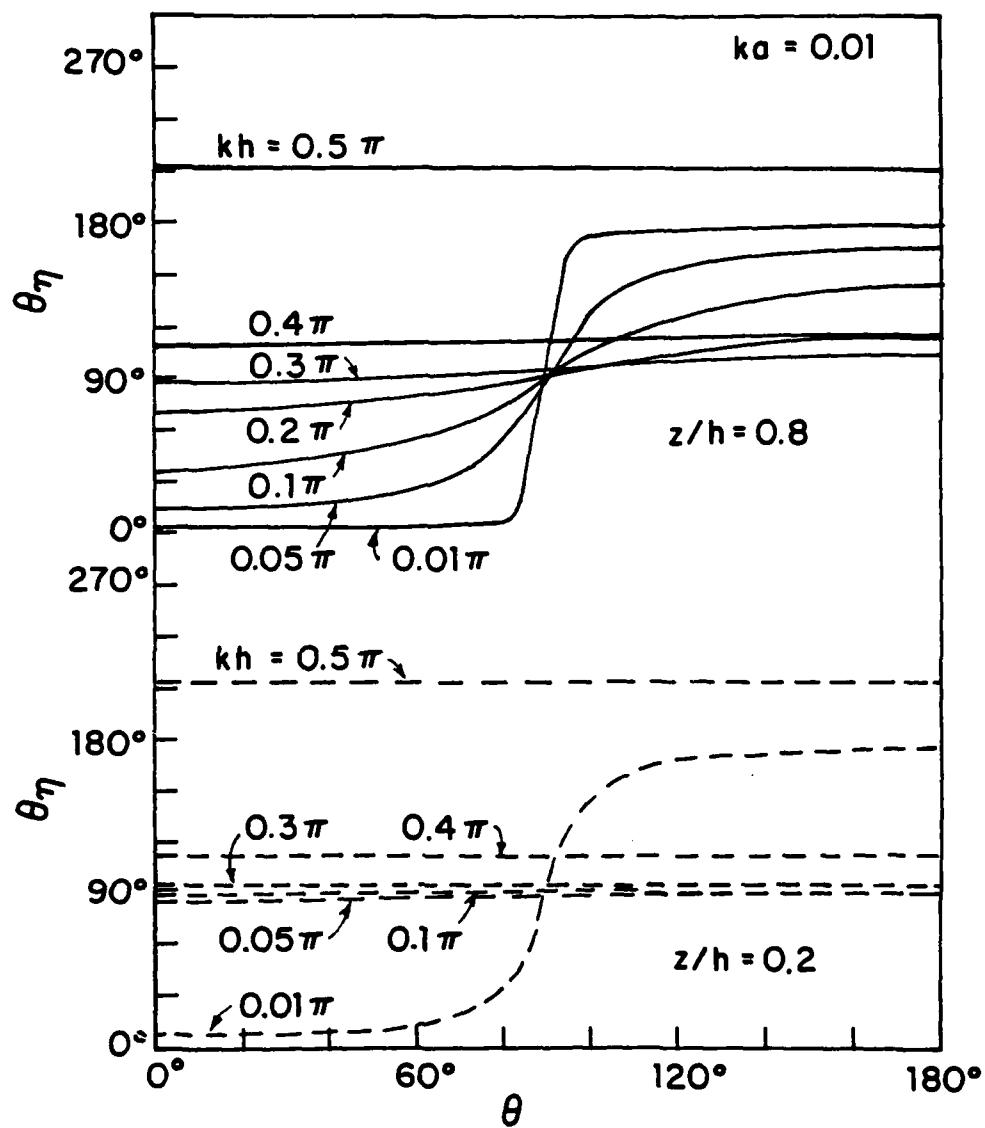


Figure 17b. Phase of Surface Density of Charge on Tubular Cylinder; E-Polarization.

0.01,  $B_H = -10.053$  mA/V; when  $ka = 0.05$ ,  $B_H = -10.265$  mA/V. When  $kh > 1$ ,  $A_H(kx)$  and  $B_H(kx)$  with H-polarization are small compared with  $A(kz)$  with E-polarization. However, when  $kh \leq 0.166\pi$  for  $ka = 0.05$  or  $kh \leq 0.1\pi$  for  $ka = 0.01$ ,  $A(kz)$  becomes smaller than  $B(kz) \doteq B_R = -2/Z_0 = -5.3$  mA/V which is comparable with  $A_H$ . The reason is simple.  $A_{HR} = -H_x^{(i)}$  is the circulating current  $K_\theta$  required to set up an axial magnetic field that cancels the incident axially directed magnetic field in the perfectly conducting tube. Similarly,  $B_R = -2H_x^{(i)}$  is the axial current  $K_z(\theta)$  required to cancel the incident transverse magnetic field  $H_x^{(i)}$  in the perfectly conducting cylinder along the  $z$ -axis. These are the components of current that are required in the absence of all resonances to satisfy the boundary conditions. When the conductors are sufficiently thin ( $ka \leq 0.1$ ) and short ( $kh < 1$ ), end-reflected and resonant currents are small compared with the currents required to cancel the incident magnetic field in the perfectly conducting tube.

The axial currents  $K_x(\theta, x)$  generated in a cylinder parallel to the incident magnetic field by reflections at the open ends are given by

$$K_x(\theta, x) \doteq iB_H'(kx)\sin \theta \quad (21)$$

When  $ka \leq 0.1$ ,  $|B_H'(kx)|$  is quite small compared with  $A_H(kx)$ . That is, the axial current density is small compared to the transverse current density in cylinders that are sufficiently thin and excited by an H-polarized field.

## SECTION V

### COMPARISON WITH MEASUREMENTS

Since the theory of Kao in Reference 1 involves no assumptions other than those implicit in the idealized model of a perfectly conducting cylinder with zero wall thickness — which is well approximated by a thin-walled metal tube — a comparison of theoretical results with measured ones serves primarily as a means of checking the accuracy of the experimental techniques and apparatus including especially probes. Extensive very satisfactory comparisons have been made and reported in References 3 and 4 on all aspects of the distributions in amplitude and phase of the current and charge densities on cylinders with  $ka = 1$  and electrical lengths between  $kh = 1.5\pi$  and  $3.5\pi$ . A similar but less extensive set of measurements with  $ka = 0.05$  and  $kh = 0.0375\pi, 0.075\pi$  and  $0.175\pi$  has been carried out. A sample given in Reference 5 is shown in Fig. 18 for the axial and transverse currents on a tube with  $ka = 0.05$  and  $kh = 0.175\pi$ . The graphs give the currents at cross sections quite close to the open end where the axial and transverse densities have comparable magnitudes and where the rotationally symmetric part of the axial current is substantially smaller than near the center. The measured graphs for  $|K_z(\theta, z)|$  are for the outside current which, as seen from Fig. 12a, has a significant relative magnitude at  $z = h$  when  $ka = 0.05$  and  $kh = 0.175\pi$ . The graphs in Fig. 18 indicate that in the approximate formula,  $K_z(\theta, z) \doteq A(kz) + B_R(kz)\cos \theta$ , the zero-order term  $A(kz)$  is smaller in magnitude than the first-order term  $B_R(kz) \times \cos \theta$ . This is evident from the deep minima at  $\theta = 90^\circ$  and  $270^\circ$  and the associated phase change of approximately  $180^\circ$ . The measured variation with  $\theta$  is consistent with that shown in Fig. 13a at  $z = 0$  where, however, the rotationally symmetric term is relatively more important than near the open end. The slow decrease of  $|K_z(\theta, z)|$  with  $z/h$  as the open end is approached agrees with Fig. 12a for the outside current.

The measured transverse current shown at the top in Fig. 18 is in excellent agreement with the approximate formula, Eq. (20), according to which  $K_\theta(\theta, z) \sim \sin \theta$ . Note that Figs. 12a and 14a indicate that close to the open end  $|K_\theta(\theta, z)|$  and the outside part of  $|K_z(\theta, z)|$  are comparable in magnitude. The very rapid increase in  $|K_\theta(\theta, z)|$  as the open end is approached is evident from the family of curves in Fig. 18 and consistent with the theoretical results shown in Fig. 14a.

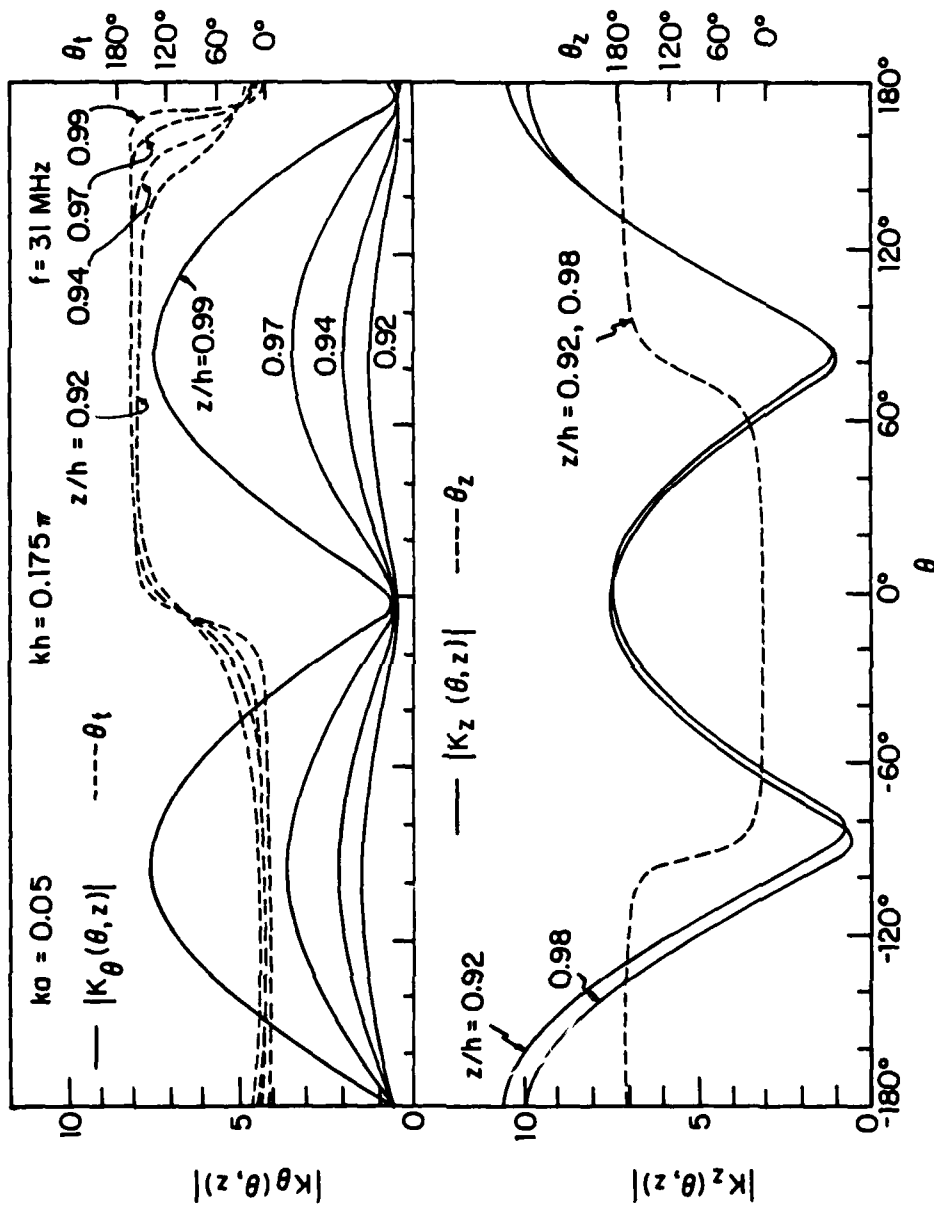


Figure 18. Measured Axial and Transverse Current Densities on Tubular Cylinder; E-Polarization. ( $|K|$  in Arbitrary Units.)

## SECTION VI

### INTERSECTING ELECTRICALLY THIN CYLINDERS; $ka \leq 0.1$

The determination of the surface currents and charges on the intersecting tubular cylinders shown in Fig. 1 is advantageously treated in two parts of which the first, relating to tubes with  $ka \leq 0.1$ , is considered in this section; the second, dealing with cylinders with  $ka > 0.1$ , is discussed in a later section. When  $ka \leq 0.1$ , the surface density of current induced in the vertical tube by the normally incident E-polarized field is well approximated by  $K_z(\theta, z) \doteq A(kz) + B_R(kz)\cos \theta$  and  $K_\theta(\theta, z) \doteq iB'(kz)\sin \theta$ . Except within a radial distance of each open end,  $B_R(kz) \doteq B_R$  and  $K_\theta(\theta, z)$  is negligible. Similarly, the current induced in the horizontal member by the normally incident H-polarized field is well approximated by  $K_\theta(\theta, x) \doteq A_H(kx) + B_H(kx)\cos \theta$  and  $K_x(\theta, x) \doteq iB_H'(kx)\sin \theta$ . Here  $A_H(kx) \doteq A_{HR}$ ,  $B_H(kx) \doteq iB_{HI}$ , and  $K_x(\theta, x)$  is negligible except within a radial distance of each open end. These are the currents induced in the cylinders when individually isolated. They must now be modified to include the effects of the mutual interaction by coupling and the common junction. This can be accomplished by treating the zero-order rotationally symmetric component and the higher-order components separately. Such a separation is particularly useful when  $ka \leq 0.1$  since then  $B_R \doteq -2/Z_0$ ,  $A_{HR} \doteq -1/Z_0$ , and  $B_{HI} \doteq -2ka/Z_0$  with  $1/Z_0 = H_x^{(1)} = 2.65 \text{ mA/V}$  when  $E_z^{(1)} = 1 \text{ V/m}$ . Thus,  $B_{HI}$  is negligible and  $B_R$  and  $A_{HR}$  are determined directly by the incident magnetic field in a manner independent of both the radius and the length of the conductor. This means that the presence or absence of a junction has only local significance insofar as the equal and opposite axial currents given by  $B_R \cos \theta$  and the circulating currents  $A_{HR}$  are concerned. Specifically, these components are substantially the same for the intersecting and the isolated cylinders. Accordingly, they can be determined for the latter and subsequently combined with the rotationally symmetric currents  $A(kz)$ .

When the vertical conductor is electrically so short that  $B_R \gg |A(0)|$ , the rotationally symmetric component of the current is negligible. It is seen from Fig. 10 that  $B_R \geq 5|A(0)|$  when  $kh \leq 0.06\pi$  with  $ka = 0.05$  and  $kh \leq 0.04\pi$  when  $ka = 0.01$  where  $h$  stands for  $h_1$  or  $h_2$ . The same conclusion is true for the horizontal conductor if it is electrically short. When the rotationally symmetric component of current is negligible compared to the equal and opposite first-order current with amplitude  $B_R \cos \theta$ , the entire current on that conductor can be determined as if it were isolated in the

same incident field. If both of the intersecting conductors are electrically short, the entire significant current on each is that obtaining when it is isolated in the same incident field. This applies specifically to currents induced by the sufficiently low-frequency components of an incident electromagnetic pulse.

When the conductors forming the cross are not electrically short, the rotationally symmetric component of current  $A(kz)$  is dominant and can be determined separately taking full account of end and junction conditions and of inter-arm coupling. The contribution by the first-order component  $B_R(kz)\cos\theta$  can be combined with  $A(kz)$  to obtain the entire current  $K_z(\theta, z) \doteq A(kz) + B_R(kz)\cos\theta$ , where  $B_R(kz) \doteq B_R$ . It remains to determine  $A(kz)$ . This can be accomplished with so-called thin-wire theory which is very well developed.

Since the zero-order current  $[K_z(z)]_0 = A(kz)$  induced in the vertical conductor is rotationally symmetric, it can be expressed in terms of the total axial current  $I_z(z) = 2\pi aA(kz)$ . There is no such current induced in the horizontal conductor by the incident field when its electric vector is parallel to the vertical conductor as in Fig. 1(b). However, a current  $I_x(x)$  is induced by charges on the vertical conductor. When the incident electric field has a component parallel to the horizontal conductor as in Fig. 1(a),  $\psi \neq 0$ , it induces a current  $I_x(x)$ . In order to determine both  $I_z(z)$  and  $I_x(x)$ , it is necessary to derive and solve the relevant coupled integral equations subject to boundary conditions at the open tubular ends of the conductors and at the junction. With reference to Fig. 1, the conditions on the currents at the ends of the four arms are:

$$I_{1z}(-h_1) = I_{2z}(h_2) = I_{3x}(-l_1) = I_{4x}(l_2) = 0 \quad (22)$$

The conditions at the junction must relate the currents and the charges per unit length in the four arms. Strictly they must involve these quantities at electrically short distances from the junction where they are still rotationally symmetric. However, since with  $ka \leq 0.1$ , the electrical surface area of the junction region is very small — of the order  $(ka)^2 \leq 0.01$  — its shape is immaterial, and the total charge on its surface is negligible. Accordingly, no significant error is introduced, insofar as currents and charges at electrically very small distances from the junction are concerned, if it is as-

sumed that each arm and its rotationally symmetric current and charge per unit length extend to the junction point  $x = z = 0$  as if concentrated along the axes of the conductors. The junction conditions can then be imposed at this point. For a vertical conductor with radius  $a_1$  and a horizontal conductor with radius  $a_3$ , they include the Kirchhoff condition on the currents, from Reference 13,

$$I_{1z}(0) - I_{2z}(0) + I_{3x}(0) - I_{4x}(0) = 0 \quad (23)$$

and the following three conditions on the charges per unit length, from Reference 7,

$$q_1(0)\Psi_1 = q_2(0)\Psi_2 = q_3(0)\Psi_3 = q_4(0)\Psi_4 \quad (24)$$

where, for conductors at least a quarter wavelength long,

$$\Psi_1 = \Psi_2 = 2[\ln(2/ka_1) - 0.5772] \quad ; \quad \Psi_3 = \Psi_4 = 2[\ln(2/ka_3) - 0.5772] \quad (25)$$

Note that these parameters are independent of the lengths of the conductors. For shorter conductors, the length is significant and

$$\Psi_1 = \Psi_2 = 2 \ln[(h_1 h_2)^{1/2}/a_1] \quad ; \quad \Psi_3 = \Psi_4 = 2 \ln[(\ell_1 \ell_2)^{1/2}/a_2] \quad (26)$$

When all radii are equal ( $a_1 = a_3 = a$ ),  $\Psi_1 = \Psi_2 = \Psi_3 = \Psi_4$  in Eq. (24) and this reduces to the equality of charges per unit length, not the surface density  $\eta = q/2\pi a$ .

The use of thin-cylinder theory with its significant simplifications is an acceptable approximation only when the following inequalities are satisfied:

$$ka_1 \ll 1 \quad ; \quad a_1 \ll h_1 \quad , \quad a_1 \ll h_2 \quad (27a)$$

$$ka_3 \ll 1 \quad ; \quad a_3 \ll \ell_1 \quad , \quad a_3 \ll \ell_2 \quad (27b)$$

Significantly, these conditions actually contain the following:

$$kh_1 \geq 1 \quad ; \quad kh_2 \geq 1 \quad , \quad k\ell_1 \geq 1 \quad , \quad k\ell_2 \geq 1 \quad (28)$$

These are recognized to be the conditions previously imposed to assure that the rotationally symmetric, zero-order component  $[K_z(z)]_0 = A(kz)$  is large compared to the first-order component  $[K_z(\theta, z)]_1 \approx B_R \cos \theta$ . It follows that when thin-cylinder theory is properly used, the significant currents are rotationally symmetric. The analytical determination of the currents and charges induced in intersecting thin cylinders by an electromagnetic wave with the wave normal directed as shown in (a) of Fig. 1 and with the components given in Eqs. (1a,b) is outlined below.

The coupled integral equations that govern the rotationally symmetric currents  $I_z(z)$  in the vertical conductor and  $I_x(x)$  in the horizontal one are best obtained in a form that permits the convenient application of the end and junction conditions in Eqs. (22), (23) and (24) which involve the currents and charges per unit length explicitly. Equations that are expressed in terms of the scalar and vector potentials are inconvenient and have been used, for example in References 14-16, with conditions requiring the continuity of the potentials at the junction instead of the charge per unit length. Since the potentials are in any case continuous, such a procedure is redundant and merely rearranges the form of the equations without taking correct account of the behavior of the charge per unit length.

The required equations in the desired form are readily derived, as in References 17 and 18, from the one-dimensional boundary conditions on the surface of the conductors. These are

$$E_z(z) = E_z^{(i)} - \partial\phi(z)/\partial z - j\omega A_z(z) = 0, \quad -h_1 \leq z \leq h_2 \quad (29a)$$

$$E_x(x) = E_x^{(i)} - \partial\phi(x)/\partial x - j\omega A_x(x) = 0, \quad -\ell_1 \leq x \leq \ell_2 \quad (29b)$$

When the integrals for the scalar potential  $\phi$  and the components of the vector potential  $A$  are substituted in Eqs. (29a,b), the following pair of simultaneous integral equations is obtained for the unknown currents  $I_x(x)$  and  $I_z(z)$ . Note that  $q(z) = (j/\omega)\partial I_z(z)/\partial z$ ,  $q(x) = (j/\omega)\partial I_x(x)/\partial x$ .

$$\begin{aligned} \int_{-h_1}^{h_2} I_z(z') K(z, z') dz' - \frac{j\omega}{k^2} \frac{\partial}{\partial z} \left[ \int_{-h_1}^{h_2} q(z') K(z, z') dz' + \int_{-\ell_1}^{\ell_2} q(x') K(z, x') dx' \right] \\ = -(j4\pi/\omega\mu_0) E_z^{(i)}(z) \end{aligned} \quad (30a)$$



$$\int_{-l_1}^{l_2} I_x(x') K(x, x') dx' - \frac{j\omega}{k^2} \frac{\partial}{\partial x} \left[ \int_{-l_1}^{l_2} q(x') K(x, x') dx' + \int_{-h_1}^{h_2} q(z') K(x, z') dz' \right] = -(j4\pi/\omega\mu_0) E_x^{(i)} \quad (30b)$$

where  $E_z^{(i)}(z)$  and  $E_x^{(i)}$  are given in Eqs. (1a,b). The kernels are defined as follows:  $K(z, z') = \exp(-jkR_z)/R_z$  with  $R_z = [(z - z')^2 + a_1^2]^{1/2}$ ,  $K(x, x') = \exp(-jkR_x)/R_x$  with  $R_x = [(x - x')^2 + a_3^2]^{1/2}$ ;  $K(z, x') = \exp(-jkR_{cz})/R_{cz}$  with  $R_{cz} = [z^2 + x'^2 + a_3^2]^{1/2}$ ;  $K(x, z') = \exp(-jkR_{cx})/R_{cx}$  with  $R_{cx} = [x^2 + z'^2 + a_1^2]^{1/2}$ . Note that  $K(z, z') = K_R(z, z') + jK_I(z, z')$  with  $K_R(z, z') = \cos(kR_z)/R_z$ ,  $K_I(z, z') = -\sin(kR_z)/R_z$ . The equations (30a,b) are to be solved for  $I_z(z)$  and  $I_x(x)$  subject to the four end conditions in Eq. (22), and the four junction conditions in Eqs. (23) and (24).

Analytical solutions of these equations have been obtained when  $a_1 = a_3 = a$  under two sets of conditions which encompass the most significant aspects of the possible distributions of current and charge in a relatively simple form. They are first, from Reference 10, a normally incident field with the electric vector parallel to the vertical conductor as in Fig. 1(b) and arm lengths that are arbitrary and, secondly, from Reference 11, a generally incident field as in Fig. 1(a) but with arm lengths that are all equal. More general cases than these two are readily formulated and evaluated by analytical or numerical methods. Zero- and first-order currents and charges have been calculated for a wide range of arm lengths in Reference 17; only zero-order currents are given in Reference 18. Measured currents and charges are in Reference 19. Details of the analytic solution and explicit formulas for the coefficients are given in Reference 16. The method used is iterative with simple zero-order terms used to obtain the first-order solution.

Zero-order terms alone are generally adequate for very thin conductors with electrical arm lengths not near integral multiples of  $\pi/2$  and  $kh > 1$ . For normal incidence with the electric field parallel to the  $z$ -axis, the zero-order currents are given in Reference 17 as:

$$[I_{1z}(z)]_0 = -AW[\sin k(h_1 + z) + \sin k(h_2 - z) - \sin k(h_1 + h_2) + F(\ell_1, \ell_2) \times \cos kh_2(\cos kz - \cos kh_1)] , -h_1 \leq z \leq 0 \quad (31a)$$

$$[I_{2z}(z)]_0 = -AW[\sin k(h_1 + z) + \sin k(h_2 - z) - \sin k(h_1 + h_2) + F(\ell_1, \ell_2) \times \cos kh_1(\cos kz - \cos kh_2)] , 0 \leq z \leq h_2 \quad (31b)$$

$$[I_{3x}(x)]_0 = AW(\cos kh_2 - \cos kh_1)\sin k(\ell_1 + x)/\cos k\ell_1 , -\ell_1 \leq x \leq 0 \quad (31c)$$

$$[I_{4x}(x)]_0 = -AW(\cos kh_2 - \cos kh_1)\sin k(\ell_2 - x)/\cos k\ell_2 , 0 \leq x \leq \ell_2 \quad (31d)$$

where

$$A = -(j4\pi E_{z0}^{(i)}/\omega\mu_0\Psi) = (-j/60\pi\Psi)(E_{z0}^{(i)}\lambda) \quad (32)$$

$$W = [\sin k(h_1 + h_2) + F(\ell_1, \ell_2)\cos kh_1 \cos kh_2]^{-1} \quad (33)$$

and

$$F(\ell_1, \ell_2) = \tan k\ell_1 + \tan k\ell_2 \quad (34)$$

The associated charges per unit length are:

$$[q_1(z)]_0 = (-jkAW/\omega)[\cos k(h_1 + z) - \cos k(h_2 - z) - F(\ell_1, \ell_2)\cos kh_2 \sin kz] \quad (35a)$$

$$[q_2(z)]_0 = (-jkAW/\omega)[\cos k(h_1 + z) - \cos k(h_2 - z) - F(\ell_1, \ell_2)\cos kh_1 \sin kz] \quad (35b)$$

$$[q_3(x)]_0 = (jkAW/\omega)(\cos kh_2 - \cos kh_1)\cos k(\ell_1 + x)/\cos k\ell_1 \quad (35c)$$

$$[q_4(x)]_0 = (jkAW/\omega)(\cos kh_2 - \cos kh_1)\cos k(\ell_2 - x)/\cos k\ell_2 \quad (35d)$$

Note that at the junction,  $x = z = 0$ ,

$$[q_i(0)]_0 = (-jkAW/\omega)(\cos kh_1 - \cos kh_2) ; i = 1, 2, 3, 4 \quad (36)$$

The charges per unit length on all arms have the same value as the junction is approached. This is zero only when  $h_1 = h_2$ . (When higher-order terms are included, Eq. (36) does not vanish when  $kh_1$  and  $kh_2$  differ by  $n\pi$ .) In this case, Eqs. (31b,c) and (35c,d) show that all currents and charges vanish at all points on the horizontal cylinder. In the absence of a component of the electric field along the horizontal conductor, currents and charges are induced only when there is a nonzero charge on the junction at  $z = 0$ . With a normally incident field this occurs only when the junction is at the center of the vertical cylinder. Currents that are excited on the horizontal conductor by periodically varying charges at  $x = 0$  are necessarily oppositely directed near  $x = 0$ . The discontinuity in the vertical current at the junction is  $I_{1z}(0) - I_{2z}(0) = -AW(\tan kl_1 + \tan kl_2)(\cos kh_2 - \cos kh_1)$ . It is, of course, the negative of the discontinuity in the horizontal current,  $I_{3x}(0) - I_{4x}(0)$ , so that Kirchhoff's law in Eq. (23) is obeyed.

The distributions of current and charge per unit length on the vertical member include one set of terms characteristic of the cylinder in the absence of the transverse member and a second set of terms that takes account of the interaction with the horizontal cylinder. The former are more easily recognized when expressed in terms of the coordinate  $z_0$  with origin at the center of the vertical tube and the half-length  $h = (h_1 + h_2)/2$ . With these it follows directly that in Eqs. (31a,b),  $\sin k(h_1 + z) + \sin k(h_2 - z) - \sin k(h_1 + h_2) = 2 \sin kh (\cos kz_0 - \cos kh)$  and in Eqs. (35a,b),  $\cos k(h_1 + z) - \cos k(h_2 - z) = 2 \sin kh \sin kz_0$ . Thus, these terms represent the simple shifted cosine distribution of the current and sinusoidal distribution for the charge per unit length but referred to an arbitrarily located origin for  $z$ . They provide a zero charge per unit length at the center, but a non-zero value at the junction so long as this is not centered. It is this charge which generates the currents on the horizontal cylinder. The second set of terms in Eqs. (31a,b) and (35a,b) is multiplied by the coupling factor  $F(l_1, l_2)$  that takes account of the horizontal currents on the cross. In Eqs. (31a,b) they are shifted cosines with respect to each arm length; they provide a discontinuity at the junction so that there can be currents in the side arms in accordance with Kirchhoff's law in Eq. (23). In Eqs. (35a,b) the terms multiplied by  $F(l_1, l_2)$  are simple sinusoids which provide no charge at the junction. The currents and charges in the horizontal arms consist of

one term only and this is multiplied by the coupling coefficient,  $\cos kh_2 - \cos kh_1$ . Note that the current in the horizontal member is distributed in the form  $\sin k(l - |x|)$  which is quite different from the shifted cosine distribution in the vertical member. The latter is induced by the uniform incident electric field, the former by charges at the junction that induce oppositely directed currents in the two arms.

When the electrical length of any of the four arms is at or near an integral multiple of  $\pi/2$ , first-order terms must be included. Sample distributions of current and charge for such cases are discussed later in this section.

In order to induce currents on the side arms, it is necessary either to have a component of the incident electric field along the horizontal element or to maintain a nonzero charge on the vertical cylinder at the junction. When the junction is at the center of the vertical member, this can be accomplished by non-normal incidence as indicated in Fig. 1(a). When the incident field in Eqs. (1a,b) induces currents in a cross with equal arms, the effect of non-normal incidence in maintaining charges at the junction is separated from the effect of unequal arm lengths already determined for normal incidence. The properties of currents induced by uniform electric fields and by those with a progressive phase shift can be examined individually.

The solution of Eqs. (30a,b) with  $a_3 = a_1 = a$  and  $h_2 = h_1 = l_1 = l_2 = h$  is relatively simple in zero-order. The currents on both vertical and horizontal elements consist of parts that are even in the coordinate, i.e.,  $I_{\text{even}}(-v) = I_{\text{even}}(v)$ , and parts that are odd, i.e.,  $I_{\text{odd}}(-v) = -I_{\text{odd}}(v)$  where  $v = x$  or  $z$ . The four currents are conveniently represented as follows in Ref. [18]:

$$[I_{1z}(z)]_0 = I_{\text{even}}(z) - I_{\text{odd}}(z), \quad -h \leq z \leq 0 \quad (37a)$$

$$[I_{2z}(z)]_0 = I_{\text{even}}(z) + I_{\text{odd}}(z), \quad 0 \leq z \leq h \quad (37b)$$

$$[I_{3x}(x)]_0 = I_{\text{even}}(x) - I_{\text{odd}}(x), \quad -h \leq x \leq 0 \quad (37c)$$

$$[I_{4x}(x)]_0 = I_{\text{even}}(x) + I_{\text{odd}}(x), \quad 0 \leq x \leq h \quad (37d)$$

where the even and odd parts of the currents are

$$I_{\text{even}}(z) = -(A \cos \psi) \left[ \frac{\cos kz \cos qh - \cos qz \cos kh}{\sin \theta \cos kh} \right] \quad (38a)$$

$$I_{\text{odd}}(z) = -(j/2)(A \cos \psi) \left[ \frac{\sin k|z| \sin qh - \sin q|z| \sin kh}{\sin \theta \sin kh} + \frac{\cos kz \sin qh - \sin q|z| \cos kh - \sin k(h - |z|) \cos \theta}{\sin \theta \cos kh} \right] \quad (38b)$$

$$I_{\text{even}}(x) = -(A \sin \psi) \left[ \frac{\cos kx - \cos kh}{\cos kh} \right] \quad (38c)$$

$$I_{\text{odd}}(x) = (j/2)(A \cos \psi) \left[ \frac{\sin qh - \sin kh \cos \theta}{\sin \theta \sin kh} \right] \left[ \frac{\sin k(h - |x|)}{\cos kh} \right] \quad (38d)$$

The associated charges per unit length are presented in the same sequence as the currents. Note that odd charges are derived from even currents and vice versa.

$$[q_1(z)]_0 = -q_{\text{odd}}(z) + q_{\text{even}}(z) \quad (39a)$$

$$[q_2(z)]_0 = q_{\text{odd}}(z) + q_{\text{even}}(z) \quad (39b)$$

$$[q_3(x)]_0 = -q_{\text{odd}}(x) + q_{\text{even}}(x) \quad (39c)$$

$$[q_4(x)]_0 = q_{\text{odd}}(x) + q_{\text{even}}(x) \quad (39d)$$

where

$$q_{\text{odd}}(z) = (jk/\omega)(A \cos \psi) \left[ \frac{\sin k|z| \cos qh - \sin q|z| \cos kh \cos \theta}{\sin \theta \cos kh} \right] \quad (40a)$$

$$q_{\text{even}}(z) = (k/2\omega)(A \cos \psi) \left[ \frac{\cos kz \sin qh - \cos qz \sin kh \cos \theta}{\sin \theta \sin kh} \right]$$

$$+ \frac{\sin k|z| \sin qh + \cos qz \cos kh \cos \theta - \cos k(h - |z|) \cos \theta}{\sin \theta \cos kh} \quad (40b)$$

$$q_{\text{odd}}(x) = (jk/\omega)(A \sin \psi) \left[ \frac{\sin k|x|}{\cos kh} \right] \quad (40c)$$

$$q_{\text{even}}(x) = (k/2\omega)(A \cos \psi) \left[ \frac{\sin qh - \sin kh \cos \theta}{\sin \theta \sin kh} \right] \left[ \frac{\cos k(h - |x|)}{\cos kh} \right] \quad (40d)$$

At the junction,  $x = z = 0$ , and with  $i = 1, 2, 3, 4$ ,

$$[q_i, 0]_0 = [q_{\text{even}}(0)]_0 = (k/2\omega)(A \cos \psi) \left[ \frac{\sin qh - \sin kh \cos \theta}{\sin \theta \sin kh} \right] \quad (41)$$

The conditions for zero charge per unit length in each arm as the junction is approached are seen to be  $\psi = \pi/2$  and  $\theta = \pi/2$ . When  $\psi = \pi/2$ , the electric vector has no component along the vertical conductor and, since it is constant in phase along the horizontal tube, the charge per unit length at its center vanishes. When  $\theta = \pi/2$ , the wave is normally incident with the component  $E_0^{(1)} \cos \psi$  parallel to the vertical conductor, the component  $E_0^{(1)} \sin \psi$  parallel to the horizontal one.

The several terms in the currents in Eqs. (37a-d) and in the charges per unit length in Eqs. (39a-d) are readily identified. The current  $I_{\text{even}}(z)$  in Eq. (38a) and the first fraction in  $I_{\text{odd}}(z)$  in Eq. (38b) are, respectively, the even and odd currents induced in the vertical cylinder in the absence of the horizontal conductor (Refs. 11 and 12). Similarly,  $I_{\text{even}}(x)$  in Eq. (38c) is the same as the current induced in the horizontal cylinder when the vertical one is absent. The associated charges are given by the corresponding terms in Eqs. (40a-c). Note that  $q_{\text{odd}}(z)$  in Eq. (40a) and  $q_{\text{odd}}(x)$  in Eq. (40c) are zero at the junction so that they are not coupled either to each other or any other charges in the intersecting cylinders. The entire current  $I_{\text{odd}}(x)$  in Eq. (38d) is excited by charges at the junction. Its distribution but not its amplitude is independent of  $\theta$ . The second fraction in  $I_{\text{odd}}(z)$  in Eq. (38b) is the current in the vertical conductor generated by the oscillations in the horizontal cylinder. It includes a term,  $-\sin k(h - |z|) \cos \theta$ , with a distribution like that in  $I_{\text{odd}}(x)$  but there are other,  $\theta$ -dependent terms that contribute to the fairly complicated distribution.

However, as can be seen from the corresponding terms in Eq. (40b), the associated charges vanish at the junction,  $z = 0$ . In the vertical cylinder all of the charges at the junction are given by the first fraction in Eq. (40b); they are generated by the part of the odd current that would remain if the horizontal cylinder were removed (Refs. 11 and 12). Thus, the charges at the junction associated with the part of the current that is associated with the isolated vertical cylinder excite the charges and associated currents in the horizontal cylinder to satisfy the three junction conditions on the charges. This resulting modification in the charges on the vertical cylinder is associated with new currents that combine with the currents on the horizontal cylinder to satisfy Kirchhoff's condition at the junction.

When the junction of intersecting cylinders is not centered on the vertical element and the exciting wave is not normally incident, both the even and odd components of the current on the vertical cylinder have associated charges at the junction which generate odd currents in the horizontal member in a manner readily understood from a combination of the effects described in conjunction with Eqs. (31a-d), (35a-d) on the one hand, and Eqs. (37a-d), (39a-d) on the other hand. The corresponding zero-order currents and charges can be derived from solutions of the general integral equations, but they are sufficiently complicated to make a simple interpretation difficult. In general, first-order solutions must be obtained from these equations in order to have a quantitative picture of the currents and charges on the intersecting cylinders. This is true particularly near and at resonance. For example in the cross with all arms equal, resonant oscillations along the horizontal and vertical cylinders and from one vertical arm to one horizontal arm all occur at the same frequency according to zero-order theory. Actually, an oscillation from one vertical to one horizontal arm involves quite different coupling between the halves of the oscillating circuit so that it occurs at a frequency somewhat different from that along a horizontal or vertical cylinder. Since zero-order theory does not include the effects of coupling, it cannot distinguish between the two cases. It is the first-order terms that take account of mutual interaction.

Sample first-order distributions of current and charge per unit length on three different, thin-cylinder crosses are shown in Figs. 19 through 21. Specifically, in Fig. 19,  $k(h_1 + h_2) = 4\pi + 2\pi = 6\pi$ , an antiresonant

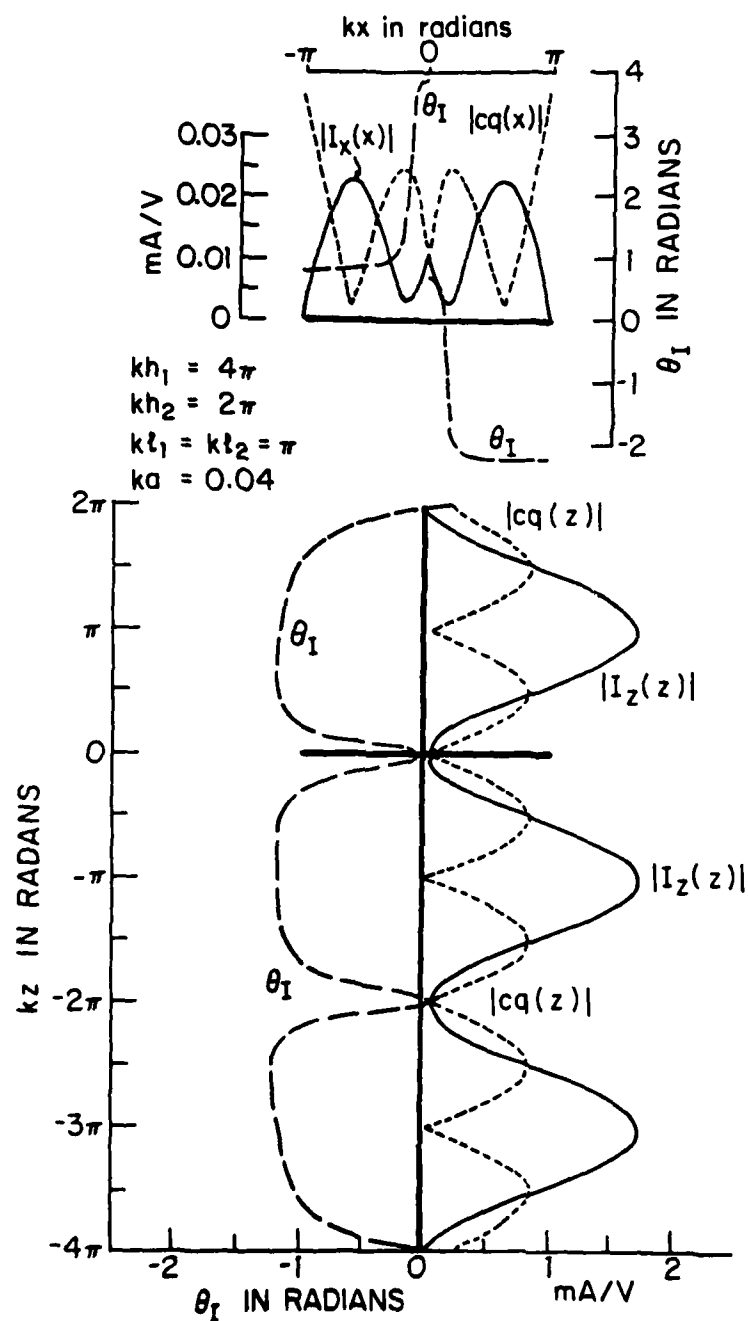


Figure 19. Currents and Charges Per Unit Length on Crossed Cylinders in Normally Incident Field;  $\vec{E}^{(i)} = \hat{z} E_z^{(i)}$ .



$$kh_1 = 3\pi; \quad kh_2 = k\ell_1 = k\ell_2 = \pi; \quad kh = 0.04$$

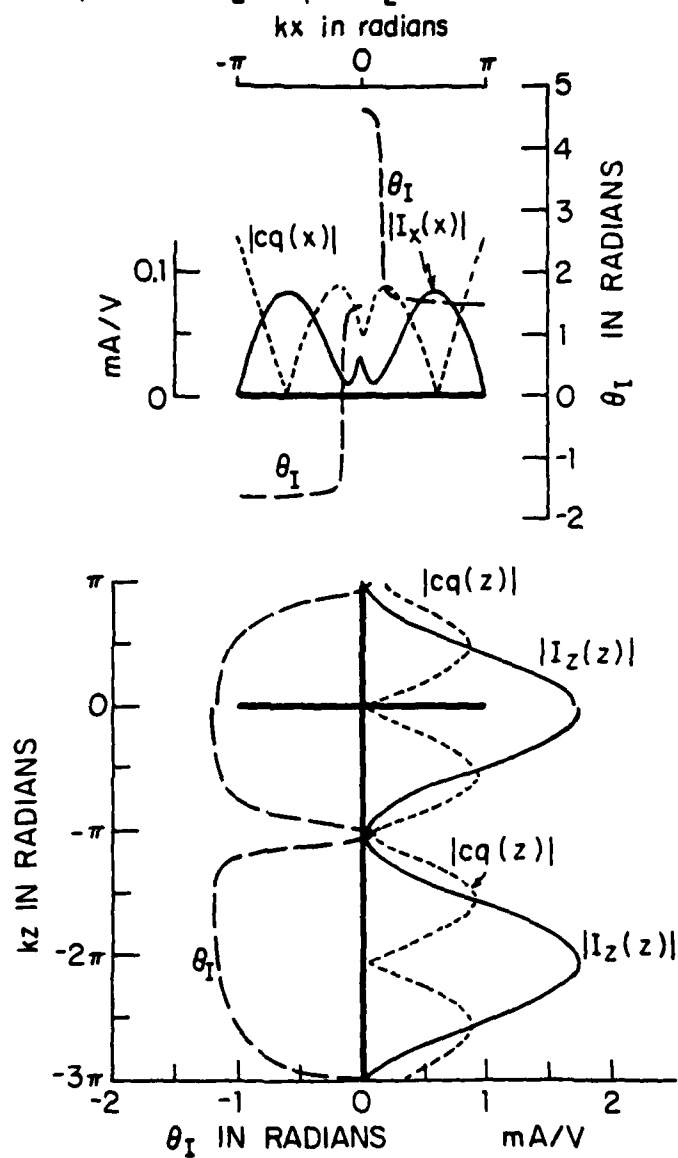


Figure 20. Currents and Charges Per Unit Length on Crossed Cylinders in Normally Incident Field;  $\vec{E}^{(i)} = \hat{z} E_z^{(i)}$ .

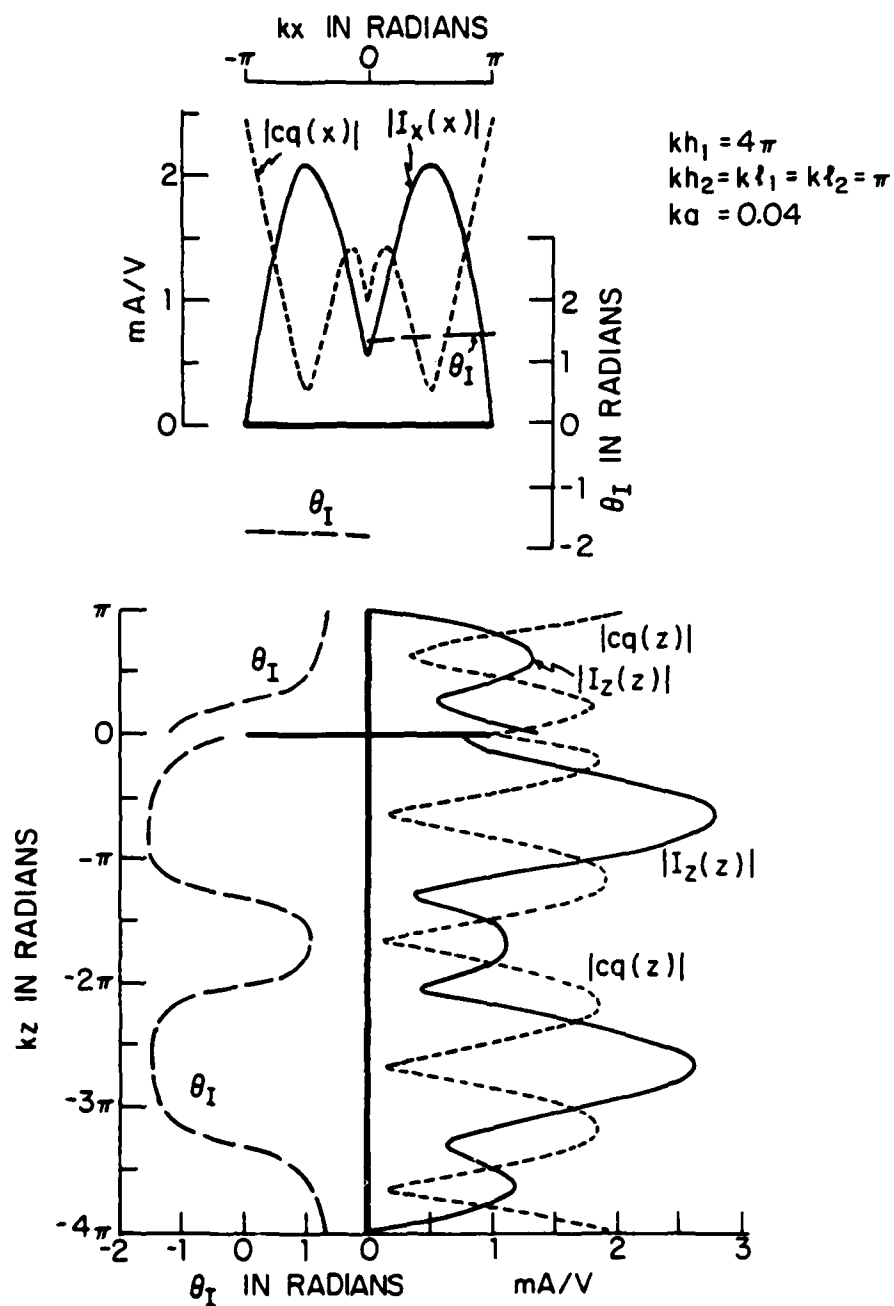


Figure 21. Currents and Charges Per Unit Length on Crossed Cylinders in Normally Incident Field;  $\vec{E}^{(1)} = \hat{z} E_z^{(1)}$ .

length with a minimum of current and a minimum of charge per unit length at the junction,  $kz = 0$ . Since  $k\ell_1 = k\ell_2 = \pi$ , each side arm is individually self-resonant, but is only weakly excited owing to the minimum of charge per unit length at the junction. Note that the maximum of  $I_x(x)$  on the horizontal arms is less than 0.02 of the maximum of  $I_z(z)$  on the vertical member. In Fig. 20,  $k(h_1 + h_2) = 3\pi + \pi = 4\pi$ , again an antiresonant length but now with a current maximum and a charge minimum at the junction. Since again  $k\ell_1 = k\ell_2 = \pi$ , the side arms are self-resonant but are only weakly excited owing to the relatively small charge at the junction. Almost all of the large current in the vertical cylinder continues through the junction with very little entering the side arms. In Fig. 21,  $k(h_1 + h_2) = 5\pi$ , a resonant length with a minimum of current and close to a maximum of charge per unit length at the junction,  $kz = 0$ . With  $k\ell_1 = k\ell_2 = \pi$ , each side arm is individually self-resonant and is now strongly excited by the large charge at the junction. As a consequence, the maximum of  $I_x(x)$  is almost as great as the maximum of  $I_z(z)$ . Measured currents and charges per unit length on electrically thin crossed cylinders over a ground plane are shown in Reference 19. They are in general agreement with the graphs in Figs. 19 through 21, but are not directly comparable since they involve the image of the cross. In general, when the incident electric field is parallel to the vertical cylinder, the currents excited in the side arms are largest when these are individually self-resonant and are located at a charge maximum in the standing-wave distribution along the vertical conductor.

## SECTION VII

### INTERSECTING ELECTRICALLY THICK CYLINDERS; $ka > 0.1$

When intersecting cylinders are not electrically thin, the simplifying approximations that are permitted when  $ka \leq 0.1$  and that underlie thin-cylinder theory are invalid. The concepts of a total axial current and a charge per unit length are not useful since the zero-order, rotationally symmetric components contribute only fractionally to the surface densities and even for them the electrically large cross section introduces highly significant phase differences in the interaction of the elements of current and charge distributed around a circumference due to the finite velocity of propagation of electromagnetic effects. These are negligible when  $ka \ll 1$  so that the currents and charges can effectively be treated as though concentrated along the axis for purposes of calculating fields. Furthermore, transverse components of current and associated charges (which are ignored in thin-cylinder theory because they are negligible when  $ka \ll 1$  and  $kh > 1$ ) are very important with E-polarization and completely dominate with H-polarization as  $ka$  approaches and exceeds one. There is no way of determining either the transverse variation of the axial current or any part of the transverse current from thin-cylinder theory.

The conditions on the currents and charges at the intersection of thin cylinders are expressed in terms of fictitious, rotationally symmetric, total currents and charges per unit length at a junction that has so small a surface area that its shape and the charges on it can be ignored. The thin-cylinder junction conditions are designed to give the correct currents and charges per unit length at distances of a radius or two from the junction, but they provide no detailed information about the current and charge densities very near to and on the surfaces of the junction. Actually, they have no valid application when  $ka$  is not quite small. The absence of rotational symmetry in the axial currents, the presence of significant transverse currents, the fact that the surface area of the junction region itself is not electrically small and carries large currents and charges, and the dependence of the surface density of charge on the spatial rates of change of both axial and transverse components of current all combine to make the thin-cylinder junction conditions meaningless when  $ka > 0.1$ . The conditions at the junction of electrically thick cylinders are contained in the general requirement that the component of the electric field tangent to all parts of the perfectly conduct-

ing surfaces of the junction vanish. In the sharp grooves at the junction lines of the intersecting tubes the component of the electric field perpendicular to the surface must vanish since the normal to one of the intersecting surfaces has a component tangent to the other surface. It follows that the charge density along the bottoms of the grooves must be zero and with it the component along the groove of the vector surface density of current. Thus, this latter must be directed perpendicularly across each groove. These conditions actually apply equally to intersecting electrically thick or thin cylinders and must be used for all values of  $ka$  if the distributions of current and charge on and very near the junction are to be determined. When  $ka \ll 1$ , a knowledge of these distributions is not required to determine the total rotationally symmetric currents and charges per unit length not too close to the junction.

No analytical or numerical determinations of the surface currents and charges on intersecting electrically thick cylinders are available. However, extensive measurements of these quantities have been reported in References 20 and 21. They include three lengths for the horizontal cylinder and two locations along the vertical tube. Graphs of both the axial and transverse components of current density and of the charge density are available for  $ka = 1$  and  $ka = 2$ . Representative and very instructive examples for  $ka = 1$  are in Figs. 22 and 23 which show contour maps of the surface densities of charge, respectively, on the vertical and horizontal cylinders when the length of the former above the ground plane is  $kh = 3.5\pi$ ,  $kl_1 = kl_2 = 2\pi$ , and the junction of the intersecting axes is at  $kh_1 = 2.5\pi$ . The axial standing-wave patterns on the illuminated ( $\theta = 180^\circ$ ) and shadowed ( $\theta = 0^\circ$ ) sides are clearly shown in Fig. 24 when  $kl = \pi$ ,  $kh_1 = 2.5\pi$  and when  $kl = 1.5\pi$  with  $kh_1 = 2\pi$ . For purposes of comparison the distribution along the vertical cylinder when isolated is also shown.

These illustrations and numerous others for the phases and amplitudes of the surface densities of current and charge in References 20 and 21 lead to the following general conclusions for intersecting cylinders with  $ka \geq 1$ :

- 1) The distributions of current and charge densities are much less sensitive to changes in the lengths of the cylinders when they are electrically thick than when electrically thin.
- 2) The distribution of the charge density on an electrically thick cylinder is more sensitive to the nature of the incident

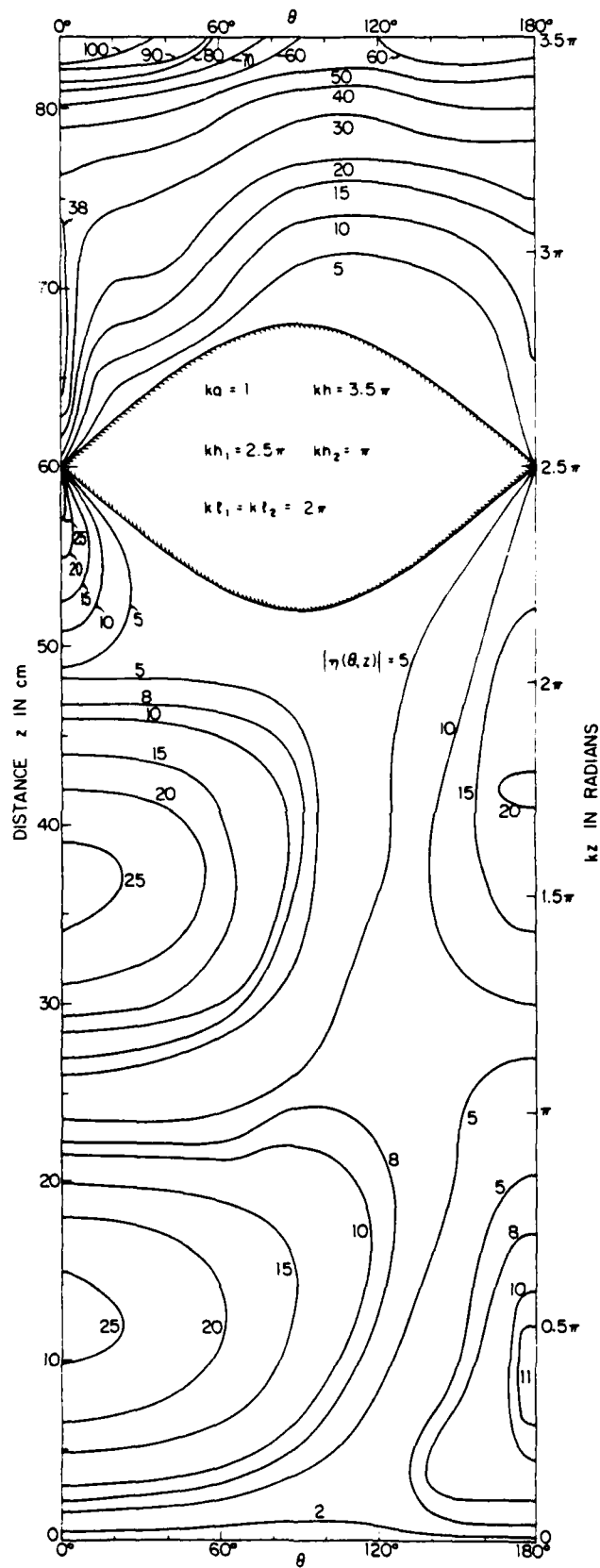


Figure 22. Measured Contours of Constant Charge Density  $|\eta(\theta, z)|$  on Vertical Members of Crossed Cylinders. ( $|\eta|$  in Arbitrary Units.)

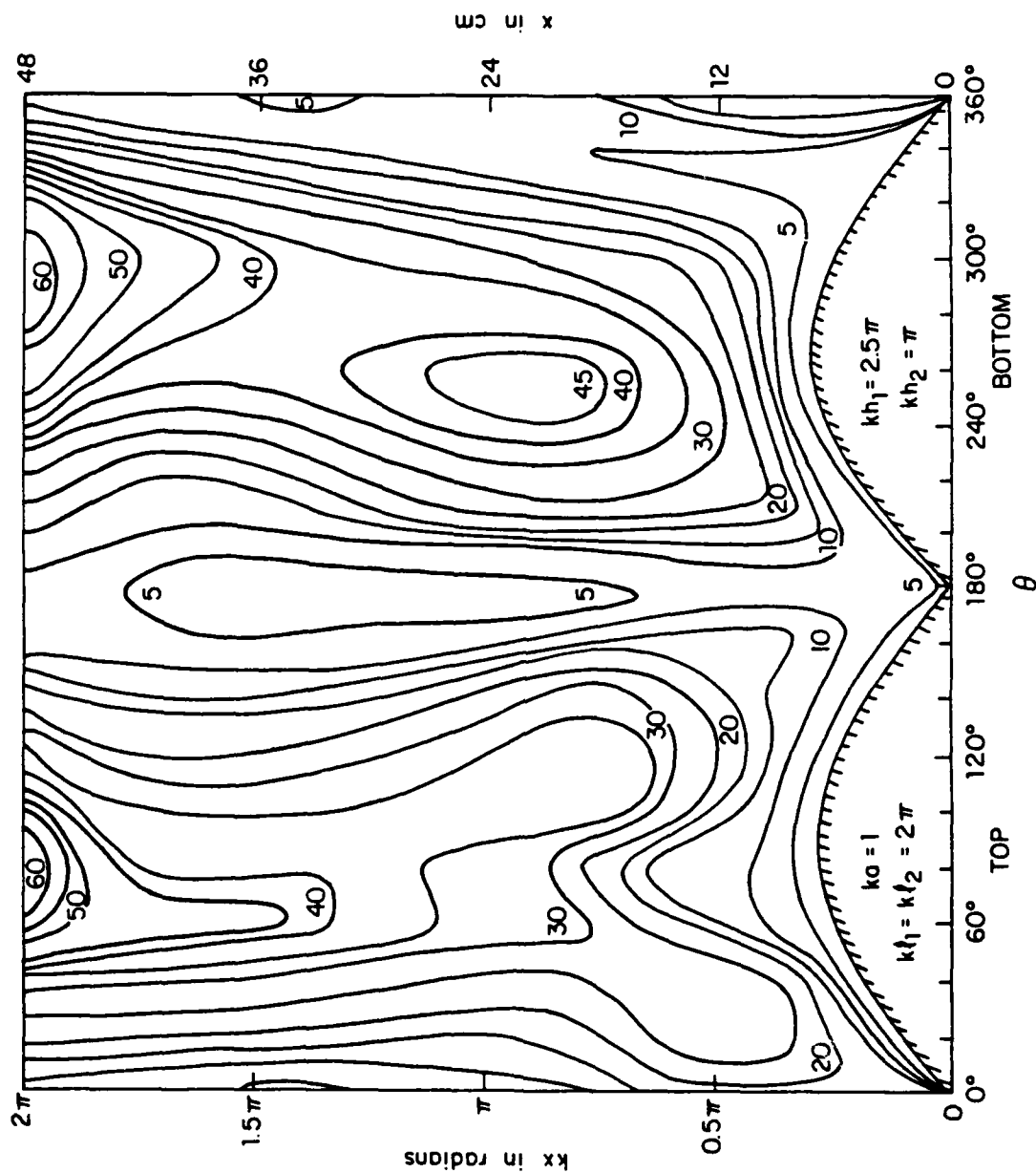


Figure 23. Measured Contours of Magnitude of Surface Density of Charge on Horizontal Member of Crossed Cylinders. ( $|\eta|$  in Arbitrary Units.)

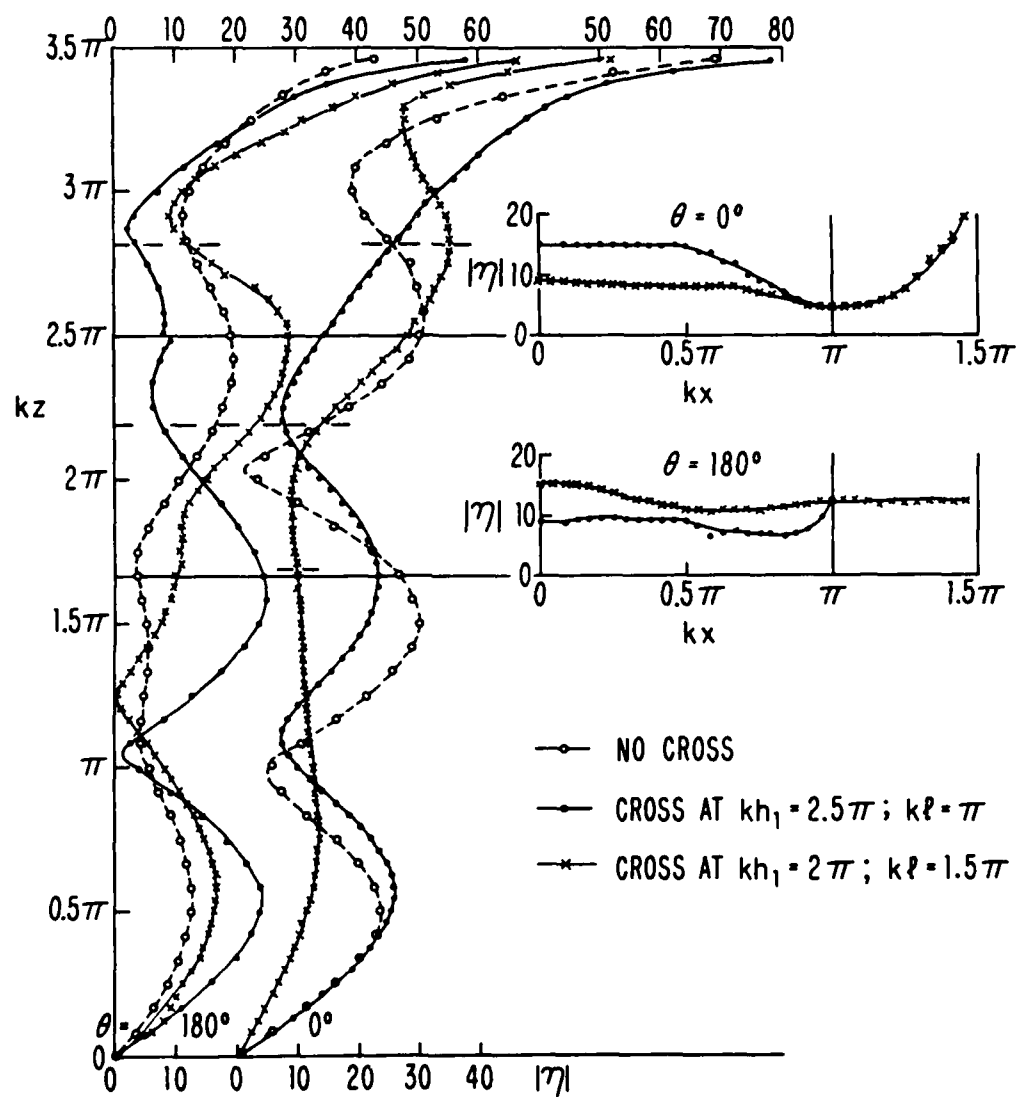


Figure 24. Measured Surface Density of Charge on Crossed Cylinders with  $kh = 3.5\pi$ ,  $ka = 1$  for Two Locations of the Junction and with No Cross. ( $|\eta|$  in Arbitrary Units.)



field and the presence, dimensions, and location of an intersecting cylinder than is the distribution of current. 3) The charge density on the vertical member when excited by an incident E-polarized field has significantly different distributions when the incident field is not plane, when the horizontal member is absent, its location is changed, or when the arm lengths are varied. The current density is much less affected. 4) The distribution of the charge density on the horizontal cylinder in an H-polarized field is insensitive to the location of its intersection with the vertical member of the cross so long as the arms are equal in length. On the other hand, the amplitude of the axial standing-wave pattern as a function of  $\theta$  is sensitive to the length of the arms. 5) As on the single cylinder, the axial current density on the vertical cylinder is substantially a superposition of forced and resonant components. The changes from the distribution along the single tube when an intersecting cylinder is present in different locations and with different arm lengths are due primarily to shifts in the relative phases of the forced and resonant components.

When  $ka = 2$ , the transverse distributions are significantly more complicated since transverse Fourier components of order 2 are large in addition to those of orders 1 and 0. The axial distributions are very similar to those with  $ka = 1$ . Sample distributions of the surface density of charge on the vertical cylinder with  $kh = 3.5\pi$  are in Fig. 25, on the horizontal cylinder with  $kl = 2\pi$  in Fig. 26. The intersection of the axes is at  $kh_1 = 2.5\pi$ . Additional graphs are in Reference 21.

In general the distributions of current and charge on the surfaces of intersecting electrically thick cylinders are quite similar to those on each of the individual cylinders alone in the same field. The relative amplitudes of the standing waves on the illuminated and shadowed sides of the vertical cylinder may differ considerably, but the standing-wave patterns are significantly changed only quite near the junction region. Thus, a knowledge of the distributions of current and charge density on single cylinders is of great value in the understanding and interpretation of these quantities on intersecting cylinders and in the rough approximation of their actual values.

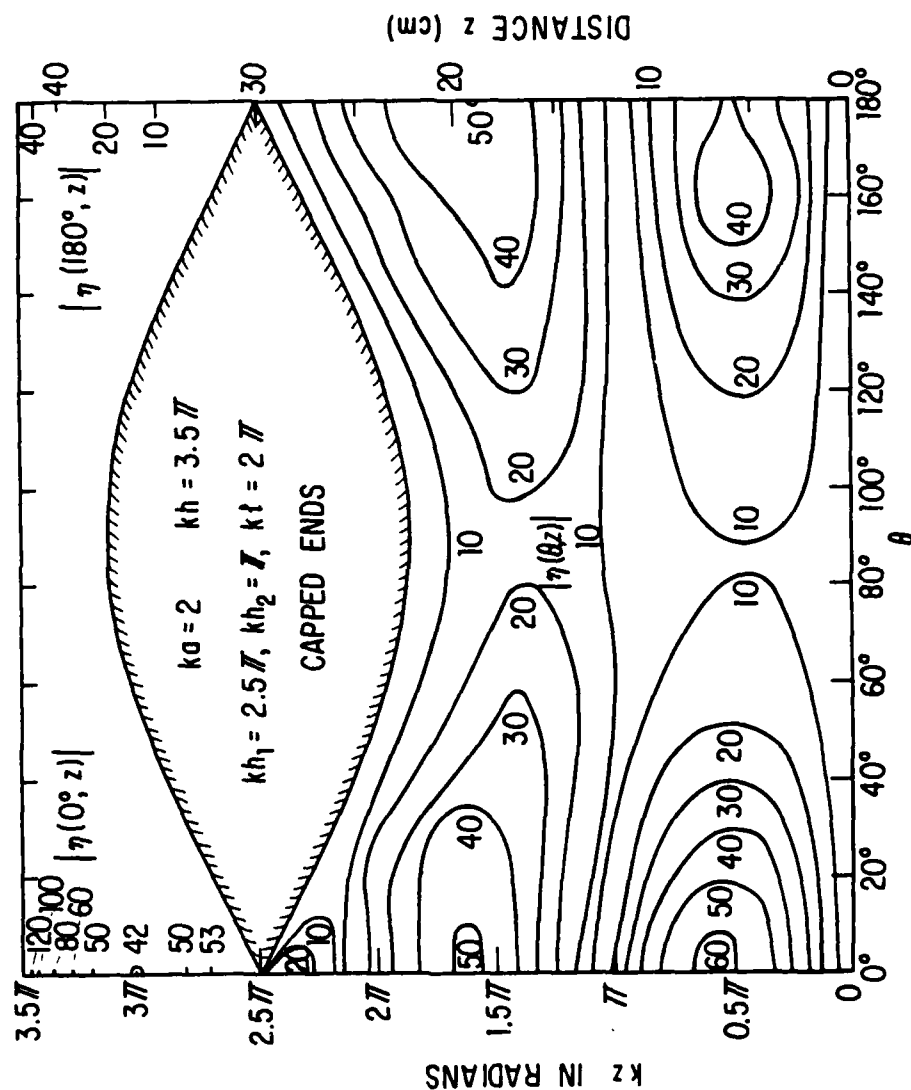


Figure 25. Measured Contours of Constant Magnitude of Surface Density of Outside Charge on Vertical Member of Crossed Cylinders with Capped Ends; E-Polarization, Normal Incidence,  $\lambda = 24$  cm. ( $|\eta|$  in Arbitrary Units.)

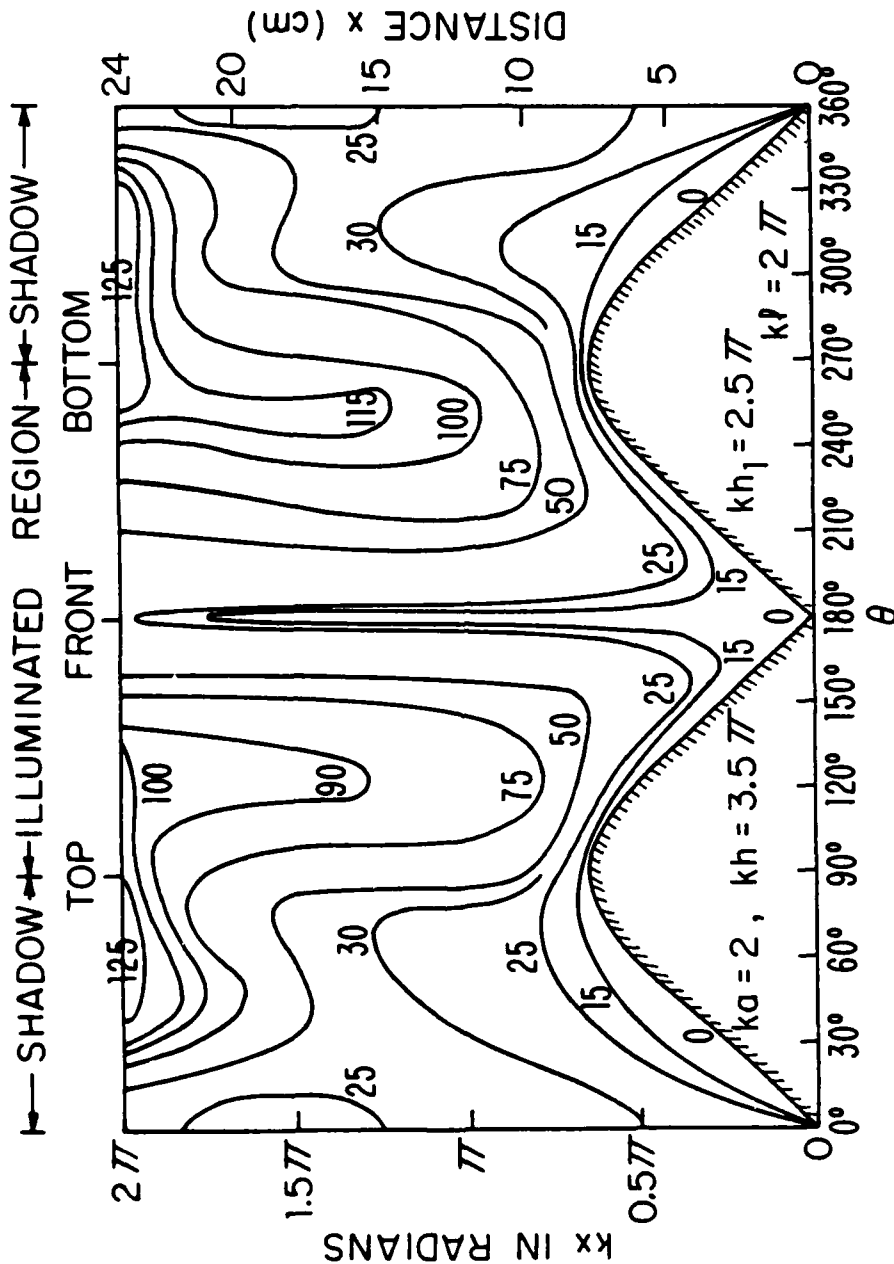


Figure 26. Measured Contours of Constant Magnitude of Surface Density of Outside Charge on Horizontal Member of Crossed Cylinders with Capped Ends; H-Polarization, Normal Incidence,  $\lambda = 24$  cm. ( $|n|$  in Arbitrary Units.)

## SECTION VIII

### INTERSECTING ELECTRICALLY THICK CYLINDER ( $ka = 1$ ) AND FLAT PLATE (BASED ON REFERENCE 22)

When the horizontal cylinder in the cross in Fig. 1 is replaced by a flat plate as shown in Fig. 27, an improved model of an aircraft is achieved. However, there are no available analytical or numerical determinations of the surface densities of current and charge induced on the surfaces of this structure when illuminated by a plane wave. Indeed, these quantities have not been evaluated for a single flat plate or strip of finite length. Fortunately, measured data are at hand, from Reference 22, for a cross that is erected on a ground plane and illuminated by a normally incident plane wave with the electric vector along the axis of the vertical cylinder. The measured data apply to a cylinder with  $kh = 3.5\pi$  and  $ka = 1$ , with a horizontal intersecting plate that has equal arms. Each of the two flat plates has the electrical length  $kl = 1.5\pi$  so that it extends to  $k(l + a) = 1.82\pi$  from the vertical axis; the electrical width of the plate is  $kL = 0.5\pi$ , its thickness is  $kT = 0.054\pi$ .

The magnitude of the measured charge density  $\eta(\theta, z)$  on the cylinder is presented in the contour diagram of Fig. 28. This shows a standing-wave pattern very much like that on the cylinder when alone. The effect of the horizontal plate is very small except in its immediate vicinity where a deep minimum surrounds it. The corresponding diagram for the charge density  $\eta(x, z)$  on the flat plate is shown in Fig. 29 for the illuminated side. The diagram for the shadowed side is in Reference 22. It is not shown here since it differs little from Fig. 29. Note that the standing-wave pattern along the edges has maxima (of opposite sign) at the corners and a half-wavelength from them. There is a deep minimum along a line increasingly displaced from the center line toward the trailing edge of the "wing" as the central cylinder is approached. There is, of course, a null along the groove of the junction line between the end of the plate where it joins the cylinder.

The current density along the cylinder is predominantly axial except quite near the open end, where large transverse currents occur. The magnitude of  $K_z(\theta, z)$  is shown in Fig. 30. The distributions resemble those along the isolated cylinder and the cylinder with an intersecting cylinder in general form. The effect of the transverse plate is seen to be very small — even smaller than the effect of a transverse cylinder. The transverse plate

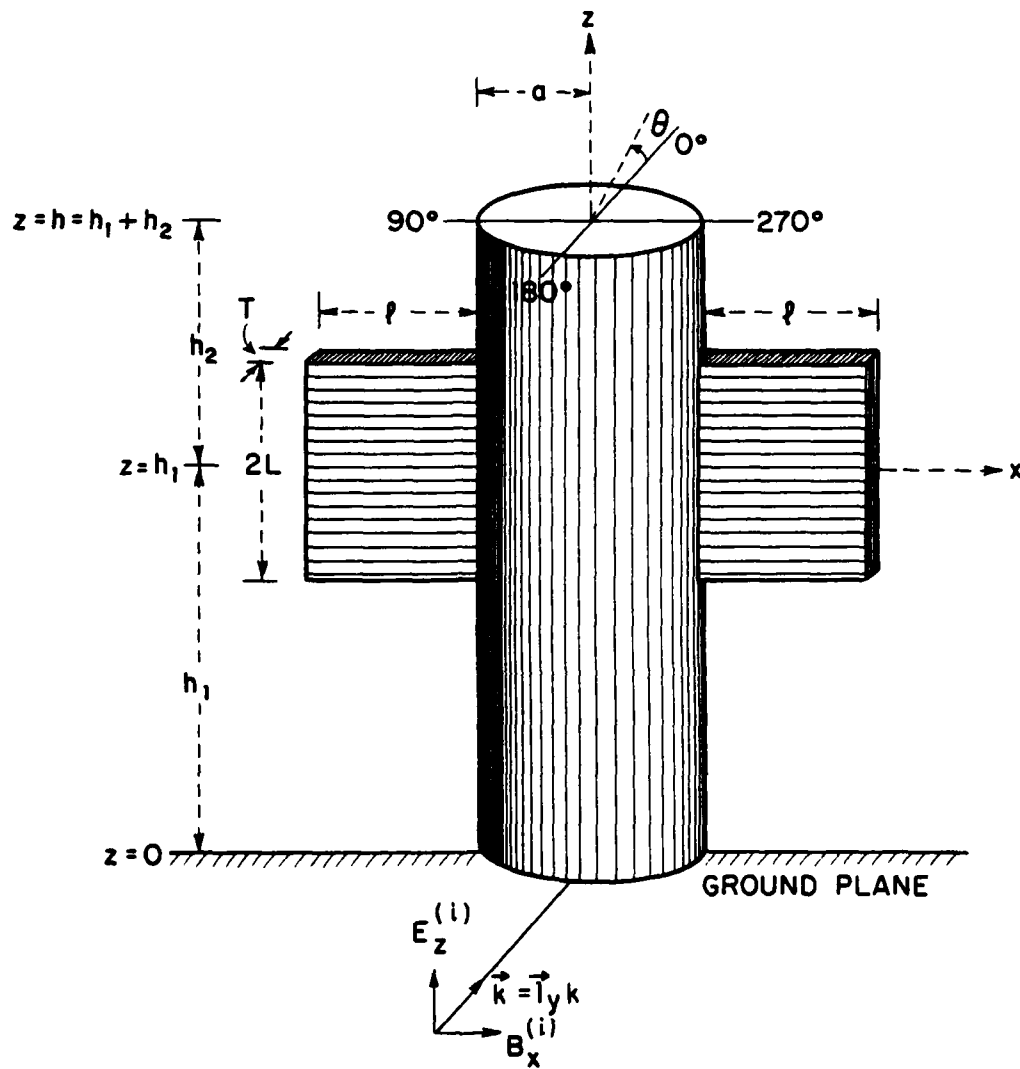


Figure 27. Diagram of Flat Plate Crossed with an Electrically Thick Cylinder Illuminated by a Normally Incident, Plane-Wave Field.

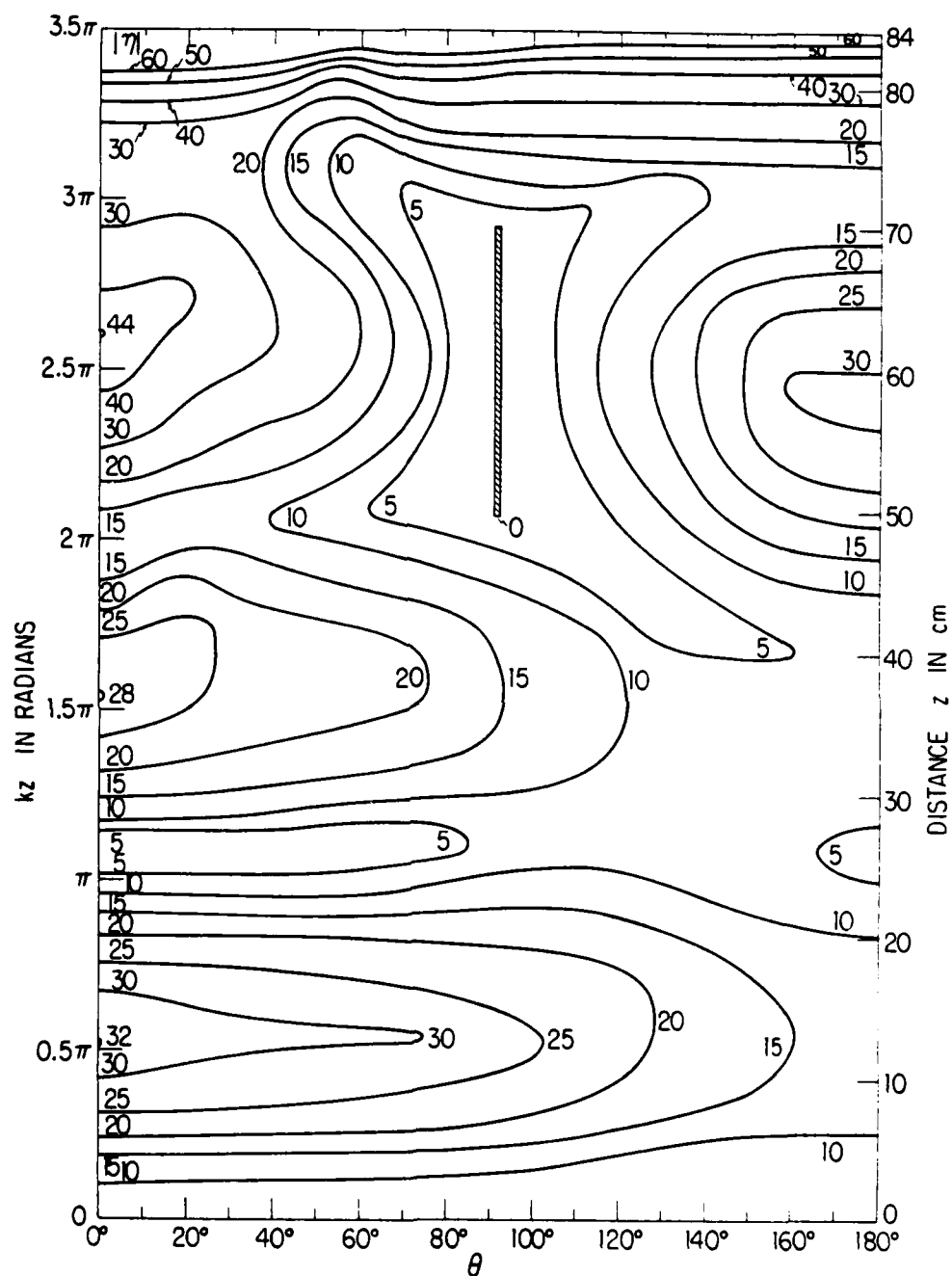


Figure 28. Contour Diagram of Measured Magnitude of Surface Density of Charge  $|\eta|$  on Tubular Cylinder with Crossed Flat Plate Centered at  $kh_1 = 2.5\pi$ ,  $kh = 3.5\pi$ ;  $k\ell$  of Plate  $= 1.5\pi$ ,  $kL = 0.5\pi$ ,  $kT = 0.054\pi$ . ( $|\eta|$  in Arbitrary Units.)

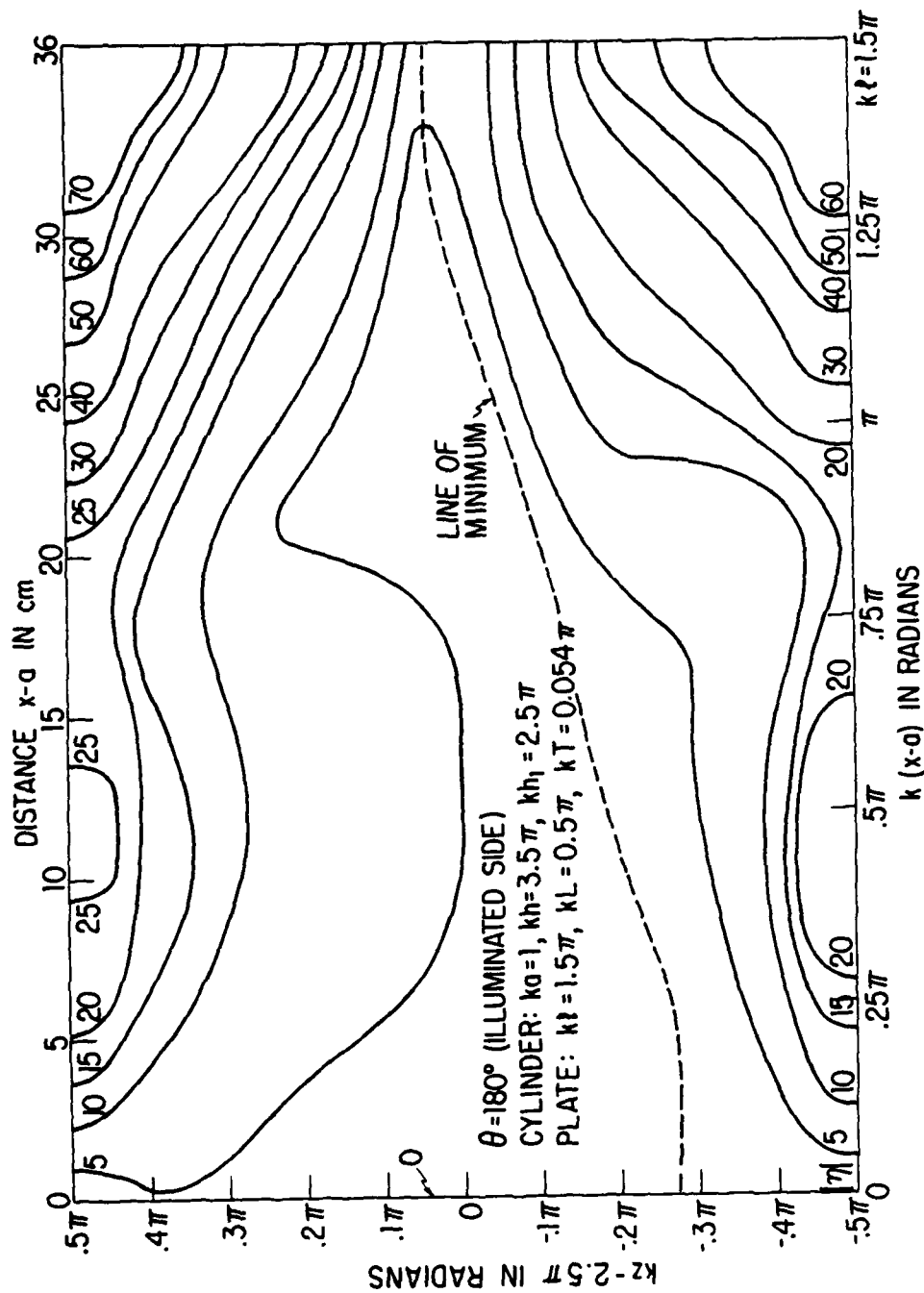


Figure 29. Contour Diagram of Measured Surface Density of Charge on Horizontal Flat Plate ( $|\eta|$  in Arbitrary Units.)

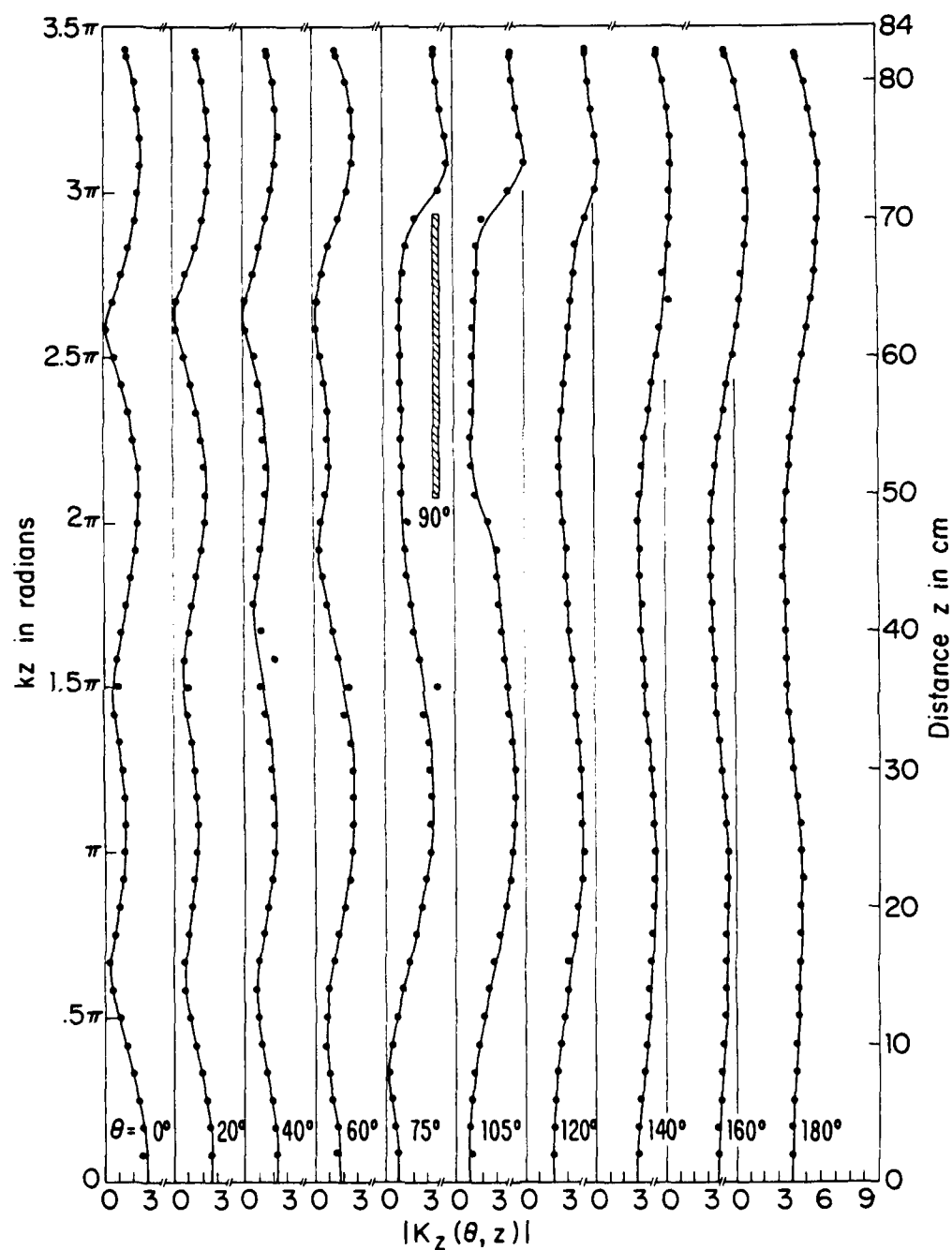


Figure 30. Measured Magnitude of Surface Density of Axial Current on Vertical Cylinder with Crossed Flat Plate;  $ka = 1$ ,  $kh = 3.5\pi$ ,  $kh_1 = 2.5\pi$ ;  $k\lambda = 1.5$ ,  $kL = 0.5\pi$ ,  $kT = 0.054\pi$ . ( $|K_z|$  in Arbitrary Units.)



is excited directly by the incident field which is H-polarized for it. The plate is wide enough so that  $K_z(x,z)$  is significant. Its magnitude on the illuminated and shadowed sides is shown in Fig. 31 as a function of  $k(x - a)$  at seven values of  $kz$  spaced across the width of the plate. It is seen to be zero at the junction with the cylinder and to increase very gradually to large values at the open edge. It is substantially greater on the illuminated side than in the shadow. The magnitude of the associated component  $K_x(x,z)$  is shown in Fig. 32, also as a function of  $k(x - a)$ . This is seen to have a standing-wave pattern to match that for the charge density in Fig. 29. The outward current has a maximum across the grooves at the junction and at a half-wavelength out toward the open edge, where it vanishes. The amplitude of  $K_x(x,z)$  as a function of  $kz$  is greatest at the long edges where  $kz = 2.5\pi \pm 0.25\pi$  and smallest along the center of the plate. More complete data, including graphs of the phases, are in Reference 22.

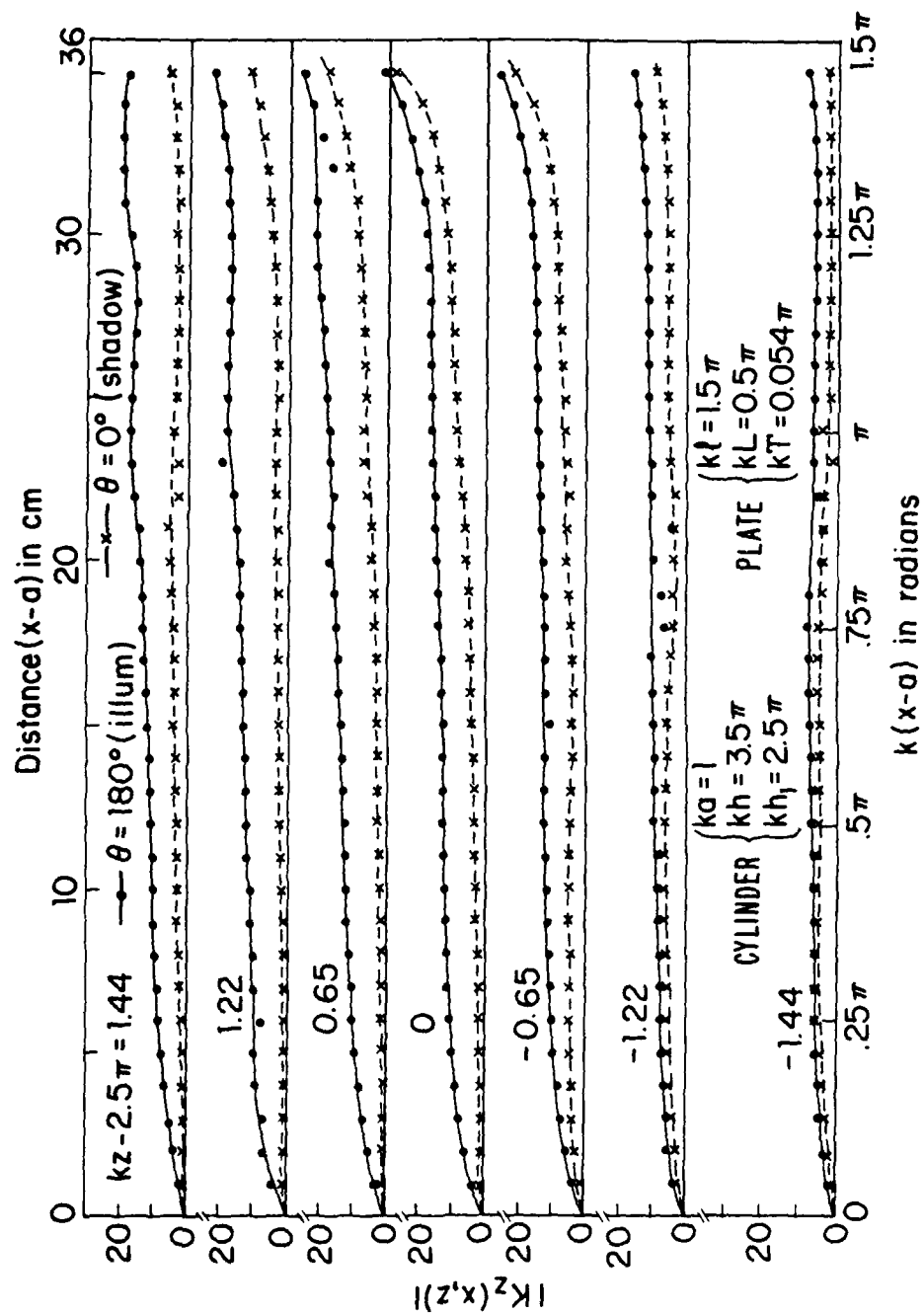


Figure 31. Measured Magnitude of Surface Density of Current  $K_z(x, z)$  on Horizontal Plate. ( $|K_z|$  in Arbitrary Units.)

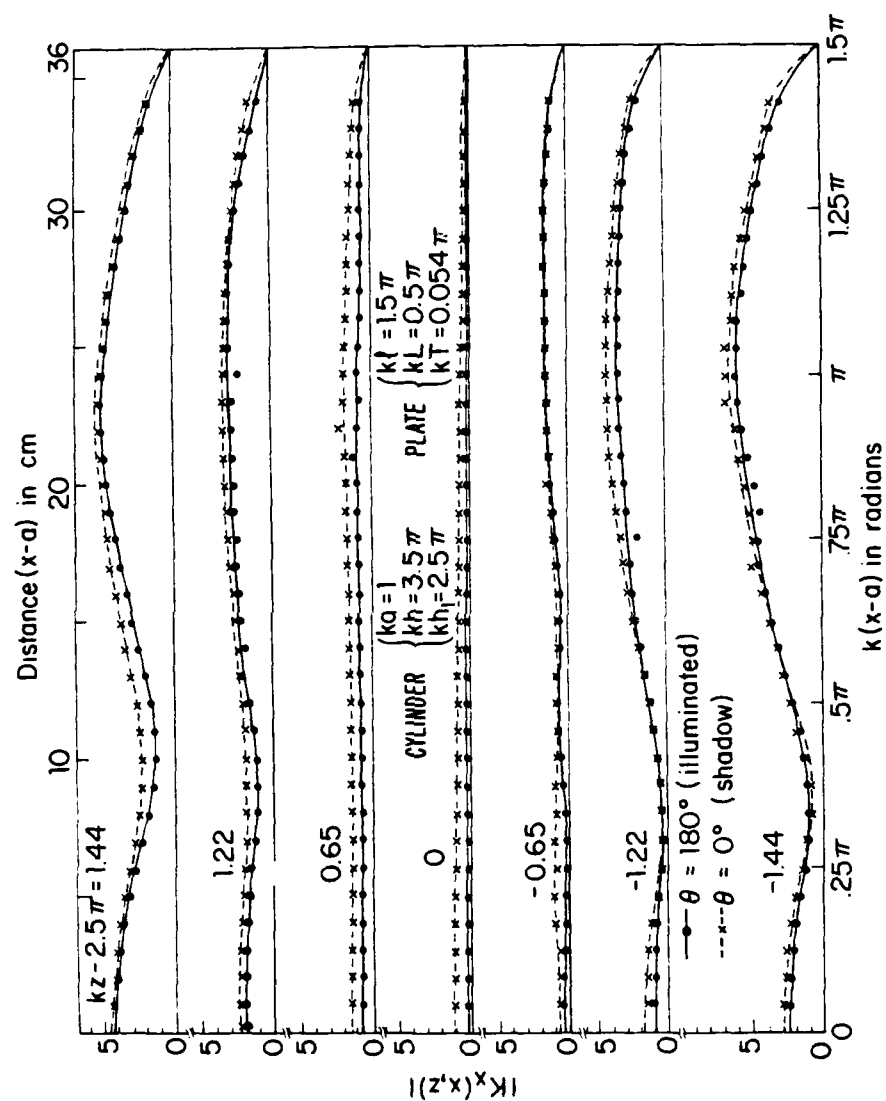


Figure 32. Measured Magnitude of Surface Density of Current  $K_x(x, z)$  on Horizontal Flat Plate. ( $|K_x|$  in Arbitrary Units.)

SECTION IX  
NON-ORTHOGONALLY INTERSECTING CYLINDERS

The determination of the currents and charges on the surfaces of conductors that intersect at angles  $\Delta$  other than  $90^\circ$  either as a continuing cross as in Reference 16 or to achieve the swept-wing configuration in Fig. 33 can be accomplished for electrically thin cylinders by a generalization of the analytical procedure described for orthogonal conductors. All of the thin-cylinder conditions previously imposed when  $\Delta = 90^\circ$  must be satisfied and, in addition, a restriction on the angle of intersection  $\Delta$  must be enforced. This is needed in order to keep the junction region electrically small enough to preserve the validity of the assumption that the total charge on its surfaces is negligible. The new condition is:

$$|\sin \Delta| \gg ka \quad (42)$$

where  $\Delta$  is the angle between adjacent arms. When  $\Delta = 90^\circ$ , this reduces to the previously imposed condition,  $ka \ll 1$ .

The integral equations for the currents in the swept-wing configuration shown in Fig. 33 are derived in the same manner as those for the orthogonal cross but several additional terms and integrals occur since the crossed conductors are now coupled inductively as well as capacitively. In order to permit the ready correlation with the equations for the orthogonal cross, the notation shown in Fig. 33 is used. As before, the vertical member extends from  $z = -h_1$  to  $z = h_2$  with the junction at the origin. The arms are taken to be equal and of length  $l$  with the variable  $s$  ranging from  $s = -l$  to  $s = 0$  along the left arm and from  $s = 0$  to  $s = l$  along the right arm. Note that when  $\Delta = 90^\circ$ ,  $s$  becomes  $x$  and the entire notation reduces to that of the orthogonal cross.

The boundary conditions requiring the vanishing of the tangential component of the electric field on the surfaces  $\rho = a$  of the conductors, each with radius  $a$ , now have the form:

$$E_z(z) = E_z^{(i)} - \partial\phi(z)/\partial z - j\omega A_z(z) = 0 \quad ; \quad -h_1 \leq z \leq h_2 \quad (43a)$$

$$E_s(s) = -E_z^{(i)} \cos \Delta - \partial\phi_3(s)/\partial s - j\omega A_{3s}(s) = 0 \quad ; \quad -l \leq s \leq 0 \quad (43b)$$

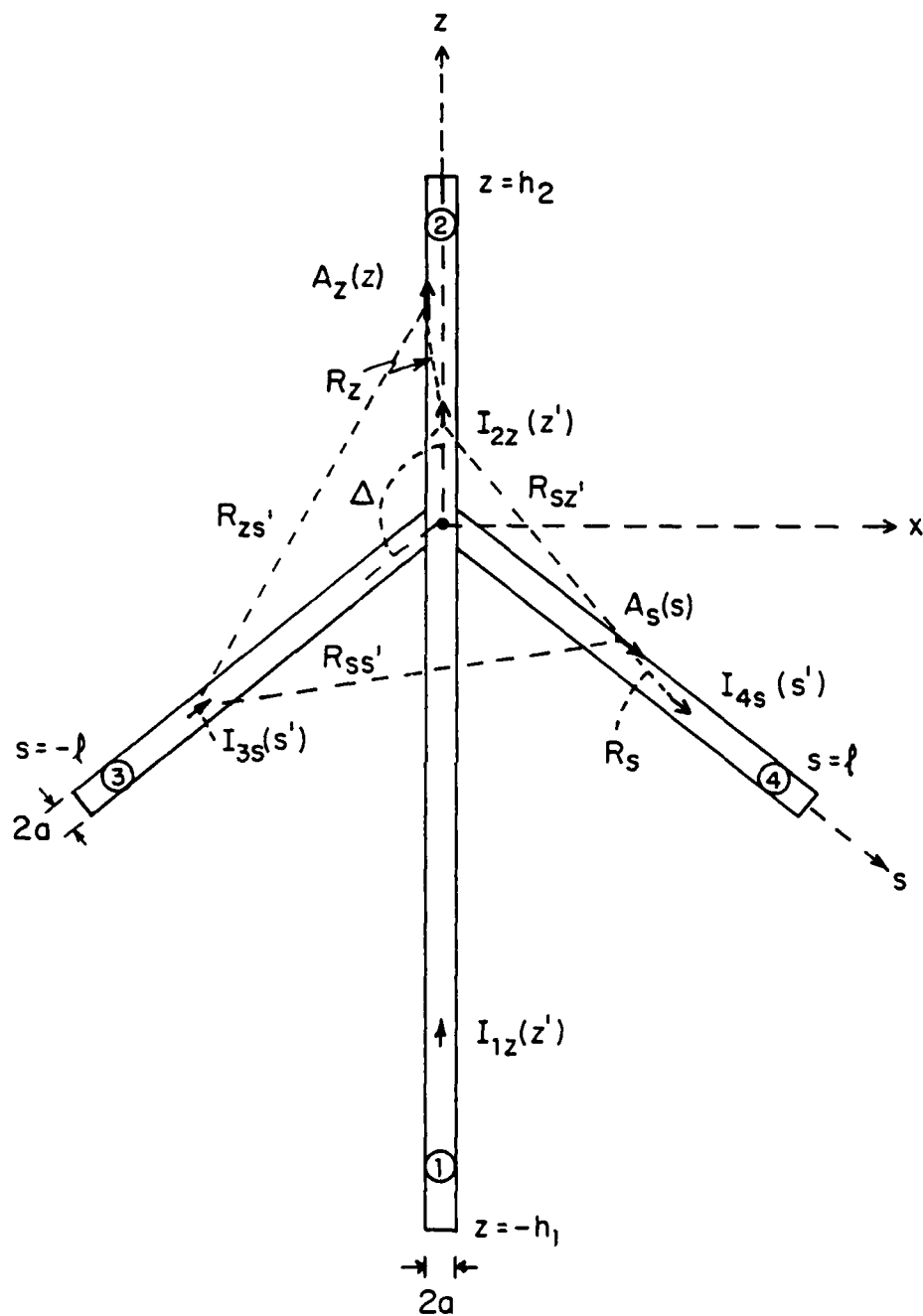


Fig. 33. Swept-Wing Thin-Wire Cross.

$$E_s(s) = E_z^{(i)} \cos \Delta - \partial \phi_4(s) / \partial s - j\omega A_{4s}(s) = 0 \quad ; \quad 0 \leq s \leq l \quad (43c)$$

for a normally incident field,  $\vec{E}^{(i)} = \hat{z} E_z^{(i)}$ . The time dependence  $e^{j\omega t}$  is used. A consequence of symmetry is that the currents and charges, and the vector and scalar potentials on the two side arms satisfy the following relations:

$$I_{3s}(-s) = -I_{4s}(s) \quad , \quad q_3(s) = q_4(-s) \quad ; \quad A_{3s}(-s) = -A_{4s}(s) \quad , \quad \phi_3(-s) = \phi_4(s) \quad (44)$$

Hence, it is necessary to determine only  $I_{1z}(z)$ ,  $I_{2z}(z)$ , and  $I_{4s}(s)$ . With the relations (44), the vector and scalar potentials in Eq. (43a) are:

$$A_z(z) = (\mu_0/4\pi) \left\{ \int_{-h_1}^{h_2} I_z(z') K(z, z') dz' + 2 \cos \Delta \int_0^l I_s(s') K(z, s', \Delta) ds' \right\} \quad (45)$$

$$\phi(z) = (1/4\pi\epsilon_0) \left\{ \int_{-h_1}^{h_2} q(z') K(z, z') dz' + 2 \int_0^l q(s') K(z, s', \Delta) ds' \right\} \quad (46)$$

where  $K(z, z') = e^{-jkR_z}/R_z$  with  $R_z = [(z - z')^2 + a^2]^{1/2}$  and  $K(z, s', \Delta) = e^{-jkR_{zs'}}/R_{zs'}$ , with  $R_{zs'} = [z^2 + s'^2 - 2zs' \cos \Delta + a^2]^{1/2}$ . Similarly, in Eq. (43c):

$$A_{4s}(s) = (\mu_0/4\pi) \left\{ \int_0^l I_s(s') [K(s, s') + K(s, s', \Delta) \cos 2\Delta] ds' + \cos \Delta \int_{-h_1}^{h_2} I_z(z') K(s, z', \Delta) dz' \right\} \quad (47)$$

$$\phi_4(s) = (1/4\pi\epsilon_0) \left\{ \int_0^l q(s') [K(s, s') + K(s, s', \Delta)] ds' + \int_{-h_1}^{h_2} q(z') K(s, z', \Delta) dz' \right\} \quad (48)$$

where  $K(s, s') = e^{-jkR_s}/R_s$  with  $R_s = [(s - s')^2 + a^2]^{1/2}$ ,  $K(s, s', \Delta) = e^{-jkR_{ss'}}/R_{ss'}$ , with  $R_{ss'} = [s^2 + s'^2 - 2ss' \cos 2\Delta + a^2]^{1/2}$  and  $K(s, z', \Delta) = e^{-jkR_{sz'}}/R_{sz'}$ , with  $R_{sz'} = [s^2 + z'^2 - 2|s|z' \cos \Delta + a^2]^{1/2}$ . When Eqs. (45) - (48) are substituted in Eqs. (43a) and (43c), the following simultaneous integral equations

in the currents and charges are obtained:

$$\begin{aligned}
 & \int_{-h_1}^{h_2} I_z(z') K(z, z') dz' + 2 \cos \Delta \int_0^{\ell} I_s(s') K(z, s', \Delta) ds' \\
 & - (j\omega/k^2) (\partial/\partial z) \left[ \int_{-h_1}^{h_2} q(z') K(z, z') dz' + 2 \int_0^{\ell} q(s') K(z, s', \Delta) ds' \right] \\
 & = -(j4\pi/\omega\mu_0) E_z^{(i)} \quad (49)
 \end{aligned}$$

$$\begin{aligned}
 & \int_0^{\ell} I_s(s') [K(s, s') + K(s, s', \Delta) \cos 2\Delta] ds' + \cos \Delta \int_{-h_1}^{h_2} I_z(z') K(s, z', \Delta) dz' \\
 & - (j\omega/k^2) (\partial/\partial s) \left\{ \int_0^{\ell} q(s') [K(s, s') + K(s, s', \Delta)] ds' + \int_{-h_1}^{h_2} q(z') K(s, z', \Delta) dz' \right\} \\
 & = -(j4\pi/\omega\mu_0) E_z^{(i)} \cos \Delta \quad (50)
 \end{aligned}$$

With  $\partial/\partial z = -\partial/\partial z'$  in  $K(z, z')$ ,  $\partial/\partial s = -\partial/\partial s'$  in  $K(s, s')$ ,  $\partial/\partial s = \partial/\partial s'$  in  $K(s, s', \Delta)$ , and integration by parts, it follows that:

$$\begin{aligned}
 j\omega(\partial/\partial z) \int_{-h_1}^{h_2} q(z') K(z, z') dz' &= -j\omega [q(h_2) K(z, h_2) - q(-h_1) K(z, -h_1)] \\
 &- \int_{-h_1}^{h_2} [\partial^2 I_z(z') / \partial z'^2] K(z, z') dz' \quad (51)
 \end{aligned}$$

$$\begin{aligned}
 j\omega(\partial/\partial s) \int_0^{\ell} q(s') [K(s, s') + K(s, s', \Delta)] ds' &= -j\omega q(\ell) [K(s, \ell) - K(s, \ell, \Delta)] \\
 &- \int_0^{\ell} [\partial^2 I_s(s') / \partial s'^2] [K(s, s') - K(s, s', \Delta)] ds' \quad (52)
 \end{aligned}$$

With these expressions, the integral equations (49) and (50) become:

$$\begin{aligned}
 & \int_{-h_1}^{h_2} [\partial^2 I_z(z') / \partial z'^2 + k^2 I_z(z')] K(z, z') dz' - F_2(z, \Delta) - F_3(z) - F_4(z, \Delta) \\
 & = - \frac{j4\pi k^2}{\omega\mu_0} E_z^{(i)} \quad (53)
 \end{aligned}$$

$$\int_0^{\ell} [\partial^2 I_s(s')/\partial s'^2 + k^2 I_s(s')] [K(s, s') - K(s, s', \Delta)] ds' - F_2(s, \Delta) - F_3(s, \Delta) - F_4(s, \Delta) - F_5(s, \Delta) = - \frac{j4\pi k^2}{\omega \mu_0} E_z^{(i)} \cos \Delta \quad (54)$$

where

$$F_2(z, \Delta) = 2j\omega(\partial/\partial z) \int_0^{\ell} q(s') K(z, s', \Delta) ds' \quad (55a)$$

$$F_3(z) = -j\omega[q(h_2)K(z, h_2) - q(-h_1)K(z, -h_1)] \quad (55b)$$

$$F_4(z, \Delta) = 2k^2 \cos \Delta \int_0^{\ell} I_s(s') K(z, s', \Delta) ds' \quad (55c)$$

and

$$F_2(s, \Delta) = j\omega(\partial/\partial s) \int_{-h_1}^{h_2} q(z') K(s, z', \Delta) dz' \quad (56a)$$

$$F_3(s, \Delta) = 2j\omega q(\ell) [K(s, \ell) - K(s, \ell, \Delta)] \quad (56b)$$

$$F_4(s, \Delta) = k^2 \cos \Delta \int_{-h_1}^{h_2} I_z(z') K(s, z', \Delta) dz' \quad (56c)$$

$$F_5(s, \Delta) = k^2(1 + \cos 2\Delta) \int_0^{\ell} I_s(s') K(s, s', \Delta) ds' \quad (56d)$$

With electrically thin conductors, the real parts of the kernels  $K(z, z')$  and  $K(s, s')$  have very sharp peaks at  $z' = z$  and  $s' = s$  so that

$$(\partial^2/\partial z^2 + k^2) I_z(z) \doteq Ak^2 + \Psi^{-1} [F_1(z) + F_2(z, \Delta) + F_3(z) + F_4(z, \Delta)] \quad (57)$$

$$(\partial^2/\partial s^2 + k^2) I_s(s) \doteq Ak^2 \cos \Delta + \Psi^{-1} [F_1(s, \Delta) + F_2(s, \Delta) + F_3(s, \Delta) + F_4(s, \Delta) + F_5(s, \Delta)] \quad (58)$$

where



$$F_1(z) = -j \int_{-h_1}^{h_2} [\partial^2 I_z(z') / \partial z'^2 + k^2 I_z(z')] K_I(z, z') dz' \quad (59)$$

$$F_1(s, \Delta) = -j \int_0^{\ell} [\partial^2 I_s(s') / \partial s'^2 + k^2 I_s(s')] [K_I(s, s') - K_I(s, s', \Delta)] ds' \quad (60)$$

and

$$\Psi = \int_{-h_1}^{h_2} K_R(0, z') dz' = 2[\ln(2/ka) - 0.5772] \quad (61a)$$

or

$$\Psi = \int_0^{\ell} [K_R(0, s') - K_R(0, s', \Delta)] ds' = \int_{-\ell}^{\ell} K_R(0, s') ds' = 2[\ln(2/ka) - 0.5772] \quad (61b)$$

The value of  $\Psi$  in Eqs. (61a,b) is valid when  $kh_1 \geq \pi/2$ ,  $kh_2 \geq \pi/2$ ,  $k\ell \geq \pi/2$ . In Eqs. (57) and (58),  $A = -(j4\pi/\omega\mu_0\Psi)E_{z0}^{(1)} = (-j/60\pi\Psi)(E_{z0}^{(1)}/\lambda)$  where  $\lambda$  is the wavelength.

The solutions of Eqs. (53) and (54) include the simple solutions of the homogeneous equations and sums of particular integrals. The formulas for the currents are:

$$I_{1z}(z) = A[C_1' \cos kz + C_1'' \sin kz + 1 + H_h(z, \Delta)/\Psi] ; -h_1 \leq z \leq 0 \quad (62a)$$

$$I_{2z}(z) = A[C_2' \cos kz + C_2'' \sin kz + 1 + H_h(z, \Delta)/\Psi] ; 0 \leq z \leq h_2 \quad (62b)$$

$$I_{4s}(s) = -I_{3s}(-s) = A[C_4' \cos ks + C_4'' \sin ks + (1 - \cos ks)\cos \Delta + H_\ell(s, \Delta)/\Psi] ; 0 \leq s \leq \ell \quad (62c)$$

where the particular integrals occurring on the right are evaluated with the formula:

$$T_1(z) = k^{-1} \int_0^z F_1(u) \sin k(z - u) du \quad (63)$$

Specifically for  $F_1(z)$ ,  $F_1(u) = Ak^2$ . This gives  $T_1(z) = 1 - \cos kz$ . The term  $\cos kz$  can be incorporated with  $C' \cos kz$ , leaving 1 as in Eq. (62a). For  $F_1(s, \Delta)$ ,  $F_1(u) = Ak^2 \cos \Delta$  and Eq. (63) gives  $T_1(s, \Delta) = (1 - \cos ks)\cos \Delta$  as shown in Eq. (62c). The terms  $H_h(z, \Delta)$  and  $H_\ell(s, \Delta)$  contain the other

particular integrals. Specifically,  $H_h(z, \Delta) = T_1(z) + \sum_{i=2}^4 T_i(z, \Delta)$  and  $H_s(s, \Delta) = \sum_{i=1}^5 T_i(s, \Delta)$  where  $T_1$  is given by Eq. (63).  $F_1(z)$  and  $F_1(s, \Delta)$  are given by Eqs. (59) and (60);  $F_i(z, \Delta)$  and  $F_i(s, \Delta)$  with  $i > 1$  are given by Eqs. (55a-c) and (56a-d). The  $C$ 's are arbitrary constants to be evaluated from the end and junction conditions. The charges per unit length corresponding to Eqs. (62a-c) are obtained with the equation of continuity,  $\partial I_z(z)/\partial z + j\omega q(z) = 0$  and  $\partial I_s(s)/\partial s + j\omega q(s) = 0$ . They are:

$$q_1(z) = (-jAk/\omega)[C_1' \sin kz - C_1'' \cos kz - jH_h'(z, \Delta)/\omega\psi] \quad (64a)$$

$$q_2(z) = (-jAk/\omega)[C_2' \sin kz - C_2'' \cos kz - jH_h'(z, \Delta)/\omega\psi] \quad (64b)$$

$$q_4(s) = q_3(-s) = (-jAk/\omega)[C_4' \sin ks - C_4'' \cos ks - jH_s'(s, \Delta)/\omega\psi] \quad (64c)$$

where  $H'$  is the derivative with respect to the argument  $kz$  or  $ks$ .

Since  $H_h(0, \Delta)$  and  $H_s(0, \Delta)$  vanish at  $z = s = 0$ , they are not involved in the application of the junction conditions,  $I_{1z}(0) - I_{2z}(0) - 2I_{4s}(0) = 0$  and  $q_1(0) = q_2(0) = q_3(0) = q_4(0)$ . These give  $C_1'' = C_2'' = C_3'' = C_4'' = C''$  and  $C_1' - C_2' - 2C_4' = 0$ . The end conditions,  $I_{1z}(-h_1) = I_{2z}(h_2) = I_{3s}(-l) = I_{4s}(l) = 0$ , must be applied to whatever order of solution is required. For a zero-order solution, they give

$$[I_{1z}(-h_1)]_0 = A[C_1' \cos kh_1 - C'' \sin kh_1 + 1] = 0 \quad (65a)$$

$$[I_{2z}(h_2)]_0 = A[C_2' \cos kh_2 + C'' \sin kh_2 + 1] = 0 \quad (65b)$$

$$[I_{4s}(l)]_0 = -[I_{3s}(-l)]_0 = A[C_4' \cos kl + C'' \sin kl + (1 - \cos kl)\cos \Delta] = 0 \quad (65c)$$

These equations can be solved for  $C_i'$ ,  $i = 1, 2, 4$ , in terms of  $C''$  and substituted in  $C_1' - C_2' - 2C_4' = 0$  to obtain:

$$C'' = \frac{\sec kh_1 - \sec kh_2 - 2(1 - \cos kl)\sec kl \cos \Delta}{\tan kh_1 + \tan kh_2 + 2 \tan kl} \quad (66)$$

Once  $C'$  and  $C''$  have been determined, the zero-order currents are known. They are:

$$[I_{1z}(z)]_0 = -AW\{\sin k(h_1 + z) + \sin k(h_2 - z) - \sin k(h_1 + h_2) + 2 \cos kh_2 \\ \times [\tan kl (\cos kz - \cos kh_1) + \cos \Delta (1 - \cos kl)\sec kl \\ \times \sin k(h_1 + z)]\} \quad (67a)$$

$$[I_{2z}(z)]_0 = -AW\{\sin k(h_1 + z) + \sin k(h_2 - z) - \sin k(h_1 + h_2) + 2 \cos kh_1 \\ \times [\tan kl (\cos kz - \cos kh_2) - \cos \Delta (1 - \cos kl)\sec kl \\ \times \sin k(h_2 - z)]\} \quad (67b)$$

$$[I_{4s}(s)]_0 = AW \sec kl\{(\cos kh_1 - \cos kh_2)\sin k(\ell - s) - \cos \Delta \sin k(h_1 + h_2) \\ \times (\cos ks - \cos kl) - 2 \cos \Delta \cos kh_1 \cos kh_2 [\sin k(\ell - s) \\ + \sin ks - \sin kl]\} \quad (67c)$$

where

$$W = [\sin k(h_1 + h_2) + 2 \tan kl \cos kh_1 \cos kh_2]^{-1} \quad (68)$$

Note that  $I_{3s}(-s) = -I_{4s}(s)$ . With  $\Delta = 90^\circ$ , these expressions reduce to those previously obtained for the currents in an orthogonal cross when  $\ell_1 = \ell_2 = \ell$ . The zero-order charges per unit length corresponding to the currents in Eqs. (67a-c) are:

$$[q_1(z)]_0 = (-jkAW/\omega)\{\cos k(h_1 + z) - \cos k(h_2 - z) - 2 \cos kh_2 [\tan kl \sin kz \\ - \cos \Delta (1 - \cos kl)\sec kl \cos k(h_1 + z)]\} \quad (69a)$$

$$[q_2(z)]_0 = (-jkAW/\omega)\{\cos k(h_1 + z) - \cos k(h_2 - z) - 2 \cos kh_1 [\tan kl \sin kz \\ - \cos \Delta (1 - \cos kl)\sec kl \cos k(h_2 - z)]\} \quad (69b)$$

$$\begin{aligned}
[q_4(s)]_0 = & (-jkAW/\omega \cos k\ell) \{ (\cos kh_1 - \cos kh_2) \cos k(\ell - s) - \cos \Delta \\
& \times \sin k(h_1 + h_2) \sin ks + 2 \cos \Delta \cos kh_1 \cos kh_2 [\cos ks \\
& - \cos k(\ell - s)] \} \quad (69c)
\end{aligned}$$

Note that  $q_3(-s) = q_4(s)$  and that, with  $i = 1, \dots, 4$ , the charge per unit length on each conductor at the junction is:

$$\begin{aligned}
[q_i(0)]_0 = & (-jkAW/\omega) \{ \cos kh_1 - \cos kh_2 + 2 \cos \Delta \cos kh_1 \cos kh_2 (1 - \cos k\ell) \\
& \times \sec k\ell \} \quad (70)
\end{aligned}$$

The effect of the presence of the side arms is especially significant when their electrical length  $k\ell$  is  $\pi/2$  or  $\pi$ . Although the zero-order formulas for the currents and charges per unit length are not quantitatively accurate when  $kh_1$ ,  $kh_2$  and  $k\ell$  are all integral multiples of  $\pi/2$ , it is possible to obtain useful, relatively simple, expressions when  $k\ell$  is  $\pi/2$  or  $\pi$  but  $kh_1$  and  $kh_2$  are not. Thus, when  $k\ell \rightarrow \pi/2$ ,  $\tan k\ell \rightarrow \infty$  and from Eq. (68),  $W \rightarrow 1/(2 \tan k\ell \cos kh_1 \cos kh_2)$ . If this is used in Eqs. (67a-c) and (69a-c), finite zero-order currents and charges per unit length are obtained. They are:

$$\begin{aligned}
[I_{1z}(z)]_0 = & -A \sec kh_1 [\cos kz - \cos kh_1 + \cos \Delta \sin k(h_1 + z)] ; \\
& -h_1 \leq z \leq 0 \quad (71a)
\end{aligned}$$

$$\begin{aligned}
[I_{2z}(z)]_0 = & -A \sec kh_2 [\cos kz - \cos kh_2 - \cos \Delta \sin k(h_2 - z)] ; \\
& 0 \leq z \leq h_2 \quad (71b)
\end{aligned}$$

$$\begin{aligned}
[I_{4s}(s)]_0 = & A \left\{ \frac{\cos kh_1 - \cos kh_2 - \cos \Delta \sin k(h_1 + h_2)}{2 \cos kh_1 \cos kh_2} \cos ks \right. \\
& \left. - \cos \Delta (\cos ks + \sin ks - 1) \right\} ; 0 \leq s \leq \ell \quad (71c)
\end{aligned}$$

$$[q_1(z)]_0 = (jKA/\omega \cos kh_1) [\sin kz + \cos \Delta \cos k(h_1 + z)] ; -h_1 \leq z \leq 0 \quad (72a)$$

$$[q_2(z)]_0 = (j k A / \omega \cos kh_2) [\sin kz + \cos \Delta \cos k(h_2 - z)] ; 0 \leq z \leq h_2 \quad (72b)$$

$$[q_4(s)]_0 = (j k A / \omega) \left\{ \frac{\cos kh_1 - \cos kh_2 - \cos \Delta \sin k(h_1 + h_2)}{2 \cos kh_1 \cos kh_2} \sin ks + \cos \Delta (\cos ks - \sin ks) \right\} ; 0 \leq s \leq l \quad (72c)$$

These formulas reveal that when low-impedance arms with  $k l = \pi/2$  are attached to the vertical member, they completely suppress the zero-order currents and charges that are induced in it in the absence of the arms. These are given by the first three terms in Eqs. (67a) and (67b), the first two terms in Eqs. (69a) and (69b). When  $\Delta = 90^\circ$ , the amplitude of the currents in the horizontal arms is determined by the discontinuity in the vertical current at the junction, viz.,  $|\sec kh_2 - \sec kh_1|$ . This can range from zero to two, depending on the values of  $kh_1$  and  $kh_2$ . When  $\Delta \neq 90^\circ$ , the vertical arms carry additional, oppositely directed currents that continue into the side arms. Also induced in the side arms are currents that are independent of the vertical member and simply oscillate in each arm. For example, in arm 4 the added current has the form  $\cos \Delta (\cos ks + \sin ks - 1)$  which is zero at  $s = 0$  and at  $s = l$  and has associated with it a charge per unit length with the form  $\cos \Delta (\cos ks - \sin ks)$ . This has the magnitude  $\cos \Delta$  at both  $s = 0$  and  $s = l$ .

When  $k l = \pi$ ,  $\tan k l = 0$  and  $W = 1/\sin k(h_1 + h_2)$ . It follows that the zero-order currents and charges are:

$$[I_{1z}(z)]_0 = -A[\sin k(h_1 + z) + \sin k(h_2 - z) - \sin k(h_1 + h_2) - 4 \cos \Delta \times \cos kh_2 \sin k(h_1 + z)]/\sin k(h_1 + h_2) \quad (73a)$$

$$[I_{2z}(z)]_0 = -A[\sin k(h_1 + z) + \sin k(h_2 - z) - \sin k(h_1 + h_2) + 4 \cos \Delta \times \cos kh_1 \sin k(h_2 - z)]/\sin k(h_1 + h_2) \quad (73b)$$

$$[I_{4s}(s)]_0 = -A\{[\cos kh_1 - \cos kh_2 - 4 \cos \Delta \cos kh_1 \cos kh_2] \times \sin ks/\sin k(h_1 + h_2) - \cos \Delta (\cos ks + 1)\} \quad (73c)$$

$$[q_1(z)]_0 = (-jKA/\omega) [\cos k(h_1 + z) - \cos k(h_1 - z) - 4 \cos \Delta \cos kh_2 \\ \times \cos k(h_1 + z)] / \sin k(h_1 + h_2) \quad (74a)$$

$$[q_2(z)]_0 = (-jKA/\omega) [\cos k(h_1 + z) - \cos k(h_1 - z) - 4 \cos \Delta \cos kh_1 \\ \times \cos k(h_2 - z)] / \sin k(h_1 + h_2) \quad (74b)$$

$$[q_4(s)]_0 = (-jKA/\omega) \{ [\cos kh_1 - \cos kh_2 - 4 \cos \Delta \cos kh_1 \cos kh_2] \\ \times \cos ks / \sin k(h_1 + h_2) + \cos \Delta \sin ks \} \quad (74c)$$

These are quite different from those with  $kl = \pi/2$ . When  $kl = \pi$  and  $\Delta = 90^\circ$ , the zero-order currents and charges per unit length on the vertical member are actually the same as when the side arms are absent. The zero-order currents on the horizontal members vanish at the junction; they oscillate in the self-resonant mode, excited by the charges maintained at the junction by the vertical currents. These are proportional to  $|\cos kh_1 - \cos kh_2|$ . When  $\Delta \neq 90^\circ$ , additional, oppositely directed currents are induced on the vertical members and these continue into the side arms where they are distributed as a shifted cosine,  $(1 + \cos ks)\cos \Delta$ . There is also an added term in the self-resonant current proportional to  $\sin ks$ .

More accurate currents and charges per unit length can be obtained for all arms and lengths by evaluating the first-order terms obtained by the substitution of the zero-order currents and charges in the particular integrals contained in  $H_h(z, \Delta)$  and  $H_h(s, \Delta)$ . Since they cannot all be evaluated analytically, numerical integration is necessary. The first-order terms are needed especially when  $kh_1$  and  $kh_2$  are integral multiples of  $\pi/2$ .

The formulas derived for the currents on the swept-wing cross are useful only within the limits of thin-cylinder theory and when  $kh_1 > 1$ ,  $kh_2 > 1$ , and  $kl > 1$ . When one or more of the arms is electrically short, the rotationally symmetric part of the current does not dominate. The transverse Fourier components of the first order with a transverse variation  $\cos \theta$  ultimately dominate as  $ka$  is reduced. The surface currents associated with this mode are readily determined as explained in an earlier section. They are proportional

to the local tangential magnetic field on each conducting surface and require no end or junction conditions.

The distributions of current and charge per unit length can be determined on the swept-wing structure for other than normally incident fields in the general manner described for the orthogonal cross with equal arms. This is true only for electrically thin structures with angles that satisfy Eq. (42). The current and charge densities on swept-wing structures composed of an intersecting electrically thick cylinder and an electrically wide flat plate can be studied experimentally in the manner described for  $\Delta = 90^\circ$ .

SECTION X  
PENETRATION OF FIELDS INTO THE INTERIOR THROUGH AN OPEN END

The intensity of an electromagnetic field that penetrates into the interior of a conducting tube through a small aperture in the cylindrical surface is proportional to the densities of current and charge on the unbroken surface at the location of the aperture. The calculation of these fields is treated in References 23 and 24. A closely related but analytically quite different problem is the field that penetrates into the interior at the open tubular end or that enters an aircraft through a conductively open, radome-covered nose. The currents and charges excited by such a field on the inner surfaces of a tubular cylinder have been calculated directly from the general analysis of Kao in Reference 1 which provides the current and charge densities on both the inside and outside surfaces of a tubular cylinder illuminated by a normally incident field. Examples of the currents on the inside surface are shown in Figs. 12a and 12b for electrically thin cylinders with  $ka = 0.05$  and  $0.01$ . Although these inside currents decrease exponentially inward from the open end, they are always equal to the outside currents at the end and are, therefore, significant even when  $ka$  is very small. When  $ka$  is not small but is below the cut-off for waveguide modes in the interior, the situation is quite similar but the distance of penetration with significant amplitude is greater. This is shown for a tube with  $ka = 1$  in Reference 3 where in Fig. 17 is shown the inside axial current, in Fig. 18 the inside transverse current, and in Fig. 19 the inside charge density. These are all significant within distances of the open end comparable with the radius of the tube. When the inside radius exceeds the cut-off value for a waveguide mode in the interior, this is excited at the open end as described and discussed in Reference 21. Since the frequency spectrum contained in an electromagnetic pulse extends over a wide range of values of  $ka$ , the three cases with  $ka \leq 0.1$ ,  $0.1 \leq ka < ka_c$ , and  $ka_c < ka$  must be included in a consideration of currents, charges, and fields inside the open or radome-covered end of a tubular conductor.



## SECTION XI

### SUMMARY AND CONCLUSION

The currents and charges induced on crossed metal structures by an incident electromagnetic pulse are best investigated in three frequency ranges. At very low frequencies when  $ka < kh < 1$ , the only significant currents are those associated with the first-order transverse Fourier component. They are directly proportional and comparable in magnitude to the component of the incident magnetic field  $H_t^{(i)}$  tangent to the metal surface. They are readily determined at each point on the surface since they are independent of all dimensional parameters. At somewhat higher frequencies when  $ka \leq 0.1$  and  $1 < kh < \infty$ , the dominant currents and charges are the total axial ones derived from the rotationally symmetrical, zero-order Fourier components, viz.,  $I = 2\pi a[K]_0$ ,  $q = 2\pi a[\eta]_0$ . They are governed by the well developed, quasi-one-dimensional integral equations of thin-wire theory with the associated end and junction conditions which have strong effects on the axial distributions. When  $ka > 0.1$ , first- and higher-order Fourier components become important in the axially directed current density and associated charge density. In addition, significant transverse currents with associated charges must be considered. They combine with the axial currents to maintain three-dimensional standing-wave patterns on the surfaces. In general, the distributions on intersecting conductors are quite similar to those on each member when isolated in the same incident field except quite near and in the junction region.

AD-A103 057

DIKEWOOD INDUSTRIES INC ALBUQUERQUE NM F/G 20/3  
INTEGRAL-EQUATION SOLUTIONS AND MEASUREMENTS FOR CURRENTS AND C--ETC(U)  
JUN 80 R W KING F29601-79-C-0149  
DC-FR-1289-4

AFWL-TR-79-135

NL

UNCLASSIFIED

2 of 2

AD-A103 057



END

DATE

FILED

9 81

DTIC

# REFERENCES

- [1] Kao, C.C., "Three-Dimensional Electromagnetic Scattering from a Circular Tube of Finite Length," J. Appl. Phys., vol. 40, November 1969, pp. 4732-4740.
- [2] Burton, R.W., R. W. P. King, and D. J. Blejer, "Surface Currents and Charges on an Electrically Thick Conducting Tube in an E-Polarized, Normally Incident, Plane-Wave Field, 2, Measurements," Radio Science, vol. 11, August-September 1976, pp. 701-711.
- [3] King, R.W.P., B. Sandler, T. T. Wu, R. W. Burton, C. C. Kao, and L. C. Shen, "Surface Currents and Charges on an Electrically Thick Conducting Tube in an E-Polarized, Normally Incident, Plane-Wave Field, 1, Theory," Radio Science, vol. 11, August-September 1976, pp. 687-699.
- [4] Burton, R.W., R. W. P. King and D. J. Blejer, "Surface Currents and Charges on an Electrically Thick and Long Conducting Tube in E- and H-Polarized, Normally Incident, Plane-Wave Fields," Radio Science, vol. 13, January-February 1978, pp. 75-91.
- [5] King, R.W.P., D. J. Blejer, and B. H. Sandler, "Current Induced on Single and Crossed Electrically Short and Thin Tubular Cylinders by a Normally Incident, Plane Electromagnetic Wave," submitted for publication.
- [6] Taylor, C.D., and C. W. Harrison, Jr., "Current and Charge Densities Induced on the Surface of a Prolate Spheroid Illuminated by a Plane-Wave Electromagnetic Field," IEEE Trans. Electromagn. Compat., vol. EMC-19, August 1977, pp. 127-131.
- [7] Burton, R.W., and R. W. P. King, "Induced Currents and Charges on Thin Cylinders in a Time-Varying Electromagnetic Field," IEEE Trans. Electromagn. Compat., vol. EMC-17, August 1975, pp. 149-155.
- [8] Chen, C.-L., and T. T. Wu, "Theory of the Long Dipole Antenna," Ch. 10 in Antenna Theory, Part I, R. E. Collin and F. J. Zucker, Eds., McGraw-Hill, New York, 1969, pp. 446-454.
- [9] Chen, C.-L., "On the Scattering of Electromagnetic Waves from a Long Wire," Radio Science, vol. 3, June 1968, pp. 585-598.

- [10] Harrington, R.F., Field Computation by Moment Methods, Macmillan Co., New York, 1968, p. 78, Fig. 4.11.
- [11] King, R.W.P., "Current Distribution in Arbitrarily Oriented Receiving and Scattering Antenna," IEEE Trans. Antennas Propagat., vol. AP-20, March 1972, pp. 152-159.
- [12] King, R.W.P., A. W. Glisson, S. Govind, R. D. Nevels, and J. O. Prewitt, "Currents and Charges Induced in an Arbitrarily Oriented Electrically Thin Conductor with Length Up to One and One-Half Wavelengths in a Plane-Wave Field," IEEE Trans. Electromagn. Compat., vol. EMC-19, August 1977, pp. 145-147.
- [13] Wu, T.T., and R. W. P. King, "The Tapered Antenna and its Application to the Junction Problem for Thin Wires," IEEE Trans. Antennas Propagat., vol. AP-24, January 1976, pp. 42-45.
- [14] Taylor, C.D., "Electromagnetic Scattering from Arbitrary Configuration of Wires," IEEE Trans. Antennas Propagat., vol. AP-17, September 1969, pp. 662-663.
- [15] Taylor, C.D., S.-M. Lin, and H. V. McAdams, "Scattering from Crossed Wires," IEEE Trans. Antennas Propagat., vol. AP-18, January 1970, pp. 133-136.
- [16] Butler, C.M., "Currents Induced on a Pair of Skew Wires," IEEE Trans. Antennas Propagat., vol. AP-20, November 1972, pp. 731-736.
- [17] King, R.W.P., and T. T. Wu, "Analysis of Crossed Wires in a Plane-Wave Field," IEEE Trans. Electromagn. Compat., vol. EMC-17, November 1975, pp. 255-265.
- [18] King, R.W.P., "Currents Induced in a Wire Cross by a Plane Wave Incident at an Angle," IEEE Trans. Antennas Propagat., vol. AP-25, November 1977, pp. 775-781.
- [19] Burton, R.W., and R. W. P. King, "Measured Currents and Charges on Thin Crossed Antennas in a Plane-Wave Field," IEEE Trans. Antennas Propagat., vol. AP-23, September 1975, pp. 657-664.

- [20] King, R.W.P., D. J. Blejer, and R. W. Burton, "Surface Currents and Charges on Crossed Electrically Thick Cylinders in a Normally Incident, Plane-Wave Field," Radio Science, vol. 13, January-February 1978, pp. 93-105.
- [21] King, R.W.P. , D. J. Blejer, S.-K. Wan, and R. W. Burton, "Currents and Charges Induced by a Normally Incident Plane Wave on Single and Crossed Tubular Cylinders with  $ka = 2$ ," Radio Science, vol. 13, January-February 1978, pp. 107-119.
- [22] King, R.W.P., D. J. Blejer, and R. W. Burton, "Surface Currents and Charges on a Cross Formed by an Electrically Thick Cylinder and a Flat Plate in a Normally Incident, Plane-Wave Field," submitted for publication.
- [23] Harrison, C.W., Jr., and R. W. P. King, "Excitation of a Coaxial Line Through a Transverse Slot," IEEE Trans. Electromagn. Compat., vol. EMC-14, November 1972, pp. 107-112.
- [24] Taylor, C.D., and C. W. Harrison, Jr., "On the Excitation of a Coaxial Line by an Incident Field Propagating Through a Small Aperture in the Sheath," IEEE Trans. Electromagn. Compat., vol. EMC-15, August 1973, pp. 127-131.

DATE  
FILMED  
— 8